SEISMOLOGICAL ANALYSIS OF FOUR RECENT MODERATE (M_L 4.8 TO 5.4) EARTHQUAKES IN UTAH

by

James C. Pechmann, Susan J. Nava, and Walter J. Arabasz
Department of Geology and Geophysics
University of Utah
Salt Lake City, Utah

CONTRACT REPORT 92-1 ***JANUARY 1992***
UTAH GEOLOGICAL SURVEY
a division of
UTAH DEPARTMENT OF NATURAL RESOURCES

THE PUBLICATION OF THIS PAPER
IS MADE POSSIBLE WITH MINERAL LEASE FUNDS

PROJECT SUMMARY

This project consisted of detailed seismological analyses of four moderate earthquakes, together with their associated foreshocks and aftershocks, that occurred in the Utah region between September 1987 and January 1989. The four earthquakes, including local magnitude (M_L) and date (UTC), were the following: (1) the M_L 4.8 Lakeside earthquake of September 25, 1987; (2) the M_L 5.3 San Rafael swell earthquake of August 14, 1988; (3) the M_L 4.8 Bear Lake earthquake of November 19, 1988; and (4) the M_L 5.4 southern Wasatch Plateau earthquake of January 30, 1989. The immediate purpose of these seismological studies was to document basic information on the spatial and temporal characteristics of the four earthquake sequences—and on the location, geometry, and sense of slip of the causative faults. The broader goal was to gain an improved understanding of the relationship between moderate earthquakes and geologic structure in Utah, which is required for more reliable assessments of earthquake hazards in the region.

The studies reported here were carried out using seismological data primarily from the University of Utah regional seismic network and from portable seismographs deployed by the University of Utah following each of the four main shocks. Supplementary data for the main shocks and larger aftershocks were obtained from other seismic networks in the Intermountain region. For each earthquake sequence, efforts were made to: (1) construct an improved velocity model for the epicentral area using sonic logs from nearby oil wells and other information, as available, (2) refine the earthquake locations using relative hypocentral location techniques, (3) determine the focal mechanisms for the main shock and larger aftershocks from P-wave first motions, (4) determine the spatial and temporal characteristics of the earthquake sequence, and (5) interpret the results in light of available geological and geophysical information for the epicentral region.

Important results include the following: (1) Of the four main shocks studied, two (Bear Lake and southern Wasatch Plateau) occurred within Utah's main seismic belt in areas characterized by significant background seismicity, whereas the other two (Lakeside and San Rafael swell) occurred outside the seismic belt in areas of low prior seismicity. (2) Three of the four main shocks were preceded by foreshocks (the southern Wasatch Plateau earthquake was the exception). (3) Not one of the main shocks had a focal mechanism typical of the basin-range-type normal faulting found throughout Utah's main seismic belt, i.e., normal dip slip on a plane of moderate dip. (The Lakeside and southern Wasatch Plateau earthquakes had strike-slip mechanisms, the San Rafael swell earthquake had an oblique-normal-slip mechanism, and the Bear Lake earthquake had an unusual type of normal-slip mechanism.) (4) None of the earthquakes studied were associated with a mapped surface fault, with the possible exception of the 1988 Bear Lake earthquake.

TABLE OF CONTENTS

INTRODUCTION

Project Background

This project originated with a proposal submitted in March 1989 to the Mineral Lease Special Projects Program of the (then) Utah Geological and Mineral Survey. The proposal requested partial support for detailed seismological analyses of the following four moderate earthquakes that occurred in the Utah region between September 1987 and January 1989 (see Figure I-1 for locations):

(1) the M_L (local magnitude) 4.8 Lakeside earthquake of September 25, 1987;

(2) the M_L 5.3 San Rafael swell earthquake of August 14, 1988;

(3) the M_L 4.8 Bear Lake earthquake of November 19, 1988; and

(4) the M_L 5.4 southern Wasatch Plateau earthquake of January 30, 1989.

Special importance was attached to this group of moderate earthquakes because they were the largest earthquakes to occur in the Utah region since the M_L 6.0 Pocatello Valley earthquake near the Utah-Idaho border in 1975.

Following agreement by the Utah Geological and Mineral Survey to fund the proposed work, the project began in July 1989. The term of the project, originally scheduled for 12 months, was extended to September 30, 1991. Additional support for this work came from the National Earthquake Hazards Reduction Program through the U.S. Geological Survey.

Purpose and Importance of Project

Moderate earthquakes below the usual threshold size for surface faulting in the Great Basin, M_L 6.0-6.5, are a significant source of seismic hazard in Utah. Earthquakes of this type that have caused considerable damage in Utah include the M_L 5.7 Cache Valley earthquake of 1962 and two earthquakes of estimated magnitude 6 that occurred near Elsinore in 1921. Seismic hazard from these moderate earthquakes is poorly understood because most of these earthquakes appear to occur on buried faults with no clear surface expression. These faults cannot be easily recognized from observations of the surface geology, and they cannot be studied using standard techniques.

The primary goal of this project was to determine the location, geometry, and sense of slip of the faults or fault segments that generated the four moderate earthquakes selected for study. Because none of these earthquakes appears to have caused any surface rupture, this information can only be obtained using seismological techniques. A secondary goal was to document the spatial and temporal characteristics of the four earthquake sequences. This work is part of a long-term effort to gain an improved understanding of the relationship between moderate earthquakes and geologic structure in Utah. It is hoped that this improved

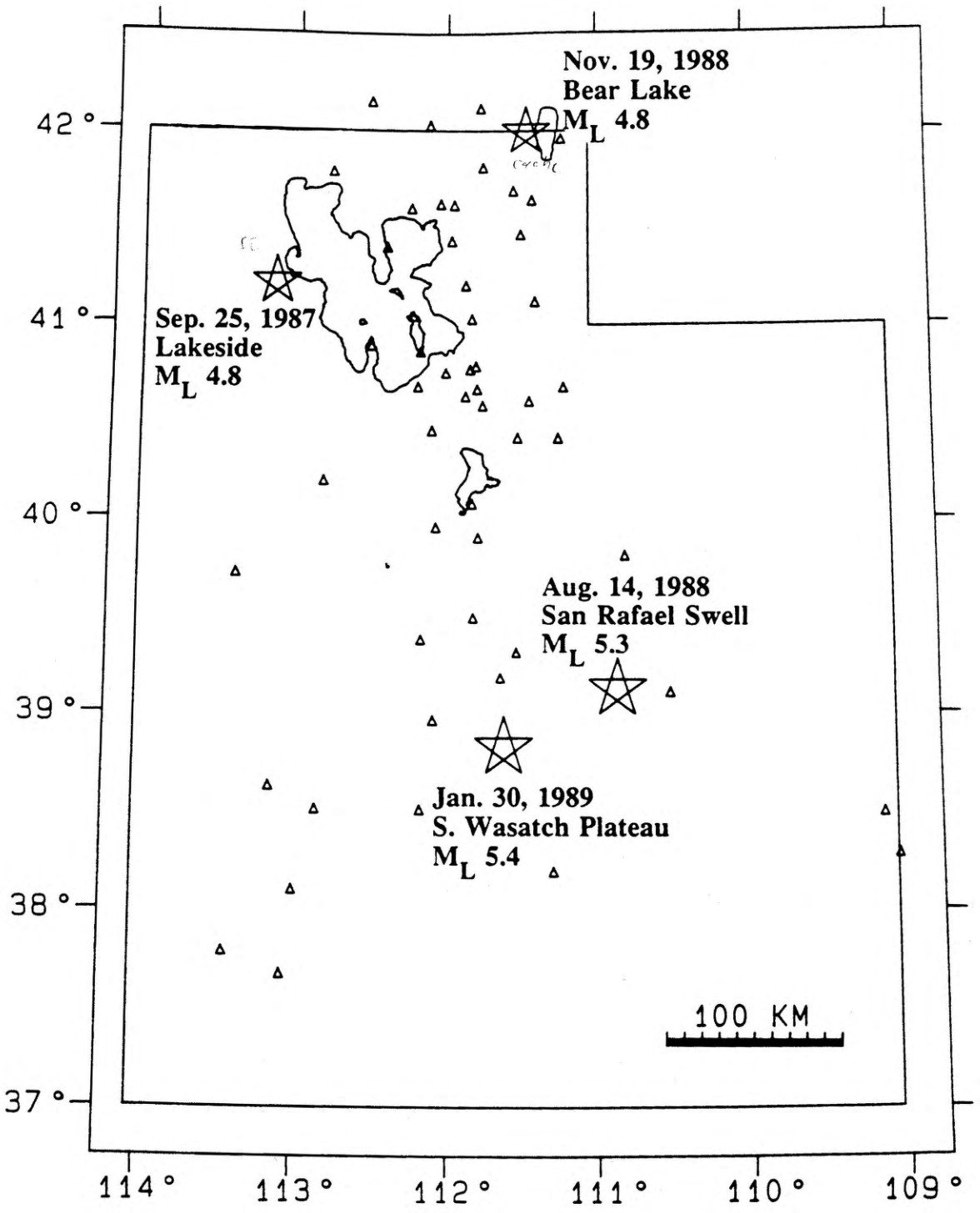

Figure I-1. Epicenters of four $M_L \geq 4.8$ earthquakes (stars) that occurred in Utah between September 1987 and January 1989. Stations of the University of Utah seismic network as of December 31, 1988, are shown as triangles.

understanding will lead to more reliable assessments of seismic hazards in Utah from moderate earthquakes on buried faults.

General Approach

We analyzed the seismological data for the selected earthquake sequences using, for the most part, standard techniques. An important subset of the data available for these studies came from local seismic stations deployed by the University of Utah during all four earthquake sequences to supplement the University of Utah's sparse permanent network (Figure 1-1). Four to five portable seismographs were deployed immediately following each of the four main shocks and operated for periods of three to fifteen days. In addition, two to four portable telemetry stations were installed following the Lakeside, San Rafael swell, and southern Wasatch Plateau earthquakes, and operated for periods of up to six months.

Data from the temporary stations provided much better control on locations of aftershocks, especially focal depths, than could be obtained using data from the permanent network alone. But even with the portable-array data, special efforts were necessary to refine the spatial resolution of the earthquake hypocenters. For each earthquake sequence, we did the following work:

(1) construct an appropriate velocity model for the epicentral area using sonic logs from nearby oil wells and other information, as available;

(2) refine the earthquake locations using relative hypocentral location techniques;

(3) determine the focal mechanisms for the main shock and larger aftershocks from P-wave first motions;

(4) determine the spatial and temporal characteristics of the earthquake sequence; and

(5) interpret the results in light of available geological and geophysical information for the epicentral region.

For the most part, this work was successful in meeting the goals of the project. For all of the main shocks except for Bear Lake, we were able to identify the location, orientation, sense of slip, and approximate size of the fault break from the focal mechanism and from planar clustering of aftershock hypocenters. However, the quality of the data varies considerably among the four sequences. The best results that we obtained were for the San Rafael swell sequence, in large part because of the excellent data from the portable instruments deployed in the area following the main shock. The deployment of portable instruments to record the San Rafael swell earthquakes was facilitated by the abundance of good seismic recording sites in the epicentral area and by the good summer weather at the time the sequence began. Comparable efforts were made to deploy instruments in the Lakeside area following the Lakeside main shock. However, the data obtained were not as good because of the inaccessibility of the immediate epicentral area, and because the coverage of the regional seismic network in this area was (and still is) quite poor (Figure 1-1). Deployment of portable

instruments after the 1988 Bear Lake earthquake and the 1989 southern Wasatch Plateau earthquake was hampered by the winter weather conditions in the mountainous terrains where these shocks occurred. Adequate data were nonetheless obtained for the southern Wasatch Plateau sequence because the earthquakes were unusually deep and because the permanent stations of the regional network provided reasonably good azimuthal coverage (Figure I-1). It became evident to us during this study that with the large station spacing of the regional seismic network in most of Utah, considerable effort must be made to deploy portable instruments during an earthquake sequence in order to obtain spatial resolution of hypocenters that is sufficient for seismotectonic interpretation.

Presentation of Results

Our detailed results for the four earthquake sequences selected for study are summarized in Chapters 1, 2, and 3. Each chapter represents, in effect, a self-contained manuscript, including references and an appendix with a listing of relocated hypocenters. Chapter 1 presents results of our studies of the 1987-1988 Lakeside earthquakes. In Chapter 2 we combine our analyses of the 1988 San Rafael swell and 1989 Southern Wasatch Plateau earthquakes into a comparative study of the two earthquakes—both of which occurred in the northwestern part of the Colorado Plateau in central Utah. Finally, Chapter 3 summarizes details of the 1988 Bear Lake earthquake.

Generalized Results

Each of the four earthquake sequences studied has distinct characteristics, the details of which we leave for Chapters 1, 2, and 3. There *are*, however, some important generalizations that can be made—useful for guiding the reader's attention. First, two of the main shocks occurred within Utah's main seismic belt in areas characterized by significant background seismicity, whereas the other two occurred in marginal areas characterized by low prior seismicity. Referring to Figure I-1, in which the density of seismograph stations follows the main seismic belt, the Bear Lake and Southern Wasatch Plateau earthquakes occurred *within* the main seismic belt; the Lakeside and San Rafael swell earthquakes, outside of it. Second, three of the four main shocks were preceded by foreshocks. The Southern Wasatch Plateau earthquake was the exception. Third, not one of the main shocks had a focal mechanism typical of basin-range-type normal faulting, i.e., normal dip slip on a plane of moderate dip. Although only the Lakeside earthquakes occurred in the Basin and Range Province proper, similar normal faulting extends east of the Basin and Range Province into the regions where the other earthquakes occurred. Two of the main shocks had strike-slip mechanisms (Lakeside and southern Wasatch Plateau), one had an oblique-normal-slip mechanism (San Rafael swell), and one had an unusual type of normal-slip mechanism (Bear Lake). Fourth, none of the earthquakes studied were associated with a mapped surface fault, with the possible exception of the 1988 Bear Lake earthquake.

1. SEISMOTECTONICS OF THE 1987-1988 LAKESIDE, UTAH, EARTHQUAKES

ABSTRACT

From September 1987 through March 1988, an earthquake sequence which included shocks of M_L 4.8 and 4.7 on September 25 and October 26, respectively, and a total of 8 events of $M_L \geq 3.8$, occurred beneath a desert basin west of the Great Salt Lake. Wood-Anderson seismograms indicate nearly identical magnitudes for the two largest earthquakes but a factor of two to five larger seismic moment for the first. The shocks were the largest in the Utah region since an M_L 6.0 main shock in 1975. Significant aspects of the 1987-88 sequence included: foreshock activity, proximity (epicentral distance, Δ, of 7 to 12 km) to a major pumping facility completed in early 1987 to lower the level of the Great Salt Lake, a strike-slip focal mechanism for the M_L 4.8 main shock, and the lack of a clear association with late Quaternary surface faults.

Despite constraints on accessibility to the epicentral area, the stations of the regional seismic network ($\Delta \geq 60$ km) were supplemented with local stations—initially four portable seismographs and later up to four telemetered stations ($2 \leq \Delta \leq 27$ km) that operated continuously from October 7, 1987, through March 1988. Well-located aftershock foci form a 6-km-square zone between 6 and 12 km depth which is steeply dipping and trends SSE, parallel to the right-lateral nodal plane of the main shock focal mechanism. Despite coincidental timing and proximity of the earthquakes to major pumping activity at the surface, the case for pumping-induced seismicity is weak.

INTRODUCTION

Between September 1987 and March 1988, an earthquake sequence which included eight shocks of $3.8 \leq M_L$ (local magnitude) ≤ 4.8 occurred beneath the Great Salt Lake desert in NW Utah, 10 km west of the Great Salt Lake (arrow, Figure 1-1). The two largest earthquakes were felt throughout northern Utah and into southern Idaho and eastern Nevada, with Modified Mercalli intensities of IV to V for the M_L 4.8 main shock on September 25 and III for an M_L 4.7 aftershock on October 26 (U.S. Geological Survey, 1987). These shocks were the largest to occur in the Utah region since the 1975 M_L 6.0 Pocatello Valley earthquake near the Utah-Idaho border (see Arabasz et al., 1981). The earthquakes attracted local attention because they were located 7 to 12 km WSW of a new 60-million dollar pumping facility built to reduce flooding along the shores of the Great Salt Lake. On April 10, 1987, the pumps had begun to pump water from the lake into the Great Salt Lake desert to form the large evaporating pond known as West Pond (Figure 1-1).

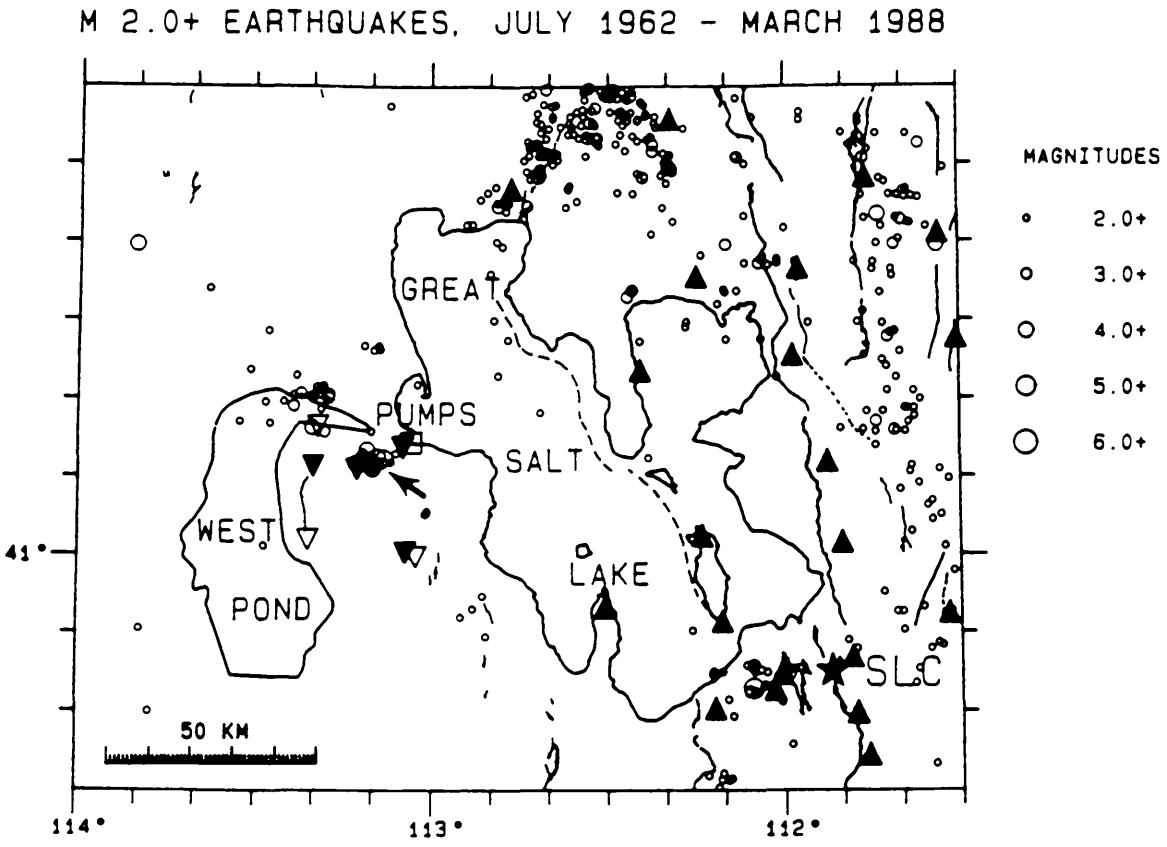

Fig. 1-1. Epicentral map of magnitude 2.0 and greater earthquakes near the Great Salt Lake located by the University of Utah from July 1962, when the University's regional seismic network began operation, through March 1988. The arrow points to the location of the 1987-1988 Lakeside sequence. Solid upright triangles show permanent stations of the University of Utah network in March 1988. Inverted open and solid triangles show locations of portable seismographs and temporary telemetered stations, respectively, installed to supplement the permanent network during the sequence. The open square labeled "Pumps" marks the location of the West Desert Pumping Station. These pumps pumped water from April 10, 1987, through June 30, 1989, from the Great Salt Lake into the Great Salt Lake Desert, lowering the level of the Great Salt Lake and creating the artificial lake labeled West Pond. The star labelled SLC shows the location of downtown Salt Lake City. Solid and dashed lines show surface traces of late Quaternary faults from the compilation of Arabasz et al. (1987b).

This report presents the results of an aftershock study carried out following the M_L 4.8 earthquake, together with focal mechanisms for the main shock and some larger aftershocks. Our principal conclusion is that the main shock was a right-lateral strike-slip earthquake on a SSE-striking fault between 6 and 12 km depth.

PRIOR SEISMICITY

The Lakeside earthquakes occurred along the western edge of the Intermountain Seismic Belt, a broad, diffuse band of seismic activity that trends north-south through central Utah following the eastern boundary of the Basin and Range Province (see Arabasz et al., 1987a,b; Smith and Arabasz, 1991). Earthquake activity had occurred episodically since at least 1965 in a broad cluster 10 to 30 km northwest of the 1987-1988 earthquakes. (Figure 1-1; see also Arabasz et al., 1987a). This activity included an M_L 4.0 event in February 1967, a swarm of ten events ($1.1 \leq M_L \leq 3.2$) in March and April of 1979, and another swarm of 9 events ($1.3 \leq M_L \leq 3.1$) in April of 1980. The University of Utah instrumental earthquake catalog, which begins in July 1962, contains only two small seismic events within 10 km of the center of the 1987-1988 activity (41° 12′ N, 113° 10.5′ W) prior to September 17, 1987. The first was an M_c (coda magnitude) 2.4 event in 1964 and the second was an M_c 1.3 event on October 18, 1986. We relocated the second earthquake according to the procedure described below. Our relocated epicenter is 8 km NE of the center of the 1987-1988 activity.

CHRONOLOGY OF THE SEQUENCE

Figure 1-2 is a plot of magnitude versus time for the Lakeside sequence from September 17 through November 5, 1987. All eight earthquakes of $M_L \geq 3.8$ occurred in September and October of 1987. The sequence began with an M_L 3.8 foreshock on September 17. No other events were detected by the University of Utah regional seismic network (Figure 1-1) until September 25, when three moderate earthquakes occurred within 70 minutes of each other: an M_L 4.1 foreshock, the M_L 4.8 main shock at 04:27 UTC (10:27 p.m. MDT, September 24), and an M_L 4.3 aftershock. An M_L 4.7 event followed on October 26. Following the M_L 4.7 earthquake, frequent small aftershocks of $M_L \leq 3.1$ continued through March 1988, after which the rate of aftershock activity declined substantially. The University of Utah Seismograph Stations located a total of 237 earthquakes in the Lakeside area from September 1987 through March 1988, including 51 of $M \geq 2.0$. In contrast, only six small earthquakes, two of which were of $M \geq 2.0$, were located in this area from April through December of 1988.

Local magnitudes determined from maximum peak to peak amplitudes on Wood-Anderson seismographs operated by the University of Utah at Dugway and Salt Lake City, Utah (using the distance corrections of Richter, 1958) are almost the same for the two largest earthquakes in the sequence, 4.8 and 4.7. However, the body-wave magnitudes determined by

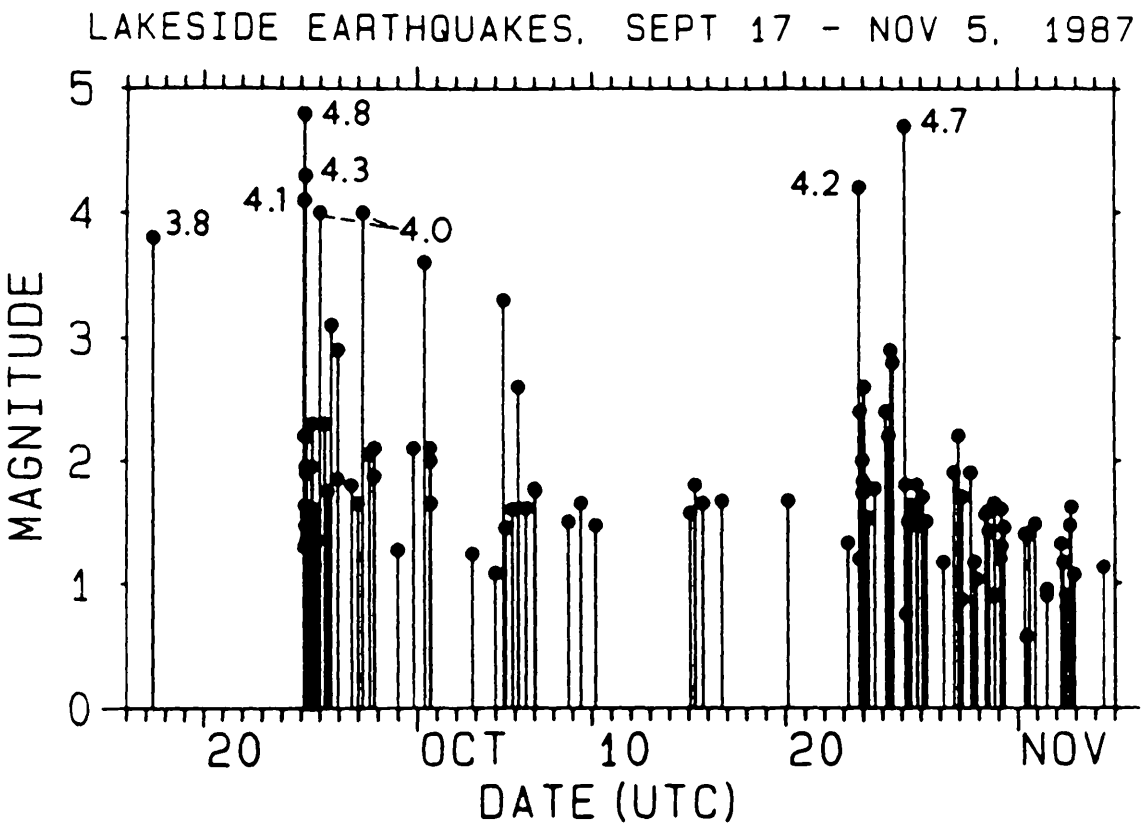

Fig. 1-2. Plot of magnitude versus time for the Lakeside earthquake sequence from September 17 through November 5, 1987 (UTC). Magnitudes of the eight $M_L \geq 3.8$ events are labeled. The plot includes all earthquakes in the University of Utah catalog within 15 km of the center of the activity (42° 12′ N, 113° 10.5′ W). The sample is believed to be complete for $M_L \geq 2.5$ (see Arabasz et al., 1987a, pp. 46-48.)

the U.S. Geological Survey (1987) are 4.7 for the September 25 event and 4.3 for the October 26 event. Examination of the Wood-Anderson seismograms shows that the signal durations and the average amplitudes for the September 25 event are noticeably larger than those for the October 26 event (Figure 1-3). Application of a method developed by Bolt and Herraiz (1983) to estimate seismic moment from Wood-Anderson seismograms yields moments of 3.8×10^{23} dyne-cm and 1.3×10^{23} dyne-cm for the September 25 and October 26 shocks, respectively. Comparing moment estimates from each Wood-Anderson station separately, the measurements from the Dugway records indicate a factor of 4.7 higher moment for the first event compared to the second, whereas the measurements from the Salt Lake City records indicate a factor of 2.4 difference. Thus, despite the similar local magnitudes, it appears that the September 25 earthquake was clearly the larger of the two, and that the October 26 earthquake can be considered an aftershock.

EARTHQUAKE LOCATIONS

Deployment of Portable Instruments

When the Lakeside sequence began, the closest seismograph station was a permanent station of the University of Utah seismograph network located 60 km to the southeast (Figure 1-1). Access to the epicentral area was difficult because of the lack of roads and because the earthquakes occurred at the northern end of the Hill Air Force Range, which is used for training and munitions testing. Nevertheless, University of Utah personnel supplemented the stations of the permanent network with temporary local stations beginning on September 26, the day after the M_L 4.8 earthquake (Table 1-1). Initially these consisted of four portable seismographs with smoked-paper recorders (open inverted triangles, Figure 1-1). Subsequently, these were replaced by four portable telemetry stations (solid inverted triangles, Figure 1-1), including one located at an epicentral distance of 2 to 6 km from the activity and that was installed by helicopter on October 29 following the M_L 4.7 earthquake. The portable telemetry stations were operated until August 16, 1988, although there were intermittent station failures after late March 1988. The seismometers at all of the temporary stations were high-gain, short-period, vertical-component velocity sensors.

Location Procedure

We relocated the Lakeside earthquakes with the computer program HYPOINVERSE (Klein, 1978) and P-wave arrival times from the eight temporary stations (generally four at any one time) plus 13 selected permanent stations located at epicentral distances of less than 125 km (Table 1-1). The velocity model used for the locations (the Wasatch Front model in Table 1-2) is a modified version of model B of Keller et al. (1975), taken from Bjarnason and Pechmann (1989). Because some of the most distant stations were important for azimuthal control,

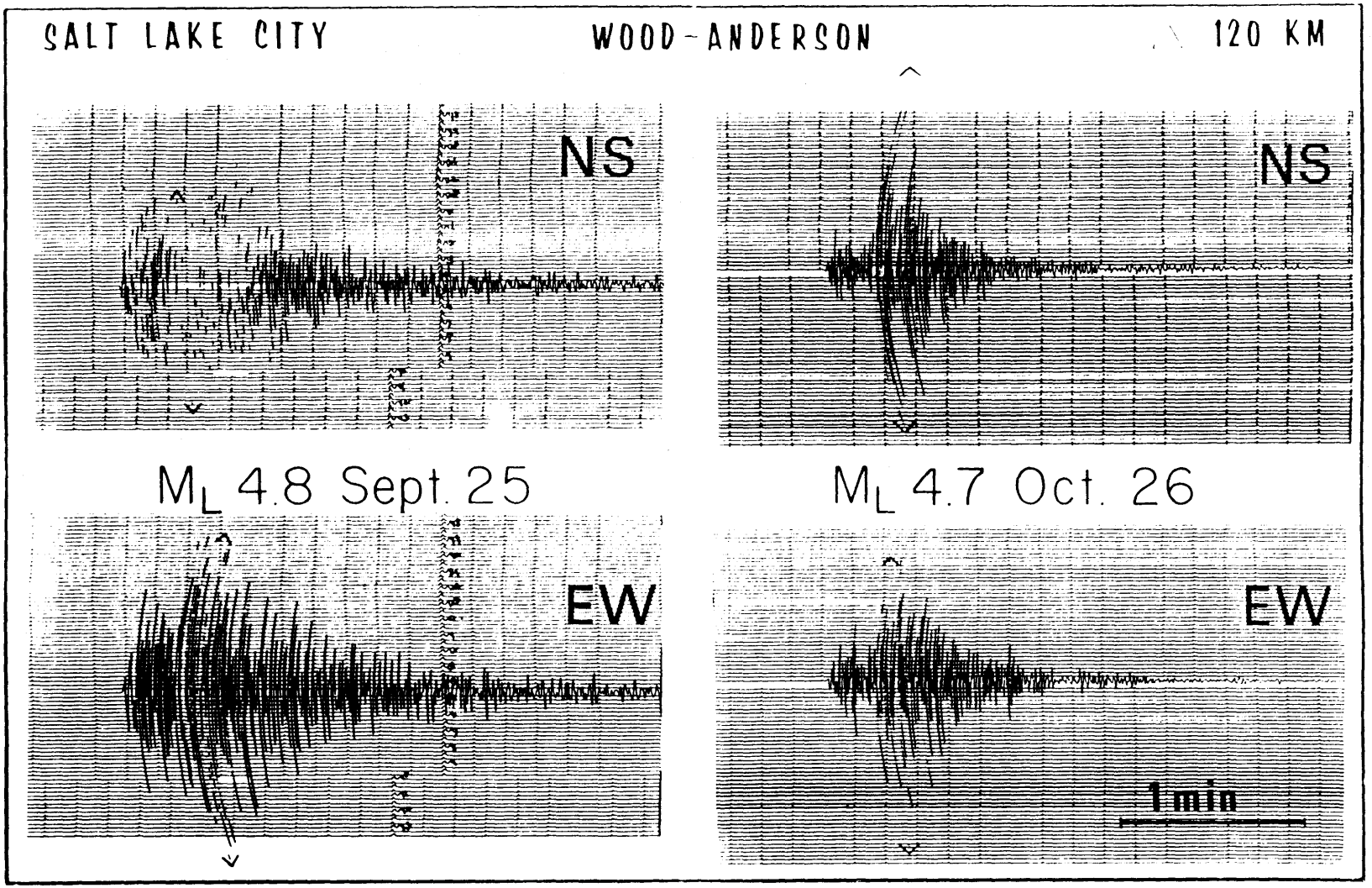

Fig. 1-3. Seismograms of the two largest Lakeside earthquakes recorded by an electronically-simulated Wood-Anderson instrument on the University of Utah campus in Salt Lake City. The epicentral distance is approximately 120 km. The V's mark the peak amplitudes used to compute the local magnitudes.

TABLE 1 - 1

STATIONS USED FOR RELOCATIONS OF THE LAKESIDE EARTHQUAKE SEQUENCE

Station Name	Type†	Latitude N	Longitude W	Elevation (m)	Station Correction (sec)	First Event Recorded (UTC)* Date	Time	Last Event Recorded (UTC)* Date	Time
ERUT	P	41° 10.89′	113° 12.51′	1309	−.11	10-29	03:42	3-26	20:34
HRUT	P	41° 13.63′	113° 04.85′	1408	−.09	10-07	00:50	3-26	20:34
HOGS	M	41° 13.76′	113° 04.83′	1414	.00	9-26	00:28	10-07	01:39
NFUT	P	41° 11.26′	113° 19.93′	1378	−.02	10-07	00:50	3-26	20:34
NNFU	M	41° 16.42′	113° 19.04′	1289	−.18	9-26	06:55	10-07	01:39
SJRU	M	41° 01.84′	113° 20.84′	1292	−.05	9-26	06:55	10-07	01:39
GVUT	P	41° 00.23′	113° 04.48′	1530	+.04	10-07	00:50	3-26	20:34
GRMU	M	40° 59.63′	113° 02.69′	1493	+.08	9-28	00:28	10-07	01:39
SNUT	R	40° 53.14′	112° 30.54′	1652	+.19	9-17	08:31	3-26	20:34
EPU	R	41° 23.49′	112° 24.53′	1436	+.11	9-17	08:31	3-26	01:00
HVU	R	41° 46.78′	112° 46.50′	1609	+.17	9-17	08:31	3-26	20:34
ANU	R	41° 02.38′	112° 13.90′	1353	−.06	9-17	08:31	3-02	02:29
CPU	R	40° 40.34′	112° 11.78′	2377	−.04	9-17	08:31	3-21	07:24
GZU	R	41° 25.53′	111° 58.50′	2646	−.12	9-17	08:31	3-26	01:00
PTU	R	41° 55.76′	112° 19.48′	2192	−.04	9-17	08:31	3-21	07:24
MOUT	R	41° 11.94′	111° 52.73′	2743	−.07	9-17	08:31	3-21	07:24
WVUT	R	41° 36.61′	111° 57.55′	1828	+.05	9-17	08:31	3-21	07:24
FPU	R	41° 01.58′	111° 50.21′	2816	−.19	9-17	08:31	3-02	02:03
DUG	R	40° 11.70′	112° 48.80′	1477	+.19	9-17	08:31	3-02	02:03
NPI	R	42° 08.84′	112° 31.10′	1640	+.01	9-17	08:31	3-02	02:03
CWU	R	40° 26.75′	112° 06.13′	1945	−.04	9-17	08:31	3-21	07:24

†R= UUSS regional network, M= microearthquake recorder, P= portable telemetry
*From September 17, 1987, through March 31, 1988

TABLE 1 - 2

LAKESIDE VELOCITY MODELS

Region	P-Wave Velocity (km/sec)	Depth to Top of Layer (km)*
Wasatch Front	3.4	0.0
	5.9	1.5
	6.4	17.1
	7.5	28.0
	7.9	42.0
Colorado Plateau	3.4	0.0
	5.9	1.5
	6.2	17.1
	6.8	27.5
	7.9	42.0
Southeast Idaho	3.4	0.0
	5.9	1.5
	6.8	17.1
	7.9	42.0

*Datum is 1500 m above sea level

we chose not to apply any distance weighting to the data. We did not use any S-wave arrival times for our relocations because there were no horizontal-component records from nearby stations to provide reliable S-wave data.

Initial epicentral locations for nearly all of the events that occurred before the installation of the portable instruments scattered to the east of the epicenters for the later events. This observation suggested that the earlier events were being systematically mislocated because of the poor azimuthal distribution of stations (Figure 1-1) and an inadequate velocity model. In an attempt to alleviate this problem, we used an inversion program written by Walter C. Nagy at the University of Utah to solve simultaneously for station delays for the 21 stations in Table 1-1, the velocity of the second layer of the model, and for hypocenters of 170 Lakeside earthquakes which had reasonably good preliminary locations. Both this program and the version of HYPOINVERSE that we used took the elevation differences of the stations into account in calculating the travel times. Velocity inversion was attempted only for the second layer of the model because this layer contains all of the hypocenters for the events used in the inversion, and the ray paths from these hypocenters to the 21 stations lie primarily within this layer. The velocity of the second layer remained within 0.06 km/sec of the starting value of 5.9 km/sec. Because the velocity did not change very much, and because it is questionable whether or not the data are of sufficiently good quality for a velocity inversion, we decided to hold the velocity model fixed and solve only for station delays and hypocenters. Tests showed that the station delays computed by the program were not very sensitive to the parameters of the inversion.

After determining the station delays, we used them with the program HYPOINVERSE to relocate all of the Lakeside earthquakes, starting from a trial hypocenter at 9 km depth at the center of the activity. Even when using the station delays, we found it advantageous to fix the focal depths of the 26 earthquakes that were recorded before the portable instruments were installed. Otherwise, the locations for these events suffered from an unconstrained tradeoff between focal depth and epicentral location. The focal depths of the first 26 earthquakes were fixed to 12 km if the magnitude was 3.8 or greater and to 9 km if the magnitude was smaller. Use of the station delays reduced the median root-mean-square of the weighted travel time residuals from 0.13 sec to 0.11 sec for the 221 earthquakes in 1987 and 1988 that we relocated.

HYPOCENTRAL DISTRIBUTION

Figure 1-4 shows epicenters of 221 Lakeside earthquakes that occurred from September 1987 through March 1988 (see the Appendix for a listing). The sample includes all but 16 of the 237 earthquakes that occurred during this time period in the area shown and were large enough to trigger the centralized digital recording system of the regional seismic network. The other 16 earthquakes are not included because they have less than five measured P-wave arrival times or azimuthal gaps between stations of more than 300°.

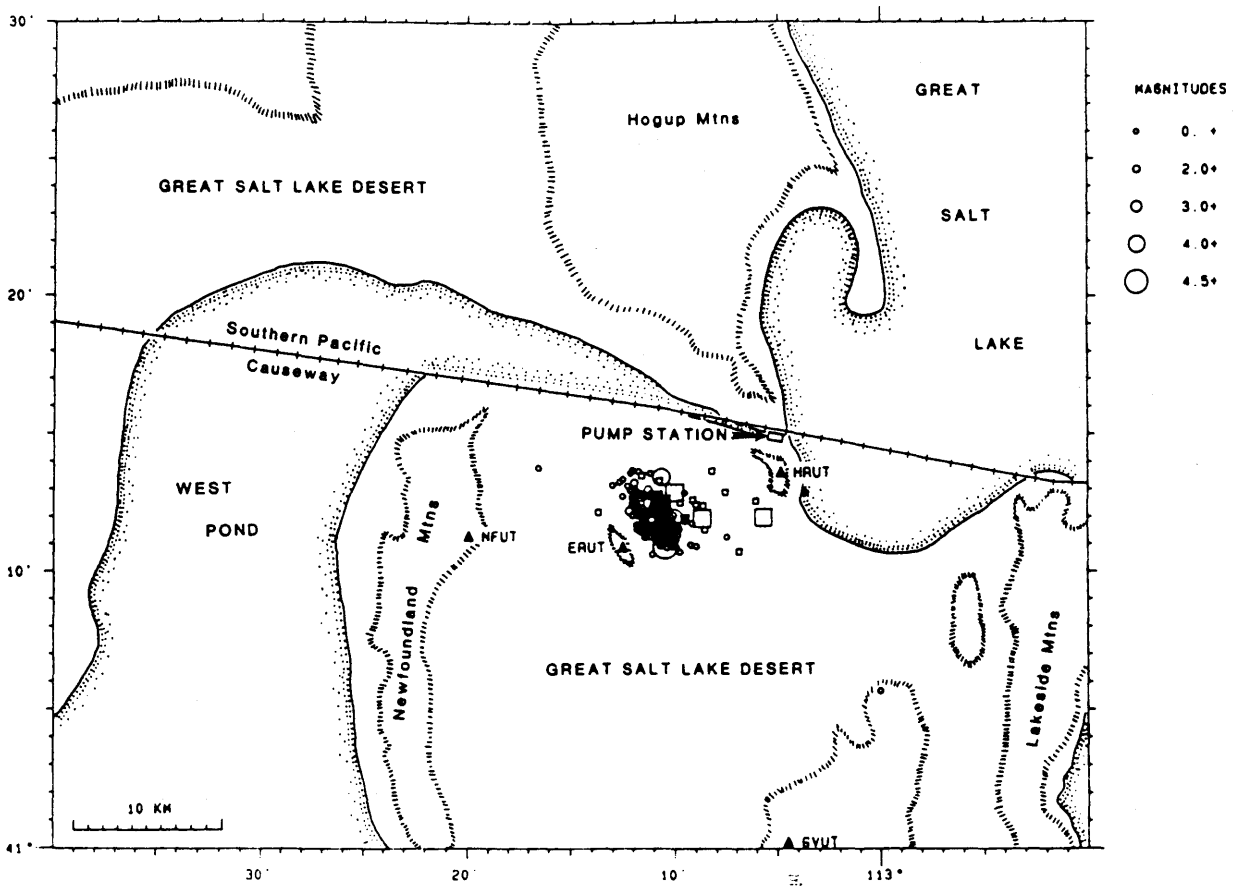

Fig. 1-4. Relocated epicenters for 221 Lakeside earthquakes that occurred from September 1987 through March 1988. Circles indicate earthquakes that occurred after the first portable stations were installed on September 26, and squares indicate earlier events for which we fixed the focal depths. Symbol sizes are scaled by magnitude as shown. The triangles show the locations of the four portable telemetry stations that were installed in October (Table 1-1). The shoreline of the Great Salt Lake is shown at its approximate location in late 1984.

Most of the earthquakes in Figure 1-4 concentrate within a SSE-trending zone that is 6 km long. About half of the epicenters of the early events with fixed focal depths (squares) scatter to the east of this zone, but the scatter is less than when no station delays are used. The epicentral pattern is similar but better-defined on Figure 1-5, which shows 154 of the best-located earthquakes from Figure 1-4. The selection criteria were: (1) distance to the nearest station equal to 15 km or less, (2) maximum azimuthal gap between stations of 180°, (3) minimum of six arrival times used for the location, and (4) maximum horizontal and vertical standard errors of 1.5 km. These criteria unfortunately exclude the September 17 foreshock, the September 25 main shock, and aftershocks that occurred during the first day following the main shock. Cross sections along line A-A′ on Figure 1-5 show that the aftershocks concentrate between 6 and 12 km depth (Figure 1-6). The hypocenters of all three well-located earthquakes of $M_L \geq 4$ lie in the bottom third of this depth range. The aftershock zone appears to have a dip greater than 65°, and perhaps near vertical, but the direction of dip is not clear from Figure 1-6.

A space-time plot of the earthquakes located in this study shows the epicenters of the main shock and its two recorded foreshocks to be near the center of the aftershock zone (Figure 1-7). This observation weakly suggests bilateral rupture, but is not definitive because of the poor quality of the locations of the earliest events. The epicenter of the largest aftershock is at the southeastern end of the aftershock zone. Most of the other aftershocks in late October are within 2 km of this M_L 4.7 event. There are no resolvable changes in focal depths with time.

FOCAL MECHANISMS

We attempted to determine focal mechanisms from P-wave first motions for all eight earthquakes in the Lakeside sequence of $M_L \geq 3.8$. Because these earthquakes occurred on the western edge of the University of Utah seismic network, we augmented the data from this network, when possible, with data from seismograph stations in Nevada, Idaho, and Washington. Takeoff angles for the first-arriving P waves were calculated using the relocated hypocenters and three different one-dimensional velocity models for stations located in different regions (Table 1-2). These velocity models and the accuracy of the takeoff angles computed from them are discussed in Bjarnason and Pechmann (1989).

Only the focal mechanism for the M_L 4.8 main shock is well constrained by the available data (Figure 1-8). The main shock focal mechanism indicates right-lateral strike-slip motion on a SSE-striking fault that dips steeply to the SW or, alternatively, left-lateral strike-slip motion on a nearly vertical fault that strikes ENE. This focal mechanism is fortunately not very sensitive to focal depth which, as explained above, is poorly controlled due to the lack of nearby stations and was fixed at 12 km. The SSE trend of the aftershock zone is parallel to the right-lateral nodal plane of the focal mechanism, suggesting that this nodal plane is the fault plane.

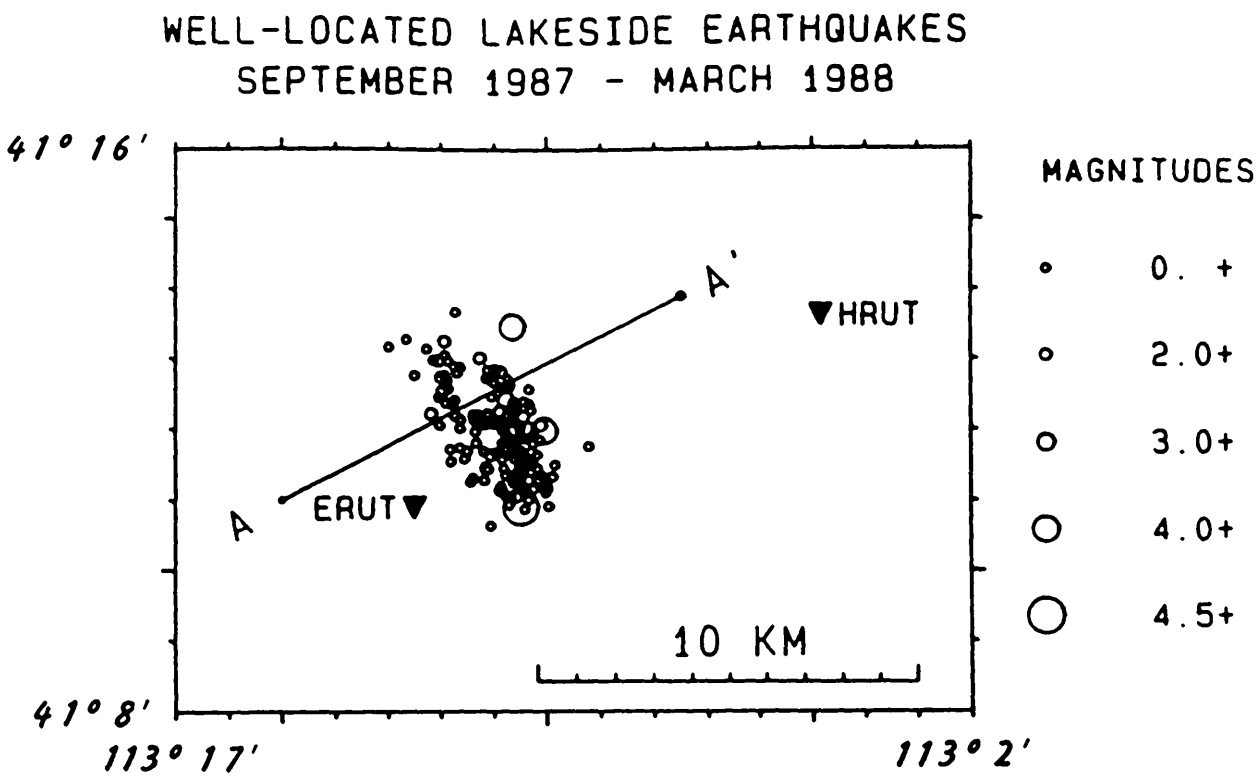

Fig. 1-5. Map view of 154 well-located Lakeside aftershocks that occurred from September 26, 1987, through March 21, 1988. See text for selection criteria. The two closest portable telemetry stations are shown as inverted triangles. The line A-A′ shows the direction of the cross sections in Figure 1-6, and is taken perpendicular to the preferred nodal plane of the main shock focal mechanism (Figure 1-8).

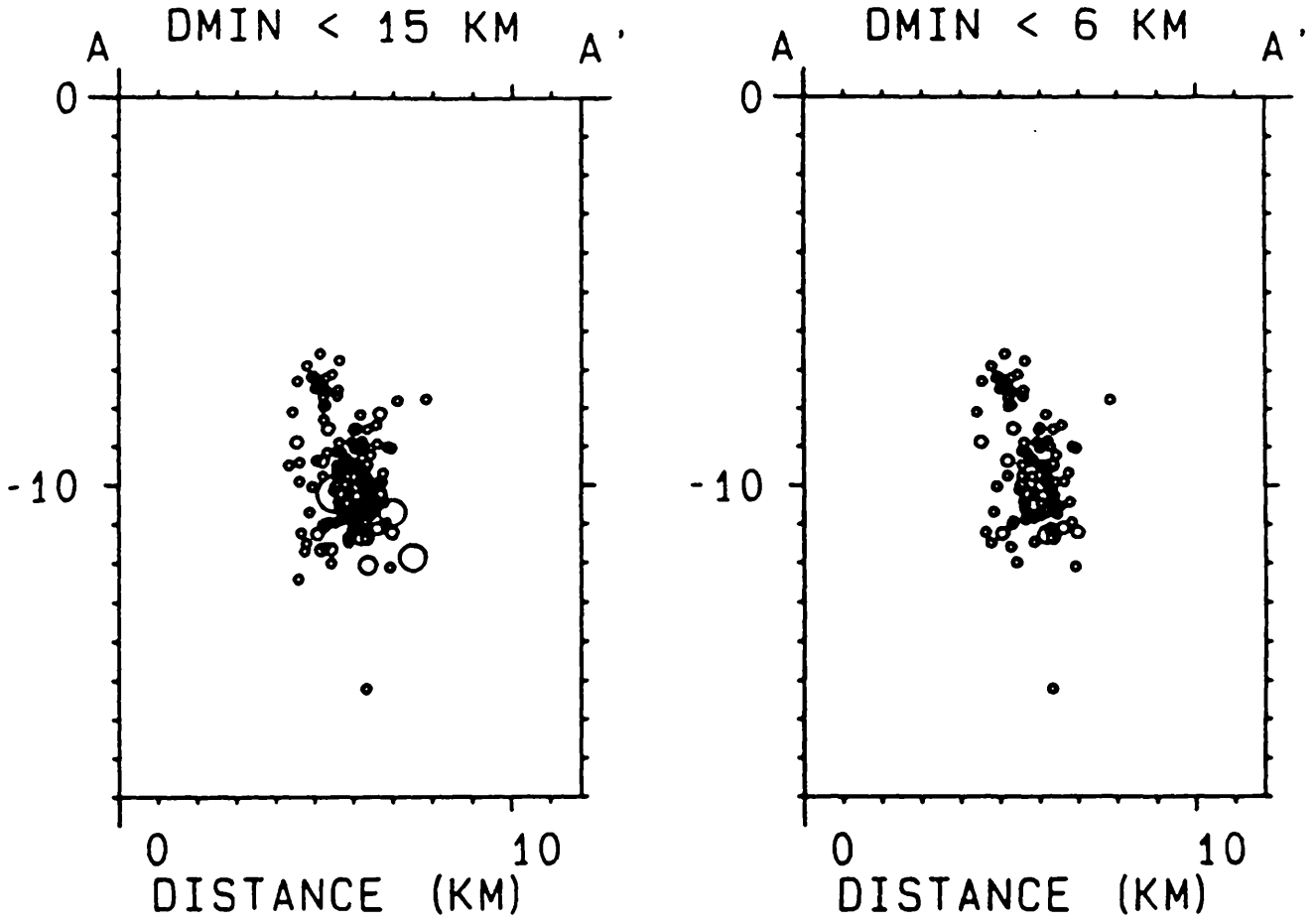

Fig. 1-6. Hypocentral cross sections with no vertical exaggeration along line A-A′ in Figure 1-5. The cross section on the left includes all of the earthquakes from Figure 1-5. The cross section on the right includes only those earthquakes from Figure 1-5 for which the distance to the nearest station used in the location, DMIN, is less than 6 km. Note that the hypocentral distribution is similar on both cross sections. Circle sizes are scaled by magnitude as in Figure 1-5.

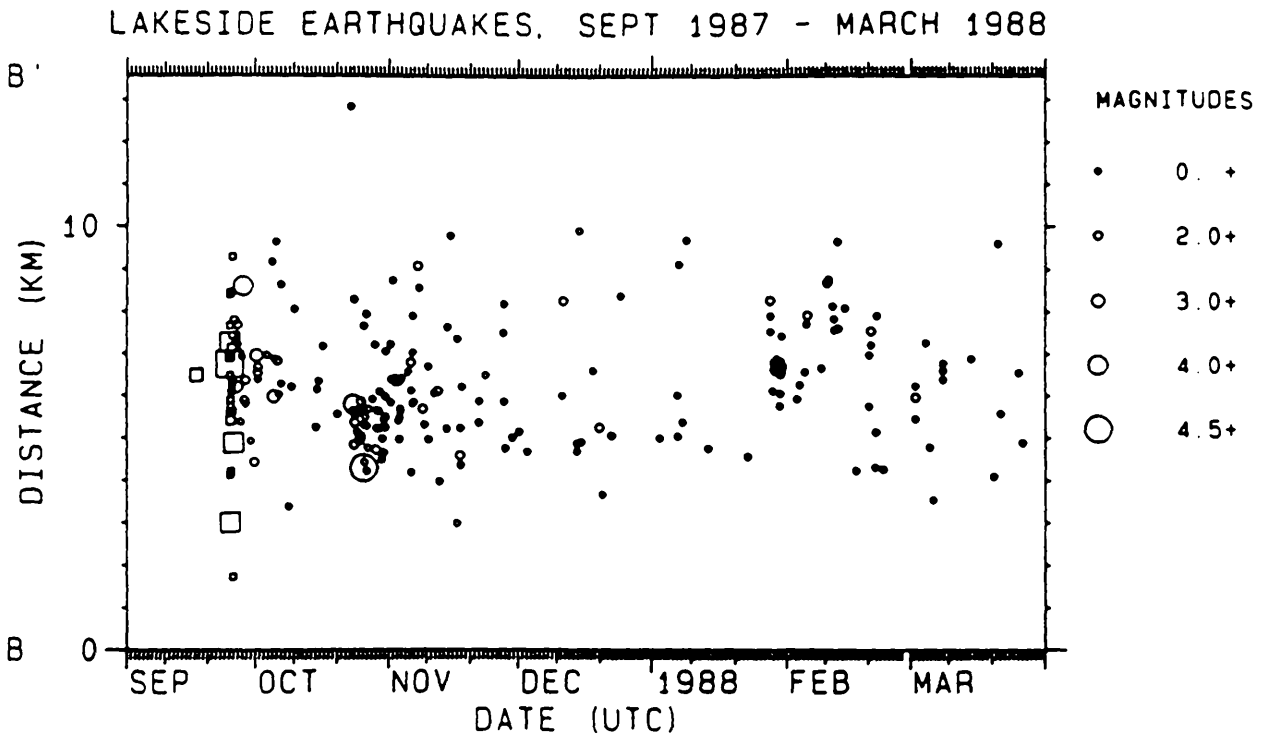

Fig. 1-7. Space-time plot of the 221 relocated epicenters for the Lakeside earthquakes shown on Figure 1-4. The space coordinate is the distance NNW along the strike of the inferred fault plane, i.e., along a line perpendicular to line A-A′ on Figure 1-5. Squares and circles as in Figure 1-4.

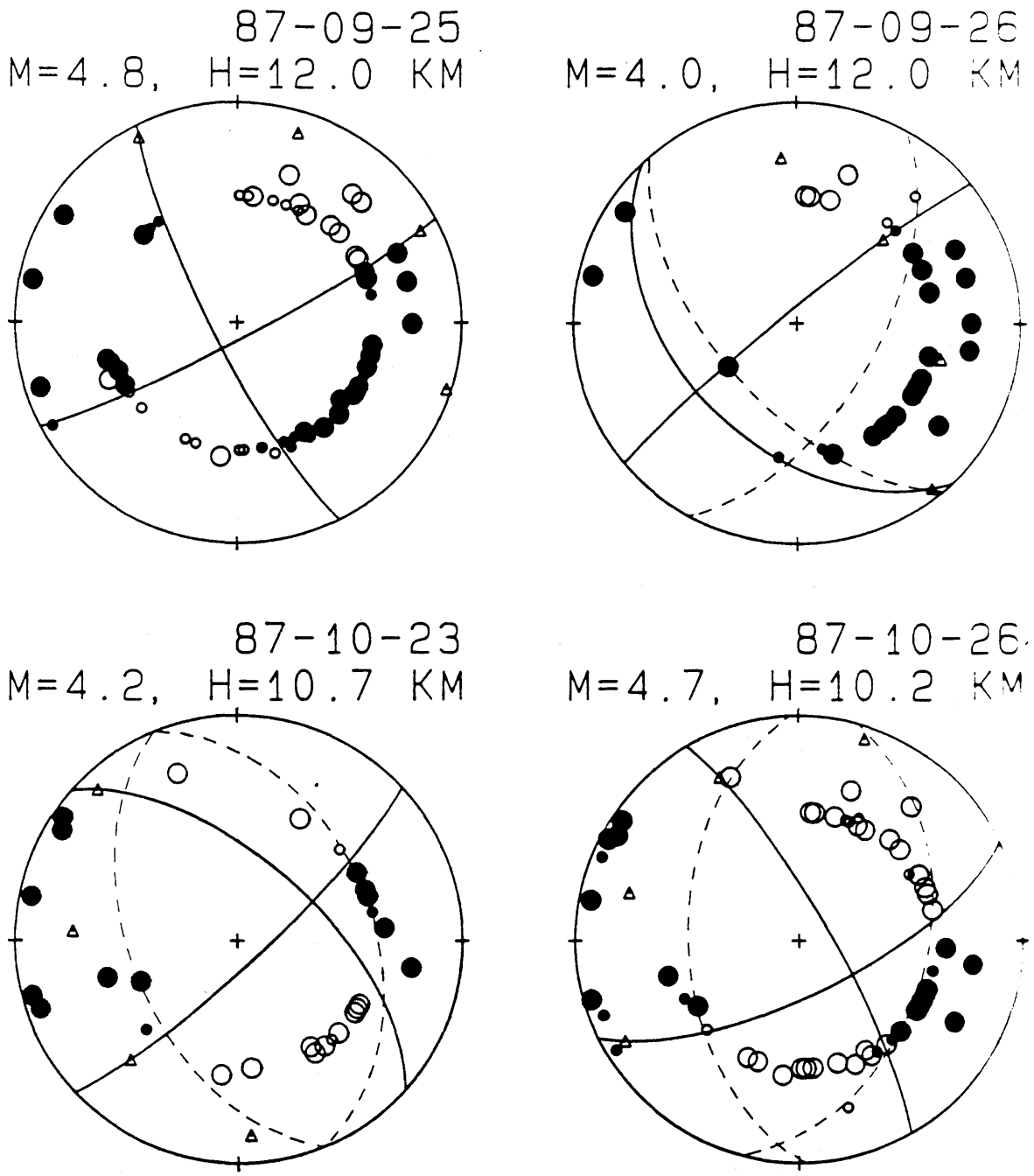

Fig. 1-8. The four best-constrained focal mechanisms that we determined for earthquakes in the Lakeside sequence, including the main shock (upper left) and largest aftershock (lower right). The date, magnitude (M), and depth (H) are given for each earthquake. P-wave first motions are plotted on a lower-hemisphere projection, with compressions shown as solid circles and dilatations as open circles. Smaller circles indicate readings of lower confidence. The triangles show slip vectors and P and T axes for the solutions shown by the solid nodal planes. The dashed nodal planes show representative alternative solutions. Based on the aftershock distribution (Figures 1-4 to 1-6), the SSE-striking nodal plane of the main shock focal mechanism is the probable fault plane.

The strike, dip, and rake of this nodal plane are 153° ± 4°, 78° ± 10°, and -174° ± 8°, respectively (following the sign convention for rake angle of Aki and Richards, 1980, p. 106).

The first motion data for the largest aftershock (Figure 1-8, lower right) is compatible with two different possible focal mechanisms: a strike-slip solution similar to that of the main shock (solid nodal planes) or else normal slip on a fault plane that dips moderately to either the W or to the ESE (dashed nodal planes). The focal mechanisms for the other six $M_L \geq 3.8$ earthquakes are less well constrained. The first motion data for these events show some variability from one event to another, but in all cases can be fit by solutions showing right-lateral strike-slip faulting on a SE- to SSE-striking plane, or normal or oblique-normal faulting on SE- to SW-striking planes (Figure 1-8). The tension (T) axes of the focal mechanisms for the main shock and the largest aftershock have shallow plunges and trend ESE-WNW. The T axes for the rest of the focal mechanisms are constrained by the data to have moderate to shallow plunges and trends between NE-SW and SE-NW.

DISCUSSION

Taken together, the focal mechanism for the main shock and the distribution of its aftershocks imply that the M_L 4.8 Lakeside earthquake involved right-lateral strike-slip motion on a fault striking SSE and dipping steeply (>65°) WSW. From the dimensions of the aftershock zone (Figures 1-5 and 1-6), we infer that slip occurred between 6 and 12 km depth on an approximately 6-km-square section of the fault. The earthquake occurred beneath the middle of a broad saline mud flat between the Newfoundland and Lakeside mountains (Figure 1-4), where no strike-slip faults have been mapped. However, the area in question has been covered by the Great Salt Lake at least twice within the last 3,000 years (Currey et al., 1984) so it is possible that evidence of late Quaternary faulting could have been obliterated due to fluctuations in the level of the lake.

Focal mechanisms for most small to moderate-size earthquakes in the Wasatch Front region show predominantly normal faulting. However, some strike-slip and oblique-slip focal mechanisms are also observed, particularly in the southern Wasatch Front area (Arabasz and Julander, 1986; Jones, 1987; Bjarnason and Pechmann, 1989). The ESE-WNW-trending T axes of the focal mechanisms for the two largest Lakeside earthquakes (Figure 1-8) are typical of Wasatch Front earthquakes (Bjarnason and Pechmann, 1989; Patton and Zandt, 1991).

It is well known that impoundment of reservoirs behind high dams occasionally triggers increased seismic activity (e.g., Simpson, 1986). The occurrence of the Lakeside earthquakes in close proximity to the West Desert Pumping Stations, and only five months after the pumps began operating, raises the question of whether or not the earthquakes might have been induced by the pumping. Although we cannot rule out this possibility, it seems unlikely for three reasons. First, in light of the previous earthquake activity of $M_L \leq 4.0$ that occurred within 30 km of the 1987-1988 Lakeside earthquakes, the latter earthquakes, although of larger magnitude, cannot be considered unusual. Secondly, few if any of the 1987-1988 earthquakes

occurred at depths shallower than 6 km (Figure 1-6); if the earthquakes were being triggered by redistribution of water at the surface, focal depths shallower than those observed would be expected (Simpson et al., 1988). Finally, the average depth of West Pond when full was only 2.5 feet and the maximum depth was only 7 feet (Ben Everitt, Utah Division of Water Resources, written communication, 1987). In comparison, the level of the Great Salt Lake rose 20.5 feet from 1963 to 1986, with 12.2 feet of this increase occurring between 1982 and 1986 (Stephens and Arnow, 1987). The elevation of the lake peaked at 4211.85 feet in June 1986 and in April 1987 (Stephens and Arnow, 1987; Mabey, 1987). The lake level declined after April 1987, in part due to the pumping but primarily because of decreased precipitation (Mabey, 1987). Thus, overall the changes in surface loads caused by the rapid rise of the Great Salt Lake between 1982 and 1986 were much larger than those caused by the subsequent pumping project. The changes in hydrology caused by the rise of the lake would also be expected to be much greater than those caused by the pumping, although the possibility of some critical local changes induced by the pumping cannot be totally excluded. Whether or not the rapid rise of the Great Salt Lake during the years preceding the Lakeside earthquakes had any causal effect is a separate question—and one that cannot be answered without further study.

CONCLUSIONS

1. The 1987 M_L 4.8 Lakeside earthquake involved right-lateral strike-slip motion on a buried fault dipping steeply to the WSW beneath a lacustrine basin W of the Great Salt Lake.

2. From the aftershock distribution, we infer that the 1987-1988 Lakeside earthquakes broke a 6-km-square segment of the fault over a depth range of 6 to 12 km.

3. Foreshocks of M_L 3.8 and 4.1 occurred eight days and 18 minutes, respectively, before the Lakeside main shock. Prior to these foreshocks, there had been very little instrumentally-recorded seismicity in the immediate epicentral area.

4. There is no compelling evidence that the 1987-1988 Lakeside earthquakes were related to the West Desert Pumping project.

ACKNOWLEDGEMENTS

We are grateful to Erwin McPherson, Ken Whipp, Ethan Brown, Julie Shemeta, Rick Benson, and Tianrun Zhang for their work installing and operating the portable stations in the Great Salt Lake Desert. Linda Hall and Tianrun Zhang measured the arrival times, Paula Oehmich computed some of the local magnitudes, Ethan Brown performed some of the initial data analyses, and Jackie Bott assisted with the focal mechanism determinations. Walter Nagy made his inversion code available to us and helped us to use it. Personnel at the University of Nevada at Reno, Lawrence Livermore National Laboratory, the University of Washington, and

Boise State University graciously provided data from their seismic networks. This research was supported by the U.S. Geological Survey, Department of the Interior, under award numbers 14-08-0001-G1349 and 14-08-0001-G1762, and by the Utah Geological Survey through contract number 89-3659. The views and conclusions contained in this report are those of the authors and should not be interpreted as necessarily representing the official policies, either expressed or implied, of either the U.S. Government or the Utah State Government.

REFERENCES

Aki, K. and P. G. Richards (1980). *Quantitative Seismology: Theory and Methods*, W. H. Freeman, San Francisco, California, 932 pp.

Arabasz, W.J. and D.R. Julander (1986). Geometry of seismically active faults and crustal deformation within the Basin and Range-Colorado Plateau transition, in *Cenozoic Tectonics of the Basin and Range Province: A Perspective on Processes and Kinematics of an Extensional Origin*, L. Mayer, Editor, *Geol. Soc. Am. Special Paper 208*, 43-74.

Arabasz, W. J., W. D. Richins, and C. J. Langer (1981). The Pocatello Valley (Idaho-Utah border) earthquake sequence of March to April 1975, *Bull. Seism. Soc. Am.* **71**, 803-826.

Arabasz, W.J., J.C. Pechmann, and E.D. Brown (1987a). Evaluation of seismicity relevant to the proposed siting of a Superconducting Supercollider (SSC) in Tooele County, Utah, *Utah Geological and Mineral Survey, Misc. Publ. 89-1*, 107 pp.

Arabasz, W.J., J.C. Pechmann, and E.D. Brown (1987b). Observational seismology and the evaluation of earthquake hazards and risk in the Wasatch Front area, Utah, in *Assessment of Regional Earthquake Hazards and Risk Along the Wasatch Front, Utah*, P.L. Gori and W.W. Hays, Editors, *U.S. Geol. Surv., Open-File Rept. 87-585*, D1-D58.

Bjarnason, I.T. and J.C. Pechmann (1989). Contemporary tectonics of the Wasatch Front region, Utah, from earthquake focal mechanisms, *Bull. Seism. Soc. Am.* **79**, 731-755.

Bolt, B.A. and M. Herraiz (1983). Simplified estimation of seismic moment from seismograms, *Bull Seism. Soc. Am.* **73**, 735-748.

Currey, D.R., G. Atwood, and D.R. Mabey (1984). Major levels of Great Salt Lake and Lake Bonneville, *Utah Geological and Mineral Survey Map 73*, scale 1:750,000.

Jones, C. H. (1987). A geophysical and geological investigation of extensional structures, Great Basin, western United States, *Ph.D. Thesis*, Massachusetts Institute of Technology, Cambridge, Massachusetts, 226 pp.

Keller, G.R., R.B. Smith, and L.W. Braile (1975). Crustal structure along the Great Basin-Colorado Plateau transition from seismic refraction studies, *J. Geophys. Res.* **80**, 1093-1098.

Klein, F. W. (1978). Hypocenter location program HYPOINVERSE, *U.S. Geol. Surv., Open-File Rept. 78-694*, 113 pp.

Mabey, D. R. (1987). The end of the wet cycle, *Survey Notes (Utah Geological and Mineral Survey)* **21,** no. 2-3, 8-9.

Nava, S. J., J. C. Pechmann, W. J. Arabasz, E. D. Brown, L. L. Hall, P. J. Oehmich, E. McPherson, and J. K. Whipp (1990). *Earthquake Catalog for the Utah Region, January 1, 1986 to December 31, 1988*, Special Publication, University of Utah Seismograph Stations, Salt Lake City, Utah, 96 pp.

Patton, H. J. and G. Zandt (1991). Seismic moment tensors of western U.S. earthquakes and implications for the tectonic stress field, *J. Geophys. Res.* **96,** 18,245-18,259.

Richter, C.F. (1958). *Elementary Seismology*, W.H. Freeman and Co., San Francisco, Calif., 768 pp.

Simpson, D.W. (1986). Triggered earthquakes, *Ann. Rev. Earth Planet. Sci.* **14,** 21-42.

Simpson, D. W., W. S. Leith, and C. H. Scholz (1988). Two types of reservoir-induced seismicity, *Bull Seism. Soc. Am.* **78,** 2025-2040.

Smith, R. B. and W. J. Arabasz (1991). Seismicity of the Intermountain Seismic Belt, in *Neotectonics of North America*, D. B. Slemmons, E. R. Engdahl, M. D. Zoback, M. L. Zoback, and D. Blackwell, Editors, *Geol. Soc. Am. SMV V-1*, in press.

Stephens, D. and T. Arnow (1987). Fluctuations of water level, water quality, and biota of Great Salt Lake, Utah, 1847-1986, in *Cenozoic Geology of Western Utah—Sites for Precious Metal and Hydrocarbon Accumulations*, R.S. Kopp and R.E. Cohenour, Editors, *Utah Geol. Assoc. Publ. 16*, 181-194.

United States Geological Survey (1987). Preliminary determination of epicenters: monthly listings, U. S. Government Printing Office, Washington, D. C.

APPENDIX

This appendix contains a listing of the relocated hypocenters determined in this study for earthquakes associated with the September 25, 1987, M_L 4.8 Lakeside earthquake. This listing includes all earthquakes in the University of Utah catalog for the time period September 1, 1986, through March 31, 1988 (Nava et al., 1990), which (1) had epicenters within 15 km of the center of the 1987-1988 activity (42° 12′ N, 113° 10.5′ W), (2) had at least five P-wave arrival time picks, and (3) had a maximum azimuthal gap between stations of 300°. The relocations were done with the computer program HYPOINVERSE (Klein, 1978) using P-wave arrival times only, the stations and station corrections in Table 1-1, the velocity model in Table 1-2, elevation corrections calculated using the top layer velocity of 3.4 km/sec, and a trial hypocenter of 41° 12.0′ N, 113° 10.5′ W, 9.0 km depth. The focal depths of the first 26 earthquakes were unconstrained because the distance to the nearest station was 60 km or more. Depending on magnitude, these depths were fixed to either 9 km ($M < 3.8$) or 12 km ($M \geq 3.8$). See text for further explanation.

The following data are listed for each earthquake:

- Year (YR), date and origin time in Universal Coordinated Time (UTC). Subtract seven hours to convert to Mountain Standard Time (MST) and six hours to convert to Mountain Daylight Time (MDT).
- Earthquake location coordinates in degrees and minutes of north latitude and west longitude, and depth in kilometers. "#" indicates fixed depth. "*" indicates poor depth resolution: no recording stations within 10 km or twice the depth.
- MAG, the computed local magnitude (M_L) for each earthquake. "W" indicates magnitude based on peak amplitude measurements from Wood-Anderson records. Otherwise, the estimate is calculated from signal durations and is more correctly identified as coda magnitude, M_C.
- NO, the number of P readings used in the solution.
- GAP, the largest azimuthal separation in degrees between recording stations used in the solution.
- DMN, the epicentral distance in kilometers to the closest station used in the solution.
- RMS, the root-mean-square of the travel-time residuals in seconds:

$$RMS = \left\{ \frac{\sum_i \left[W_i R_i \right]^2}{\sum_i \left[W_i \right]^2} \right\}^{\frac{1}{2}}$$

where: R_i is the observed minus the computed arrival time for the i-th reading, and W_i is the relative weight given to the i-th arrival time (0.0 for no weight through 1.0 for full weight).

Lakeside, Utah, Earthquake Sequence

yr	*date*	*origin time*	*latitude*	*longitude*	*depth*	*mag*	*no*	*gap*	*dmin*	*rms*
86	1018	44 18.49	41° 15.91′	113° 7.73′	9.0#	1.3	10	220	62	0.21
87	917	831 26.00	41° 12.23′	113° 10.49′	12.0#	3.8W	13	223	66	0.13
87	925	409 53.97	41° 12.89′	113° 10.03′	12.0#	4.1W	13	222	66	0.11
87	925	427 57.52	41° 12.24′	113° 10.88′	12.0#	4.8W	13	223	67	0.12
87	925	449 31.07	41° 12.28′	113° 11.04′	9.0#	2.2	12	223	67	0.20
87	925	453 58.85	41° 12.85′	113° 10.75′	9.0#	1.3	10	237	67	0.20
87	925	518 14.90	41° 11.97′	113° 5.72′	12.0#	4.3W	12	247	60	0.21
87	925	536 33.47	41° 11.81′	113° 10.21′	9.0#	1.6	12	222	65	0.19
87	925	603 48.19	41° 12.51′	113° 9.76′	9.0#	1.5	13	221	66	0.22
87	925	610 39.58	41° 11.53′	113° 8.61′	9.0#	1.4	12	220	63	0.17
87	925	633 55.25	41° 13.33′	113° 10.75′	9.0#	2.0	11	224	67	0.13
87	925	713 48.63	41° 12.17′	113° 13.67′	9.0#	2.0	12	227	70	0.15
87	925	721 16.72	41° 12.89′	113° 7.62′	9.0#	1.4	9	234	63	0.14
87	925	739 30.33	41° 11.94′	113° 9.55′	9.0#	2.2W	13	221	65	0.14
87	925	748 40.30	41° 12.44′	113° 9.02′	9.0#	1.5	11	221	65	0.24
87	925	839 9.05	41° 12.06′	113° 11.73′	9.0#	1.5	13	225	67	0.18
87	925	840 50.19	41° 11.85′	113° 10.54′	9.0#	1.4	8	266	66	0.09
87	925	1028 1.17	41° 12.56′	113° 6.08′	9.0#	1.6	12	216	61	0.25
87	925	1413 13.12	41° 11.92′	113° 10.69′	9.0#	2.0	11	223	66	0.11
87	925	1512 2.55	41° 12.65′	113° 10.42′	9.0#	2.3W	13	223	66	0.20
87	925	1651 55.56	41° 12.62′	113° 9.17′	9.0#	1.2	11	221	65	0.32
87	925	1735 39.16	41° 12.40′	113° 8.68′	9.0#	1.5	12	219	64	0.26
87	925	1810 43.77	41° 13.51′	113° 11.58′	9.0#	1.6	11	224	68	0.22
87	925	1818 23.96	41° 13.67′	113° 8.26′	9.0#	1.1	8	273	64	0.22
87	925	2100 45.55	41° 10.72′	113° 6.94′	9.0#	1.4	12	217	60	0.17
87	926	28 1.98	41° 11.94′	113° 8.73′	12.0#	4.0W	12	220	6	0.17
87	926	655 46.46	41° 12.83′	113° 11.00′	10.6	2.3W	15	87	13	0.11
87	926	1018 17.30	41° 12.63′	113° 10.70′	9.9	1.8	14	86	14	0.14
87	926	1447 49.23	41° 12.02′	113° 10.58′	12.1	3.1W	15	87	14	0.11
87	926	2314 39.37	41° 12.81′	113° 10.88′	10.2	2.9W	15	86	13	0.11
87	926	2328 38.58	41° 12.59′	113° 10.72′	10.0	1.9	14	86	14	0.22
87	927	1634 59.06	41° 11.92′	113° 9.55′	8.8*	1.8	14	165	24	0.25
87	928	28 24.84	41° 12.56′	113° 10.34′	7.8	1.6	16	86	8	0.18
87	928	606 52.05	41° 13.46′	113° 10.65′	11.9	4.0W	16	93	8	0.09
87	928	1422 45.63	41° 11.64′	113° 11.08′	11.6	2.0	16	92	10	0.14
87	928	2010 19.27	41° 11.89′	113° 10.30′	8.9	1.9	16	86	8	0.17
87	928	2032 22.23	41° 12.18′	113° 10.44′	8.1	2.1	15	97	8	0.14
87	930	35 32.41	41° 11.55′	113° 9.81′	8.8	1.3	12	140	16	0.18
87	930	1957 42.56	41° 11.17′	113° 10.01′	10.2	2.1W	16	86	9	0.19
87	1001	916 31.07	41° 12.41′	113° 10.77′	10.4	3.6W	17	87	9	0.19
87	1001	1614 43.56	41° 12.30′	113° 10.61′	10.0	2.1	17	86	9	0.14
87	1001	1656 4.54	41° 12.26′	113° 10.26′	7.9	1.6	15	85	8	0.15
87	1001	1700 17.55	41° 12.11′	113° 10.90′	10.9	2.0	17	88	9	0.10
87	1003	2033 58.54	41° 12.88′	113° 9.58′	8.4	1.2	12	132	15	0.21
87	1005	26 41.02	41° 13.60′	113° 11.17′	5.5	1.1	13	92	9	0.18

Lakeside, Utah, Earthquake Sequence

yr	*date*	*origin time*	*latitude*	*longitude*	*depth*	*mag*	*no*	*gap*	*dmin*	*rms*
87	1005	1031 2.93	41° 11.98′	113° 10.34′	10.3	3.3W	17	87	8	0.12
87	1005	1250 43.71	41° 12.02′	113° 11.65′	9.4	1.5	13	94	13	0.09
87	1005	2130 12.88	41° 13.17′	113° 13.00′	9.5	1.6	16	98	10	0.19
87	1006	444 25.59	41° 12.14′	113° 11.27′	9.6	2.6W	16	92	9	0.16
87	1006	1402 7.40	41° 11.97′	113° 10.43′	5.1	1.6	15	87	9	0.16
87	1007	50 10.02	41° 12.76′	113° 12.50′	9.4	1.8	13	133	11	0.06
87	1007	139 25.34	41° 11.98′	113° 10.81′	10.6	1.8	18	81	9	0.13
87	1008	1907 10.42	41° 10.92′	113° 9.02′	10.2*	1.5	9	220	63	0.09
87	1009	1044 8.91	41° 12.04′	113° 10.55′	8.3	1.6	10	165	9	0.17
87	1010	505 29.81	41° 12.79′	113° 11.52′	8.6	1.5	5	183	9	0.01
87	1015	230 16.92	41° 11.84′	113° 9.56′	9.1	1.6	13	120	7	0.29
87	1015	845 2.31	41° 11.91′	113° 10.78′	10.6	1.8W	15	122	9	0.18
87	1015	1823 42.95	41° 11.81′	113° 11.35′	8.3	1.6	11	135	10	0.12
87	1016	1741 7.76	41° 12.06′	113° 12.03′	9.9	1.7	13	125	10	0.08
87	1020	339 32.80	41° 11.31′	113° 11.41′	11.7	1.7	12	117	10	0.16
87	1023	553 59.84	41° 13.77′	113° 16.47′	21.4	1.3	12	179	7	0.39
87	1023	1944 50.32	41° 11.98′	113° 10.05′	10.7	4.2W	13	121	8	0.10
87	1023	2014 39.69	41° 11.70′	113° 10.48′	9.3	1.2	9	133	9	0.02
87	1023	2039 38.44	41° 11.45′	113° 11.16′	11.7	2.4W	13	118	10	0.12
87	1023	2325 22.92	41° 11.28′	113° 10.36′	11.1	2.0W	13	116	9	0.11
87	1023	2342 19.89	41° 12.77′	113° 11.94′	9.2	1.7	12	146	10	0.06
87	1024	24 32.82	41° 12.88′	113° 11.65′	10.0	1.8	11	132	10	0.13
87	1024	151 36.90	41° 11.55′	113° 10.48′	11.1	2.6W	14	119	9	0.09
87	1024	649 16.31	41° 11.59′	113° 10.62′	9.4	1.5	9	132	9	0.05
87	1024	1451 55.39	41° 11.35′	113° 10.66′	10.9	1.8	12	117	9	0.11
87	1025	435 22.67	41° 11.14′	113° 10.88′	11.0	2.4W	14	115	10	0.17
87	1025	811 27.65	41° 11.64′	113° 10.70′	10.3	2.2W	5	133	9	0.07
87	1025	1043 2.60	41° 11.33′	113° 10.52′	10.8	2.9W	14	116	9	0.11
87	1025	1317 44.35	41° 11.74′	113° 10.77′	11.4	2.8W	14	120	9	0.11
87	1026	416 0.85	41° 10.90′	113° 10.49′	10.2	4.7W	14	113	9	0.31
87	1026	432 34.25	41° 12.71′	113° 11.12′	10.0	1.8W	14	130	9	0.11
87	1026	539 13.83	41° 11.73′	113° 9.93′	2.0	0.8	7	133	8	0.12
87	1026	824 17.46	41° 11.16′	113° 10.03′	11.0	1.5	9	115	14	0.05
87	1026	1145 1.61	41° 11.64′	113° 10.46′	10.5	1.6	9	133	9	0.03
87	1026	1908 27.88	41° 10.63′	113° 11.08′	12.4	1.8	14	113	10	0.18
87	1026	1931 8.58	41° 12.88′	113° 11.12′	10.0	1.6	11	131	9	0.24
87	1026	2007 13.48	41° 11.52′	113° 10.45′	8.6	1.5	8	132	9	0.02
87	1027	223 37.06	41° 11.31′	113° 10.17′	9.5	1.7	10	116	9	0.20
87	1027	708 44.52	41° 11.68′	113° 10.66′	10.1	1.5	9	133	9	0.18
87	1028	434 28.58	41° 11.85′	113° 10.58′	8.9	1.2	10	135	9	0.06
87	1028	1730 16.06	41° 12.46′	113° 11.05′	10.7	1.9W	14	127	9	0.16
87	1028	2303 52.22	41° 11.30′	113° 10.13′	9.8	2.2W	14	116	9	0.16
87	1029	251 50.19	41° 11.35′	113° 10.79′	11.0	0.9	11	117	13	0.13
87	1029	342 21.56	41° 11.58′	113° 10.86′	10.6	1.7	14	119	3	0.12
87	1029	1412 18.39	41° 11.85′	113° 10.13′	10.4	1.9W	12	134	4	0.05

Lakeside, Utah, Earthquake Sequence

yr	*date*	*origin time*	*latitude*	*longitude*	*depth*	*mag*	*no*	*gap*	*dmin*	*rms*
87	1029	1843 59.71	41° 11.48′	113° 10.45′	10.5	1.2	6	154	3	0.03
87	1029	2120 50.79	41° 11.86′	113° 10.85′	8.7	1.0	6	163	3	0.16
87	1030	807 36.07	41° 10.93′	113° 10.72′	11.6	1.6	15	113	3	0.21
87	1030	1017 50.83	41° 11.33′	113° 9.89′	9.9	1.6	13	116	4	0.16
87	1030	1225 39.44	41° 11.39′	113° 10.30′	9.9	1.4	7	152	3	0.05
87	1030	1846 25.90	41° 11.75′	113° 10.06′	12.7	0.9	5	157	4	0.07
87	1030	1906 33.94	41° 11.05′	113° 10.68′	12.0	1.6	15	114	3	0.13
87	1031	211 56.10	41° 11.55′	113° 10.32′	10.2	1.2	6	155	3	0.01
87	1031	354 55.90	41° 12.14′	113° 11.64′	7.3	1.6	8	139	3	0.04
87	1031	358 27.88	41° 11.47′	113° 11.67′	1.3*	1.3	6	158	10	0.12
87	1031	722 2.47	41° 11.26′	113° 11.45′	11.2	1.5	13	117	2	0.14
87	1101	835 51.52	41° 12.20′	113° 11.74′	7.2	1.4	7	139	3	0.04
87	1101	1037 20.41	41° 11.87′	113° 10.41′	10.6	0.6	6	161	3	0.02
87	1101	1431 23.97	41° 12.10′	113° 10.68′	10.5	1.4	9	137	3	0.13
87	1101	2132 4.93	41° 13.05′	113° 11.93′	9.1	1.5	12	148	4	0.09
87	1102	1217 4.81	41° 11.99′	113° 10.85′	8.6	0.9	6	166	3	0.02
87	1102	1225 31.30	41° 12.27′	113° 10.30′	12.1	0.9	6	168	4	0.05
87	1103	600 57.14	41° 11.45′	113° 10.82′	7.7	1.3	10	131	3	0.14
87	1103	846 5.89	41° 12.00′	113° 10.84′	8.5	1.2	7	137	3	0.02
87	1103	1138 13.15	41° 11.31′	113° 10.49′	10.2	0.9	6	151	3	0.10
87	1103	1201 32.05	41° 11.64′	113° 10.44′	8.9	0.8	6	157	3	0.04
87	1103	1658 19.37	41° 11.72′	113° 10.55′	9.5	1.5	10	120	3	0.07
87	1103	1834 6.31	41° 11.80′	113° 10.26′	8.4	1.6	9	134	4	0.04
87	1103	2236 32.59	41° 11.74′	113° 11.65′	6.9	1.1	8	122	2	0.05
87	1105	1035 8.53	41° 12.35′	113° 10.33′	9.1	1.1	7	125	4	0.04
87	1106	302 40.19	41° 12.26′	113° 10.91′	10.7	2.0W	10	125	3	0.09
87	1106	411 16.12	41° 12.00′	113° 10.52′	10.5	0.8	7	122	3	0.09
87	1106	503 23.44	41° 10.87′	113° 10.41′	7.5	0.7	6	114	3	0.06
87	1106	1259 10.83	41° 11.67′	113° 10.89′	9.2	0.6	7	120	3	0.09
87	1106	1259 21.60	41° 12.21′	113° 11.41′	10.1	1.4	12	126	3	0.15
87	1106	1452 13.82	41° 12.73′	113° 11.44′	7.9	0.9	7	131	4	0.17
87	1106	2108 25.94	41° 11.73′	113° 10.79′	10.3	0.9	7	120	3	0.05
87	1107	1752 34.04	41° 13.25′	113° 11.94′	10.2	2.7W	12	137	4	0.12
87	1108	103 52.55	41° 12.97′	113° 11.87′	9.8	2.0	12	133	4	0.10
87	1108	2308 3.16	41° 11.69′	113° 10.63′	10.8	2.4W	16	120	3	0.12
87	1109	934 28.98	41° 11.64′	113° 10.18′	10.6	0.7	7	118	4	0.10
87	1110	425 19.66	41° 12.39′	113° 10.43′	9.0	1.8	8	126	4	0.04
87	1110	758 37.85	41° 11.25′	113° 10.65′	8.9	1.0	7	115	3	0.07
87	1111	1422 9.09	41° 11.87′	113° 10.76′	9.5	1.5	10	122	3	0.11
87	1112	1029 33.72	41° 11.90′	113° 10.76′	10.0	2.0	15	122	3	0.15
87	1112	2216 35.96	41° 10.91′	113° 9.97′	8.2	1.0	7	113	4	0.05
87	1114	1244 35.34	41° 11.45′	113° 10.53′	8.9	1.5	6	117	3	0.06
87	1114	1619 32.58	41° 12.51′	113° 11.60′	9.6	1.1	7	129	3	0.15
87	1115	953 37.58	41° 13.61′	113° 12.12′	8.6	1.1	6	141	5	0.21
87	1116	2208 45.35	41° 12.60′	113° 10.92′	9.2	0.3	8	129	4	0.10

Lakeside, Utah, Earthquake Sequence

yr	*date*	*origin time*	*latitude*	*longitude*	*depth*	*mag*	*no*	*gap*	*dmin*	*rms*
87	1116	2208 53.32	41° 11.25′	113° 7.54′	1.8	0.9	7	112	6	0.37
87	1117	1620 45.04	41° 11.05′	113° 10.57′	10.0	2.8W	15	114	3	0.11
87	1117	1635 19.37	41° 11.48′	113° 10.47′	9.0	1.0	6	117	3	0.06
87	1117	1826 32.97	41° 11.00′	113° 10.34′	9.4	0.9	6	144	3	0.01
87	1118	34 55.31	41° 11.55′	113° 11.82′	8.1	0.9	7	160	2	0.04
87	1121	2222 10.80	41° 11.28′	113° 11.20′	7.2	1.1	7	117	2	0.10
87	1121	2343 37.19	41° 11.67′	113° 10.98′	9.5	1.2	7	120	3	0.13
87	1123	1104 22.25	41° 11.72′	113° 11.83′	7.3	1.6	13	122	2	0.09
87	1127	943 46.84	41° 12.35′	113° 11.79′	6.6	1.6	9	128	3	0.09
87	1127	1445 42.86	41° 12.80′	113° 11.70′	10.6	1.6	12	131	4	0.09
87	1127	1533 27.27	41° 11.78′	113° 10.67′	10.5	1.3	7	121	3	0.12
87	1127	2205 43.48	41° 11.34′	113° 10.08′	9.9	1.0	6	116	4	0.04
87	1129	1248 53.04	41° 11.19′	113° 10.88′	7.2	0.9	7	116	2	0.09
87	1201	307 33.13	41° 11.44′	113° 10.44′	9.8	0.9	5	117	3	0.01
87	1203	28 35.16	41° 11.14′	113° 10.47′	9.6	1.3	12	115	13	0.09
87	1211	439 15.60	41° 11.99′	113° 10.35′	11.1	1.1	5	122	4	0.02
87	1211	1305 32.51	41° 12.73′	113° 12.00′	9.4	2.1	15	132	4	0.12
87	1214	1620 55.07	41° 11.17′	113° 10.40′	10.8	1.0	7	129	3	0.09
87	1214	1639 9.47	41° 11.50′	113° 9.85′	11.0	1.4	7	117	4	0.05
87	1215	451 17.74	41° 13.71′	113° 12.04′	9.2	0.8	5	142	5	0.03
87	1215	1800 10.65	41° 11.76′	113° 9.22′	7.8	1.6	12	118	5	0.10
87	1218	833 39.97	41° 12.13′	113° 10.93′	9.1	1.1	7	124	3	0.12
87	1219	2157 43.58	41° 11.52′	113° 10.38′	9.9	2.2	16	118	3	0.11
87	1220	1221 29.55	41° 10.98′	113° 9.30′	7.0	1.0	6	112	4	0.13
87	1222	1255 20.50	41° 11.30′	113° 10.67′	10.5	1.6	12	117	3	0.07
87	1222	1757 59.91	41° 11.34′	113° 10.55′	9.3	1.3	8	116	3	0.07
87	1224	2023 41.52	41° 12.89′	113° 11.76′	6.8	1.3	9	133	4	0.12
88	102	1856 49.51	41° 11.45′	113° 10.17′	10.3	1.3	9	117	3	0.04
88	106	1904 24.55	41° 11.80′	113° 10.86′	9.8	1.2	8	121	3	0.09
88	106	2110 10.28	41° 11.60′	113° 9.85′	9.4	1.3	11	118	4	0.18
88	107	411 14.57	41° 13.14′	113° 12.27′	7.7	1.1	9	137	4	0.12
88	108	136 55.32	41° 11.58′	113° 10.42′	9.7	1.5	8	118	3	0.05
88	108	2132 31.53	41° 13.39′	113° 12.49′	7.2	1.8	9	140	5	0.18
88	113	2024 16.85	41° 11.06′	113° 10.79′	7.9	0.7	6	114	2	0.07
88	122	1933 20.41	41° 11.16′	113° 10.24′	9.6	1.1	8	115	3	0.07
88	127	2322 17.04	41° 12.84′	113° 11.14′	9.4	1.9	11	131	4	0.06
88	127	2335 0.04	41° 12.66′	113° 11.02′	8.6	1.0	6	129	4	0.02
88	127	2339 26.53	41° 13.01′	113° 11.28′	9.5	2.0W	16	133	4	0.11
88	128	1345 58.51	41° 11.59′	113° 11.57′	11.5	1.4	7	121	2	0.10
88	129	58 33.59	41° 12.22′	113° 10.73′	11.4	2.8	15	124	4	0.10
88	129	109 54.94	41° 12.37′	113° 10.62′	11.1	2.0	15	126	4	0.14
88	129	1101 6.59	41° 12.23′	113° 11.13′	10.9	1.4	10	126	3	0.07
88	130	144 33.53	41° 11.97′	113° 11.37′	11.0	1.9	10	124	3	0.10
88	130	537 13.04	41° 12.22′	113° 10.86′	11.3	3.1W	15	125	3	0.12
88	130	539 44.15	41° 12.18′	113° 11.13′	10.8	2.2	15	124	3	0.05

Lakeside, Utah, Earthquake Sequence

yr	*date*	*origin time*	*latitude*	*longitude*	*depth*	*mag*	*no*	*gap*	*dmin*	*rms*
88	130	607 40.50	41° 11.54′	113° 11.14′	9.3	1.4	6	163	2	0.14
88	130	902 38.66	41° 12.17′	113° 10.73′	11.2	2.9W	15	124	3	0.14
88	130	917 29.91	41° 11.69′	113° 11.21′	11.0	1.5	12	120	2	0.10
88	130	1440 18.81	41° 12.71′	113° 10.74′	9.7	1.6	12	128	4	0.06
88	203	610 39.73	41° 11.88′	113° 10.53′	10.3	1.1	8	134	3	0.15
88	203	2312 33.37	41° 11.70′	113° 11.52′	10.0	1.2	9	121	2	0.06
88	205	227 13.80	41° 12.08′	113° 11.02′	11.5	1.3	9	123	3	0.09
88	205	836 31.01	41° 12.72′	113° 11.16′	9.8	1.8	8	130	4	0.08
88	205	1614 3.30	41° 12.53′	113° 11.98′	11.3	2.9	11	131	3	0.16
88	208	2354 1.47	41° 12.07′	113° 11.19′	10.9	1.8	9	125	3	0.05
88	210	1007 31.44	41° 12.97′	113° 12.05′	8.5	2.2W	12	135	4	0.10
88	210	1755 55.08	41° 12.98′	113° 12.15′	8.0	1.3	11	134	4	0.09
88	211	1544 15.42	41° 12.69′	113° 11.89′	7.6	1.5	7	132	3	0.04
88	211	2127 35.30	41° 12.45′	113° 12.04′	7.2	1.3	8	130	3	0.10
88	211	2350 18.62	41° 12.41′	113° 11.75′	7.5	1.0	6	128	3	0.04
88	212	1937 28.15	41° 13.67′	113° 11.73′	15.2	0.8	7	140	5	0.15
88	212	2323 49.28	41° 12.37′	113° 11.91′	7.5	1.3	7	128	3	0.06
88	214	1236 41.87	41° 12.66′	113° 11.91′	7.9	1.3	6	132	3	0.06
88	217	426 49.35	41° 11.02′	113° 10.10′	8.6	0.7	5	114	3	0.07
88	220	454 36.30	41° 12.21′	113° 11.32′	10.4	1.6	12	126	3	0.05
88	220	510 36.17	41° 11.45′	113° 11.35′	9.8	0.9	5	118	2	0.04
88	220	1524 12.08	41° 12.19′	113° 11.74′	7.4	1.1	7	126	3	0.04
88	220	1524 43.73	41° 12.22′	113° 12.19′	8.9	2.0	16	127	3	0.11
88	221	1622 38.16	41° 11.10′	113° 10.02′	9.0	0.9	7	114	4	0.07
88	221	1931 41.67	41° 11.51′	113° 10.26′	10.1	1.3	8	117	3	0.08
88	222	0 48.31	41° 12.57′	113° 11.87′	7.5	1.8	9	131	3	0.11
88	223	1318 44.38	41° 11.05′	113° 10.07′	8.3	0.7	5	114	3	0.06
88	302	203 20.75	41° 12.06′	113° 10.11′	11.2	2.8W	16	122	4	0.07
88	302	211 6.23	41° 11.68′	113° 10.29′	10.6	0.9	8	119	3	0.04
88	302	229 27.40	41° 12.06′	113° 10.53′	10.8	1.2	8	123	4	0.13
88	304	1123 28.35	41° 12.32′	113° 11.49′	6.7	0.8	5	127	3	0.02
88	305	1221 1.40	41° 11.30′	113° 10.23′	9.1	0.9	5	116	3	0.03
88	306	701 1.49	41° 10.72′	113° 9.79′	8.9	0.6	5	116	4	0.03
88	308	1430 59.65	41° 11.78′	113° 11.51′	5.9	1.7	5	122	2	0.04
88	308	1509 14.03	41° 11.92′	113° 11.48′	5.5	1.1	5	123	2	0.05
88	308	1518 35.01	41° 12.07′	113° 11.37′	6.7	0.6	5	125	3	0.02
88	315	440 30.37	41° 12.13′	113° 11.39′	7.1	1.2	9	125	3	0.06
88	320	912 58.03	41° 10.91′	113° 10.16′	8.5	0.6	5	113	3	0.06
88	321	724 58.80	41° 13.28′	113° 12.66′	10.7	1.3	13	140	4	0.14
88	321	2225 54.10	41° 11.44′	113° 11.12′	9.8	1.2	6	118	2	0.04
88	326	100 11.61	41° 11.91′	113° 11.43′	9.9	1.2	7	123	2	0.15
88	326	2034 47.00	41° 11.28′	113° 10.46′	7.6	0.9	6	116	3	0.13

number of earthquakes = 222

* indicates poor depth control
W indicates Wood-Anderson data used for magnitude calculation

2. LEFT-LATERAL SHEAR BENEATH THE NORTHWESTERN COLORADO PLATEAU: THE 1988 SAN RAFAEL SWELL AND 1989 SOUTHERN WASATCH PLATEAU EARTHQUAKES

ABSTRACT

Two moderate earthquakes that occurred in the northwestern Colorado Plateau in central Utah on August 14, 1988, and January 30, 1989 (UTC), provide important new information on earthquake hazards, contemporary deformation, and the state of stress at mid-crustal depths in this region. The first was an M_L 5.3 shock on the northwest edge of the San Rafael swell, a broad Laramide anticlinal upwarp. The second was an M_L 5.4 earthquake located 70 km WSW of the first beneath the southern Wasatch Plateau, which rims the northwestern Colorado Plateau and forms part of a transition to the Basin and Range Province to the west. These earthquakes were the largest to occur within the Colorado Plateau since an M 5½ event near the Utah-Arizona border in 1959. The San Rafael swell earthquake occurred in an area without mapped active surface faults and where historical earthquake activity has been minimal, suggesting that moderate but potentially damaging earthquakes ($5 \leq M_L \leq 6½$) could occur anywhere in the northwestern Colorado Plateau.

Following each main shock, we supplemented the University of Utah's regional seismic network with 4 to 5 portable seismographs and later 2 to 4 telemetered stations in the epicentral area. Each earthquake sequence was relocated with a velocity model based on refraction studies and sonic logs of nearby oil wells; station delays were derived from well-located aftershocks. For the San Rafael swell sequence, the 68 best-located hypocenters define a 5-km-long aftershock zone extending in depth from 11 to 18 km and dipping 60°±5° ESE. P-wave focal mechanisms for the main shock and largest aftershock (M_L 4.4) both show oblique normal faulting, with the left-lateral nodal plane dipping E to SE in a direction similar to the dip of the aftershock zone. For the southern Wasatch Plateau sequence, the 33 best-located hypocenters define an 8-km-long aftershock zone between 21 and 25 km depth, striking NNE and dipping 90°±10°. P-wave focal mechanisms for the main shock and largest aftershock (M_L 4.2) both show strike-slip faulting with the left-lateral nodal plane striking NNE, parallel to the trend of the aftershock zone.

The T axes for all four focal mechanisms are oriented between E-W and ENE-WSW, intermediate between the ESE-WNW extension direction of the Basin and Range–Colorado Plateau transition zone and the NE-SW extension direction of the interior of the Colorado Plateau. Our data imply that both main shocks were caused by buried left-lateral or oblique left-lateral and normal slip on Precambrian basement faults striking NNE to NE. Active NNE left-lateral shear at depth may explain some enigmatic aspects of the surficial tectonics—including the right-stepping, en-echelon pattern of young, N-S-trending graben on the Wasatch Plateau.

INTRODUCTION

This report is about two moderate-sized earthquakes that occurred recently in central Utah beneath the northwestern part of the Colorado Plateau: the M_L (local magnitude) 5.3 San Rafael swell earthquake on August 14, 1988, and the M_L 5.4 southern Wasatch Plateau earthquake on January 30, 1989. These two earthquakes occurred 5½ months and 70 km apart. They were the largest earthquakes to occur in the Colorado Plateau since a magnitude 5½ event near the Utah-Arizona border in 1959 (Figure 2-1). The 1988 and 1989 earthquakes provide an important insight into the contemporary tectonics of the northwestern Colorado Plateau.

Both earthquakes occurred in unpopulated areas. The closest town to the San Rafael swell earthquake was Castle Dale, 18 km NW of the epicenter, and the closest town to the southern Wasatch Plateau earthquake was Salina, 25 km NW of the epicenter. Both earthquakes were felt strongly in small towns in the vicinity with MMI (Modified Mercalli intensity) V to VI, where they caused some minor damage (U.S. Geological Survey, 1988, 1989; Case, 1988; Tingey and May, 1988). The felt areas of both earthquakes extended throughout much of Utah and into neighboring states (U.S. Geological Survey, 1988, 1989). The San Rafael swell earthquake triggered numerous rock falls within 40 km of the epicenter, possibly numbering in the hundreds, and isolated rock falls at distances of up to at least 113 km from the epicenter (Case, 1988). The southern Wasatch Plateau earthquake also triggered some rock falls, but far fewer than did the San Rafael swell earthquake (W.F. Case, personal communication, 1991).

This report presents the results of aftershock studies carried out following both earthquakes, together with focal mechanisms for the main shock and the largest aftershock of each sequence. We were able to identify the fault planes for both main shocks based on their aftershock distributions. Our main conclusion based on this work is that both earthquakes involved left-lateral or oblique left-lateral and normal slip on NNE- to NE-striking faults at mid-crustal depths. This observation suggests the possibility of large-scale left-lateral shear at depth beneath the northwestern Colorado Plateau.

GEOLOGICAL SETTING

Figures 2-2 and 2-3 depict the generalized geology of the region where the 1988 and 1989 earthquakes occurred. The area shown encompasses the transition between the Basin and Range Province on the west and the Colorado Plateau on the east. The 1988 earthquake occurred within the Colorado Plateau province beneath the northwest edge of the San Rafael swell, a broad kidney-shaped anticlinal upwarp with a monoclinal flexure on its southeastern flank (Stokes, 1986, p. 240). The San Rafael swell is underlain by sedimentary rocks ranging in age from Paleozoic at the center of the uplift to middle Cretaceous around the periphery (Figures 2-2, 2-3). The 1989 earthquake occurred beneath the southern Wasatch Plateau (WP, Figure 2-2), one of the high plateaus along the northwest edge of the Colorado Plateau that

Seismicity of the Colorado Plateau

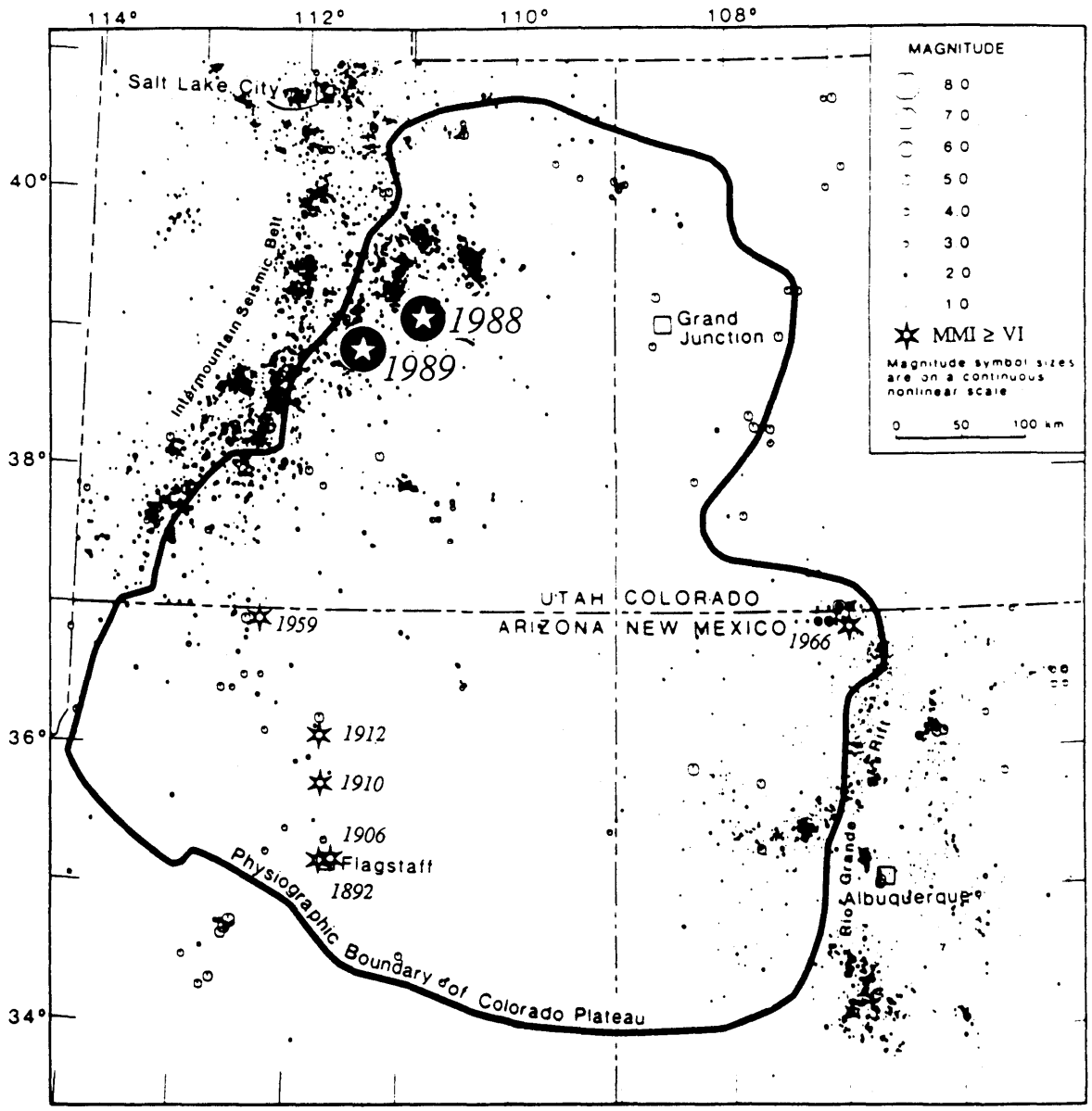

(After Humphrey and Wong, 1983)

Fig. 2-1. Locations (bold circumscribed stars) of the August 14, 1988, San Rafael swell earthquake (M_L 5.3) and the January 30, 1989, southern Wasatch Plateau earthquake (M_L 5.4), superimposed on a regional seismicity map for 1962-1981 taken from Humphrey and Wong (1983) and Wong and Humphrey (1989).

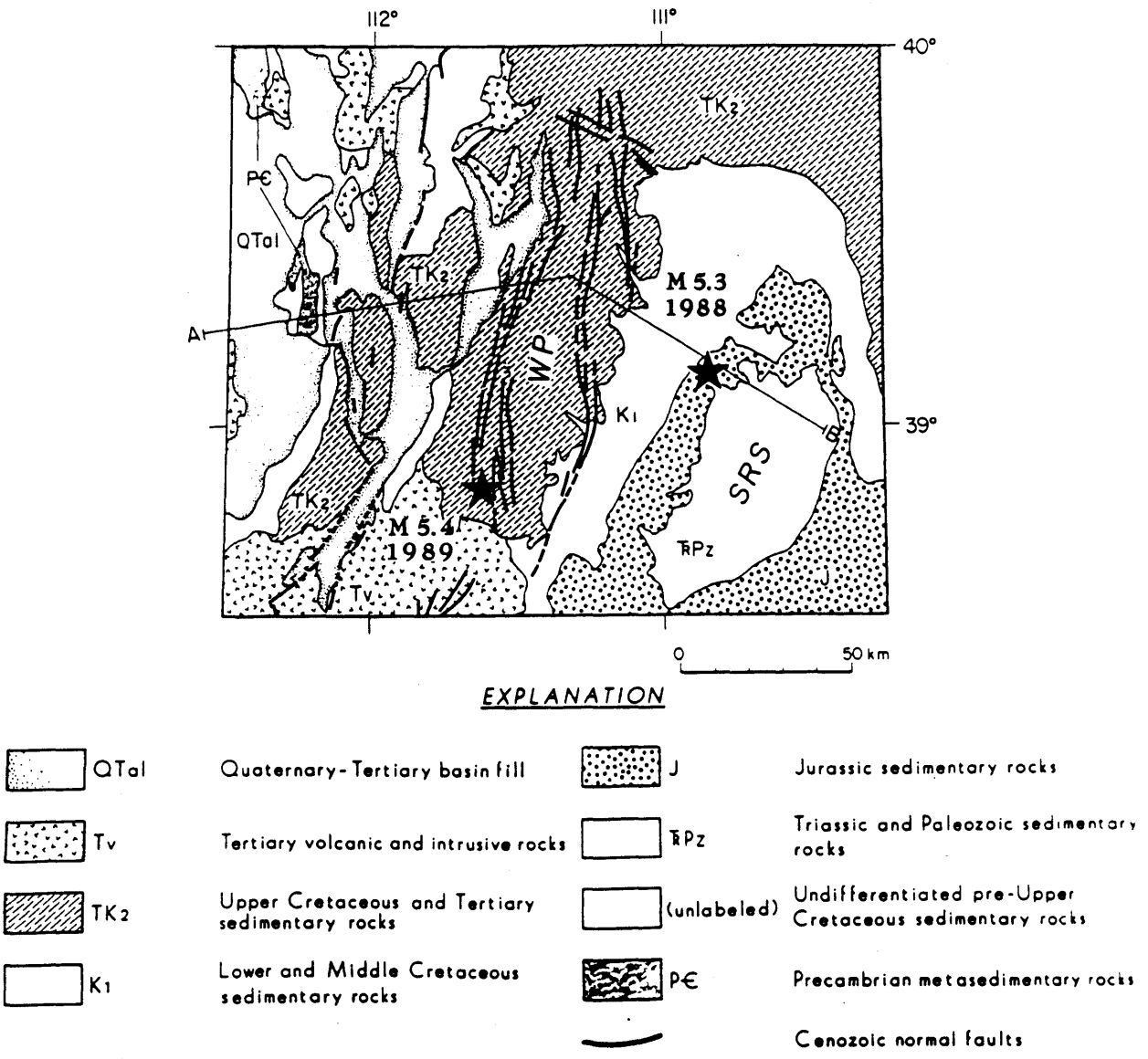

Fig. 2-2. Generalized geologic map of a portion of central Utah which includes the epicenters of the 1988 San Rafael swell and 1989 southern Wasatch Plateau earthquakes. SRS is the San Rafael swell and WP is the Wasatch Plateau. The map is generalized from the geologic map of Utah, compiled by Hintze (1980).

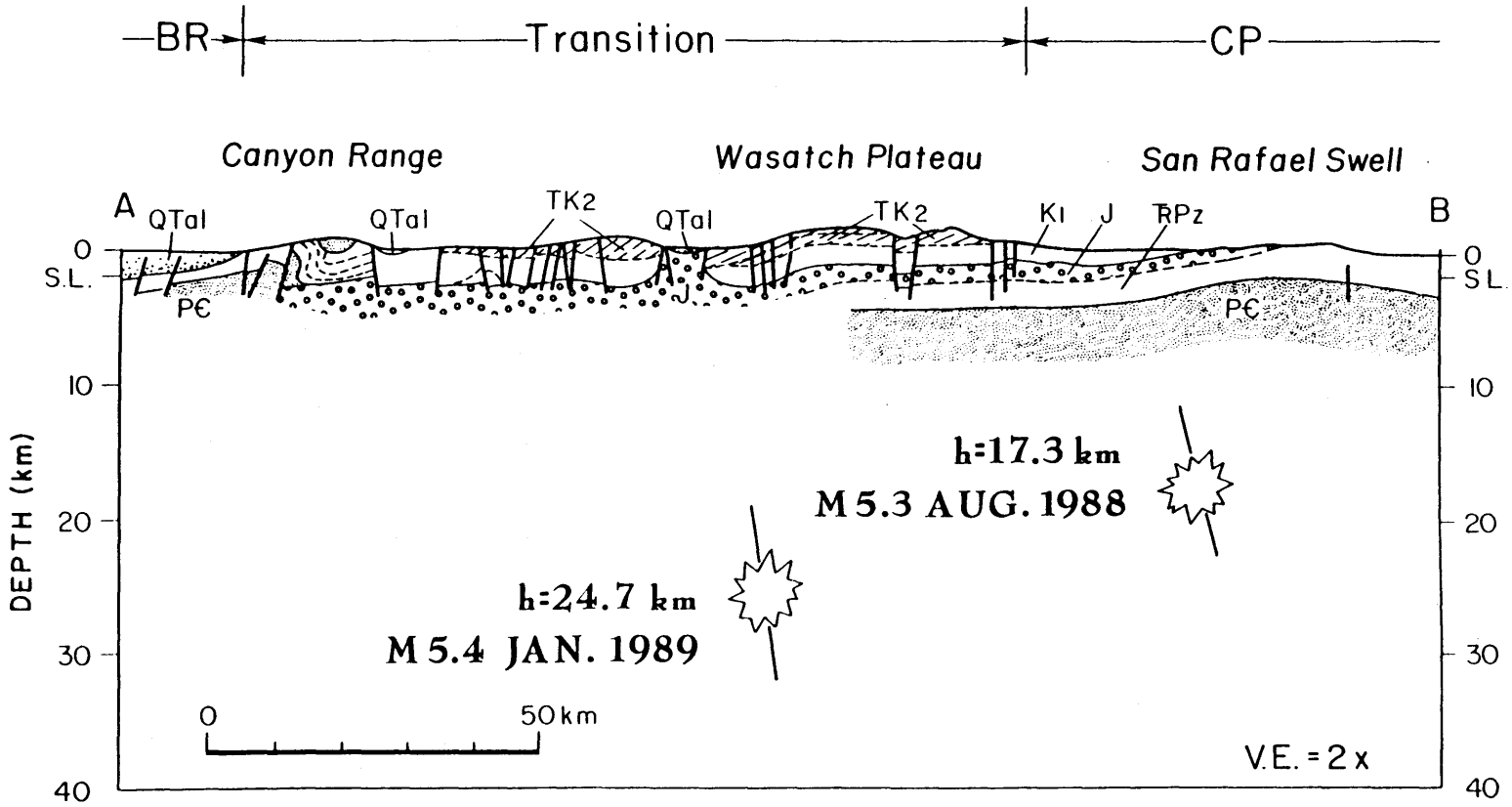

Fig. 2-3. Generalized geologic cross section, with a factor of two vertical exaggeration, along the line A-B shown on Figure 2-2. Starbursts indicate the hypocenters of the San Rafael swell and southern Wasatch Plateau earthquakes, projected onto the cross section together with the orientations of the inferred fault planes. BR is the Basin and Range Province and CP is the Colorado Plateau. This cross section is generalized from one that accompanies the geologic map of Utah (Hintze, 1980). Symbols and patterns are as in Figure 2-2.

form part of the Basin and Range–Colorado Plateau transition zone. This plateau is composed of relatively flat-lying sedimentary rocks of Upper Cretaceous and Tertiary age. It is bounded on the east by an erosional escarpment and on the west by the Wasatch Monocline (Figure 2-3; Stokes, 1986, p. 247).

The western part of the region shown in Figure 2-2 was subjected to considerable E-W upper crustal shortening from 105 to 75 m.y. ago during the Cretaceous Sevier orogeny. This crustal shortening was accommodated by eastward-directed imbricate thrust faulting and associated folding, which affected Paleozoic and Mesozoic sedimentary rocks but did not involve the underlying Precambrian basement to any great extent (Stokes, 1986, pp. 144-145; Hintze, 1988, pp. 99-100). Recent surface and subsurface data show that Sevier-age thrust faulting extends beneath the Wasatch Plateau (Standlee, 1982; Lawton, 1985; Allmendinger et al., 1986) and into the northwest San Rafael swell at least as far east as Cedar Mountain, 20 km ENE of the epicenter of the 1988 earthquake (Neuhauser, 1988). The San Rafael swell itself formed between 65 and 60 million years ago during a Paleocene episode of the Laramide orogeny, which in central Utah was characterized by compressional deformation of a different nature than that of the Sevier orogeny (Stokes, 1986, p. 148; Hintze, 1988, pp. 100-101). The San Rafael swell and other asymmetrical anticlines of Laramide age in the sedimentary rocks of the Colorado plateau are generally regarded as the surface expressions of reverse displacements along steeply-dipping faults in the underlying Precambrian basement (Davis, 1978; Stokes, 1986, p. 148). The epeirogenic uplift of the Colorado Plateau took place during the late Cenozoic, much later than the more localized uplift of the San Rafael swell. Rowley et al. (1978, 1979) infer from the areal distribution of ash flow tuffs in southwestern Utah that the uplift of the Colorado Plateau relative to the Basin and Range province in this region began some 25 to 30 m.y. ago during the late Oligocene. Extension and normal faulting in the western Utah portion of the Basin and Range Province also began at about this same time or earlier, but the main phase of Basin and Range faulting in this area did not get underway until the early or middle Miocene, 15-21 m.y. ago (Rowley et al., 1978; Hintze, 1988, pp. 74-75).

The heavy lines on Figure 2-2 indicate the surface traces of Cenozoic normal faults. The fault in the northwest portion of the map is the Wasatch fault, a major active normal fault which marks the classical physiographic boundary between the Basin and Range Province and the Colorado Plateau and Middle Rocky Mountains. This boundary is transitional in the sense that some of the characteristics of the Basin and Range Province extend 50 to 100 km eastward into the Colorado Plateau, including high heat flow and normal faulting (Best and Hamblin, 1978; Keller et al., 1979; Thompson and Zoback, 1979; Bodell and Chapman, 1982; Arabasz and Julander, 1986; Powell and Chapman, 1990). For example, there are post-Eocene normal faults in the Wasatch Plateau (Spieker, 1949), some of which show late Pleistocene and possibly Holocene movement (Foley et al., 1986). These normal faults form a right-stepping, en-echelon pattern of N-S-striking graben (Figure 2-2). COCORP seismic reflection data published by Allmendinger et al. (1986) suggest that these young normal faults might not cut into the Precambrian basement, but may instead merge with a low-angle thrust fault in the Jurassic

section which has been reactivated as a normal fault. However, Allmendinger et al. (1986, p. 261) consider this interpretation to be "somewhat tenuous given the resolution of the seismic data and the small displacements on most of the normal faults."

There are no Quaternary faults mapped within the San Rafael swell but such faults, if present, may be difficult to recognize due to the paucity of Quaternary deposits. The Paleozoic and Mesozoic sedimentary cover rocks of the swell are cut by NW- and NE-striking faults, some of which are inferred to extend into the Precambrian basement (see Hintze, 1980).

PRIOR SEISMICITY

Overview of Regional Seismicity

Most of the seismicity in the vicinity of the Colorado Plateau is concentrated around its margins (Figure 2-1). This seismicity occurs principally within the Intermountain Seismic Belt in Utah on the northwest boundary of the province and along the Rio Grande Rift in New Mexico on the southeast boundary. Figure 2-4 provides a more detailed view of the seismicity in the region surrounding the 1988 and 1989 earthquakes. The circles on this map show epicenters of earthquakes of $M \geq 2$ from July 1962, when the University of Utah regional seismic network first began operating, through 1990. The stars show epicenters of $M \geq 5$ earthquakes from 1850 through 1990. A prominent feature of the 1962 to 1990 seismicity in this area is an arcuate band of small earthquakes which follows the eastern edge of the Wasatch Plateau (the northeastern edge of the transition zone, TZ on Figure 2-4) northward to 39° 45′ N, and then trends eastward and southward along a southwest-facing escarpment known as the Book Cliffs. Earthquakes within this arcuate band of activity are apparently triggered by active coal mining in this area and have very shallow focal depths, almost exclusively less than 4 km (Dunrud et al., 1973; Smith et al., 1974; McKee, 1982; Arabasz and Julander, 1986; Williams and Arabasz, 1989; Wong et al., 1989). The intense cluster of activity centered 30 km NW of the epicenter of the San Rafael swell earthquake (Figure 2-4) is associated with large-scale coal-mining beneath East Mountain, a part of the Wasatch Plateau (McKee, 1982; Arabasz and Julander, 1986; Williams and Arabasz, 1989). Seismicity within the Basin and Range–Colorado Plateau transition zone in the western half of Figure 2-4 is shallow (depth < 15-20 km), diffuse, and not easily correlated with mapped surface faulting (McKee and Arabasz, 1982; Arabasz and Julander, 1986; Arabasz et al., 1987).

The 1988 San Rafael swell earthquake occurred in an area that had very little recorded seismicity prior to 1988. In the portion of the Colorado Plateau within 100 km of the San Rafael swell earthquake, the two largest historical earthquakes both had a maximum Modified Mercalli Intensity of V, which converts to an estimated magnitude of 4.3. They occurred in 1953 at 39° 0′ N 110° 10′ W, and in 1961 at 39° 36′ N 110° 12′ W (see Arabasz et al., 1979). Instrumental monitoring by the University of Utah detected only a few scattered earthquakes from 1962 through 1987 in the area of the San Rafael swell (Figure 2-4). The University of

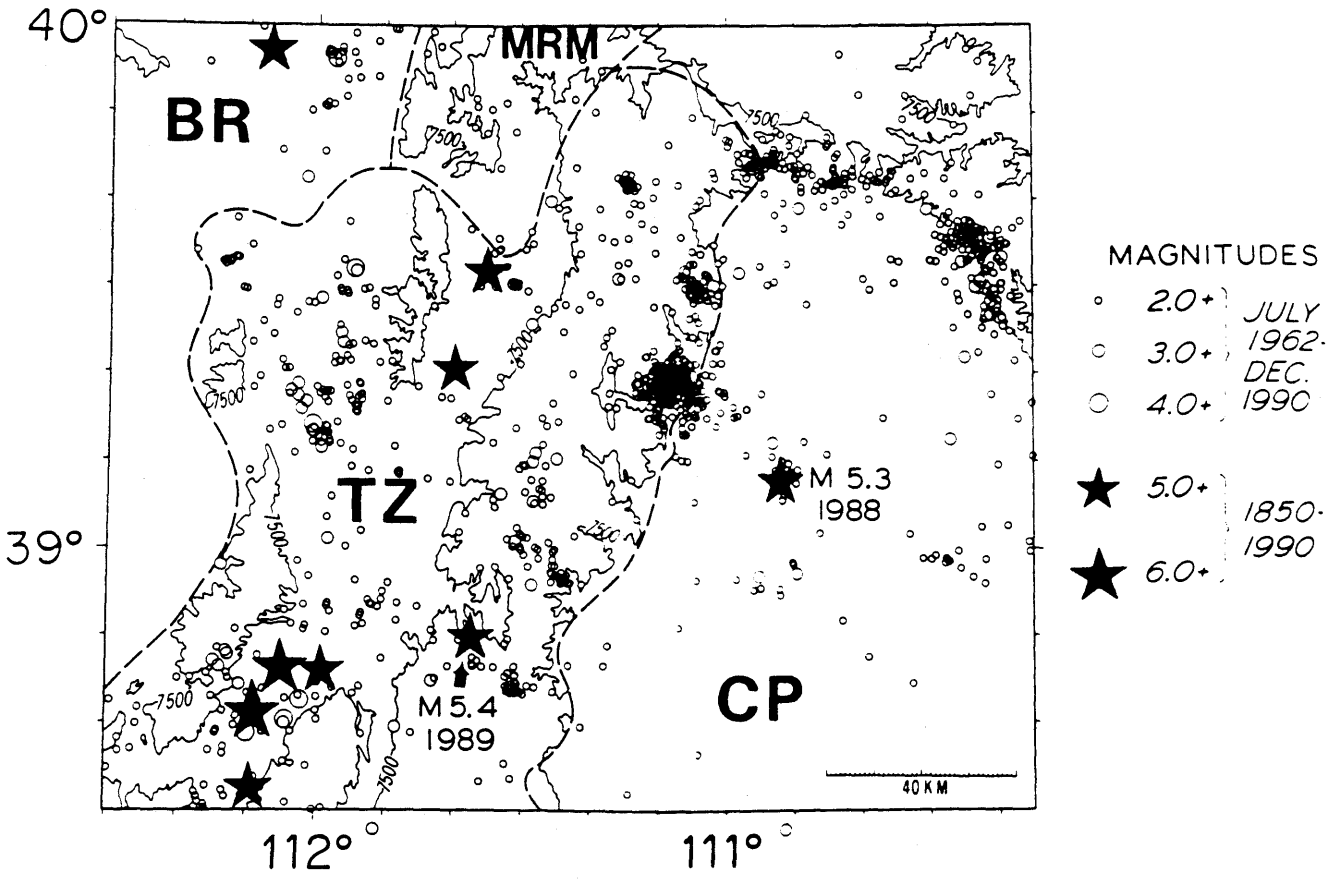

Fig. 2-4. Epicenter map of earthquakes along the northwestern margin of the Colorado Plateau from 1962 through 1990. The thin solid line is the 7500 foot elevation contour. The dashed line outlines the transition zone (TZ) between the Basin and Range Province (BR) and the Colorado Plateau (CP). MRM is the Middle Rocky Mountains physiographic province. The M 6.0+ earthquakes in the southwestern corner of the map are the M 6 ½ earthquake near Richfield, Utah, in 1901 and the two M 6 ¼ earthquakes near Elsinore, Utah, in 1921. Epicentral data are from the University of Utah Seismograph Stations earthquake catalog (see Arabasz et al., 1979, 1987). Physiographic province boundaries are from Stokes (1986).

Utah earthquake catalog lists two earthquakes of $M_L \geq 3.0$ within 25 km of the epicenter of the 1988 main shock during this time period: a shock of M_L 3.1 in 1962 located 8 km to the north of the 1988 event, and a shock of M_L 3.0 in 1964 located 21 km to the south of it (Figure 2-4). The locations of these two earthquakes are not of very high quality, however, owing to the sparseness of the University's regional seismic network at the time, and could easily be in error by several kilometers or more.

The 1989 southern Wasatch Plateau earthquake occurred on the eastern edge of a seismically active zone that includes some of the largest historical earthquakes in Utah: a magnitude 6½+ earthquake near the town of Richfield in 1901, and two magnitude 6¼ earthquakes near the town of Elsinore in 1921 (Pack, 1921; Williams and Tapper, 1953; Arabasz et al., 1979; Arabasz and Julander, 1986). Some of the seismicity between 20 and 30 km NE of the main shock epicenter (Figure 2-4) is probably related to coal mining, since there are working mines in this area. The earthquakes just to the east and south of the main shock epicenter do not appear to be associated with any mines.

Precursory Swarm and Foreshocks

The M_L 5.3 San Rafael swell earthquake was preceded by two notable bursts of seismic activity near its epicenter. The first was a swarm of seven earthquakes of $M_L \leq 2.5$ recorded by the University of Utah regional seismic network between January 14 and 20, 1988, seven months before the impending main shock. The second was a sequence of six foreshocks of magnitude 1.8 to 3.8 that occurred on August 14, 1988, during the 65 minutes prior to the occurrence of the main shock at 20:03 UTC (2:03 p.m. MDT) (Figure 2-5). The largest foreshock, of M_L 3.8 at 19:07 UTC, was felt (MMI IV) in nearby small towns (U.S. Geological Survey, 1988). During the seven-month period between the swarm and the foreshocks, the epicentral area did not experience any earthquakes large enough to be located with the University's seismic network.

Relocation of the January 1988 swarm events and the August 1988 foreshocks using the master event technique described below indicates that their epicenters are all within 2 km of the relocated main shock epicenter, and that their focal depths are generally comparable to that of the main shock. Taking into account the location errors, which are on the order of 1 or 2 km horizontally and at least 2 or 3 km vertically, the hypocenters of the foreshocks and the swarm events are not resolvably different from that of the main shock. Given this observation, and the previous low level of seismicity in the area, it seems highly probable that both the January 1988 swarm and the August foreshocks were closely related to the San Rafael swell main shock. Hence, we consider the January 1988 swarm to be a "precursory swarm," following the terminology of Evison (1977). Evison (1977) and Kanamori (1981), among others, have noted that numerous moderate- to large-size earthquakes throughout the world have been preceded by a pattern of activity similar to that which preceded the 1988 San Rafael swell earthquake: a precursory swarm followed by quiescence and then foreshocks. However, some

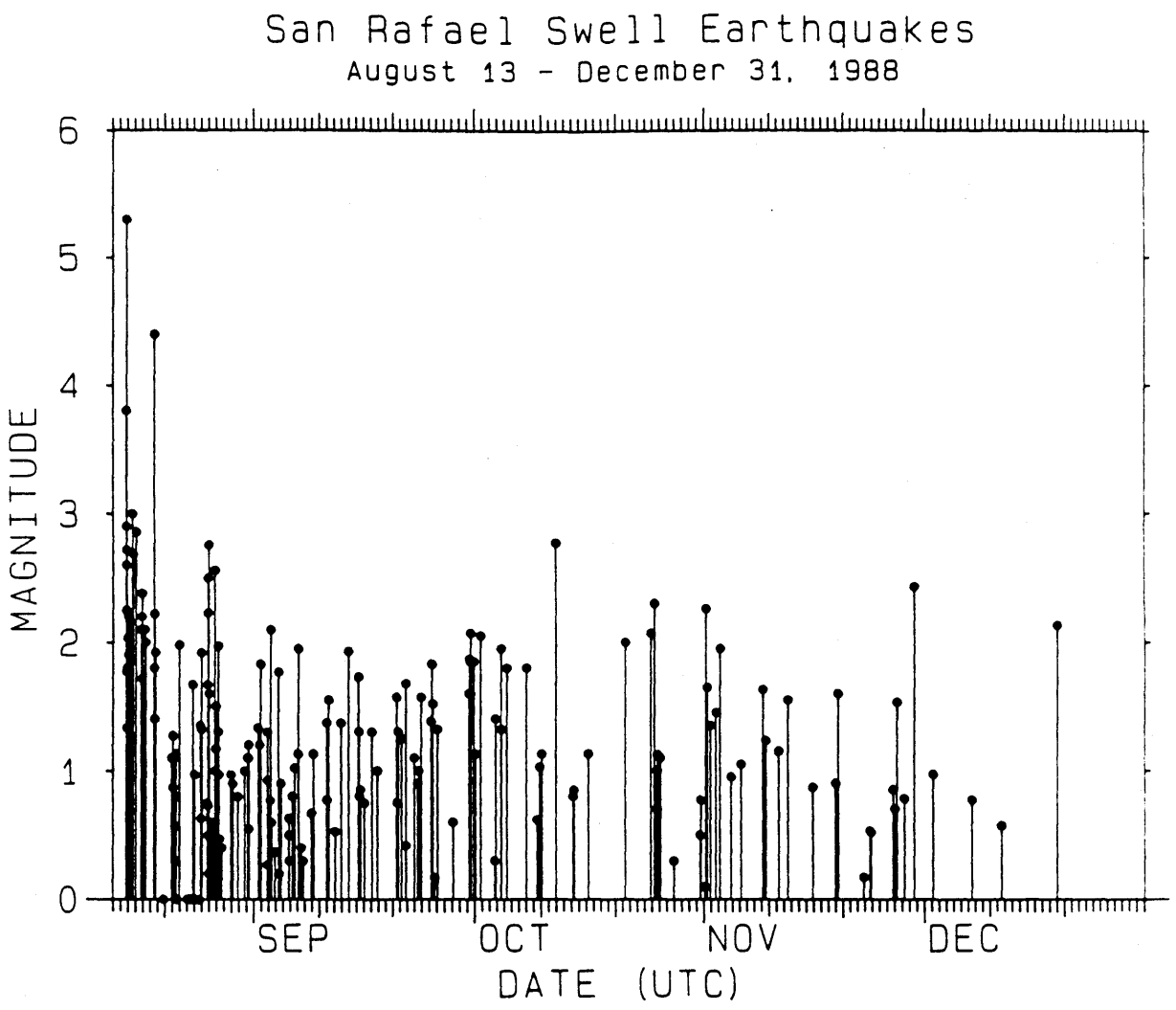

Fig. 2-5. Plot of magnitude versus time for the San Rafael swell earthquake sequence from August 13 through December 31, 1988. The plot includes all earthquakes in the University of Utah catalog within 15 km of the main shock epicenter. The sample is complete for at least $M_L \geq 2.0$. Small earthquakes recorded only on the portable seismographs were arbitrarily assigned a magnitude of 0.0, since we have not calibrated a magnitude scale for use with these instruments.

or all of the features of this typical precursory pattern fail to occur before most earthquakes, and when this pattern does occur, the details of it vary considerably from one earthquake sequence to another (Kanamori, 1981).

In contrast to the San Rafael swell earthquake, the southern Wasatch Plateau earthquake was not heralded by any unambiguous foreshocks or precursory swarms. During the two year period preceding the occurrence of the main shock at 04:06 UTC on January 30, 1989 (9:06 p.m. MST on January 29), the University of Utah network detected only a few scattered earthquakes within a 20 km radius of the main shock epicenter. The network recorded a single possible foreshock of magnitude 2.0 at 13:20 UTC on January 23, 1989 (Figure 2-6). The epicenter of the master-event relocation of this earthquake is 9 km E of the relocated main shock epicenter, in an area where there had been previous seismic activity since at least the mid 1970's. This event would qualify as a foreshock according to some definitions. However, it does not meet the criteria for "true" foreshocks proposed by Ebel (1981), because it occurred outside the aftershock zone of the main event. Thus, we do not consider the January 23 event to be a definite foreshock.

EARTHQUAKE LOCATIONS

Deployment of Portable Instruments

When the M_L 5.3 San Rafael swell earthquake occurred, the nearest seismograph station was the easternmost permanent station of the University of Utah regional network, located 20 km to the east at Cedar Mountain. Beginning the day after the main shock, University of Utah personnel deployed five portable analog seismographs with smoked-paper recorders in the epicentral area to augment the station coverage from the permanent network (Table 2-1; triangles, Figure 2-7). Four temporary seismograph stations, directly telemetered to the University's central recording lab in Salt Lake City, were installed on August 20 and 21 (Table 2-1; inverted triangles, Figure 2-7). These stations supplemented the smoked-paper seismographs until August 31, when the latter were removed. The four telemetered stations were operated until December 12, 1988.

Following the M_L 5.4 southern Wasatch Plateau earthquake, we also deployed temporary stations near the main shock epicenter to supplement the permanent network, which at the time had no stations within 40 km of the epicenter (Table 2-2). This effort was more limited than the field recording effort conducted after the San Rafael swell earthquake because of the severe winter weather conditions in the Wasatch Plateau in January 1989. The day after the southern Wasatch Plateau main shock, a University field crew installed four portable smoked-paper seismographs at the locations indicated by the triangles in Figure 2-10. These were operated for a week, but not continuously, owing to weather-related problems. On February 8, the portable analog stations were replaced with two portable telemetry stations at the sites marked by the inverted triangles in Figure 2-10. The easternmost portable telemetry station was converted

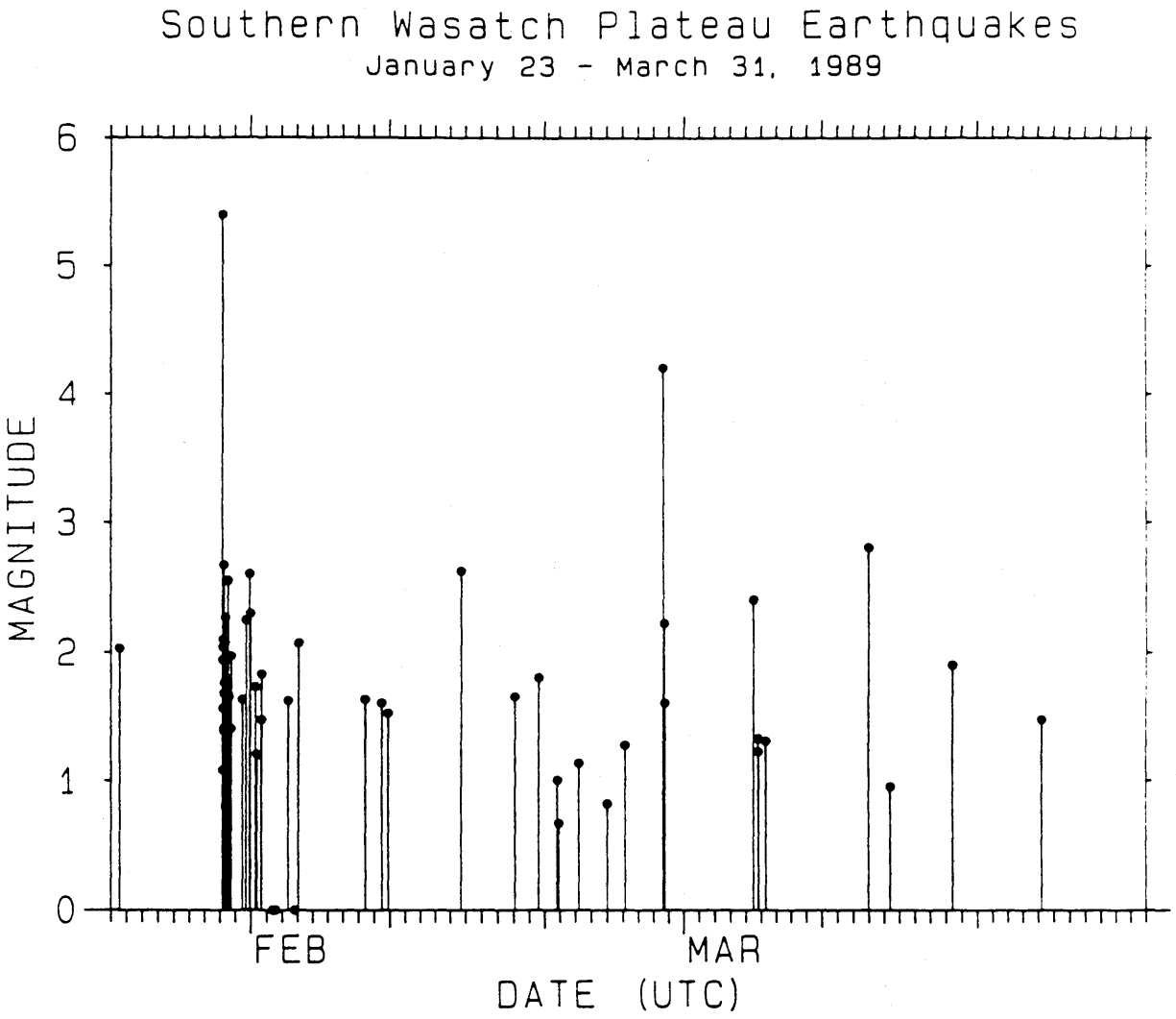

Fig. 2-6. Plot of magnitude versus time for the southern Wasatch Plateau earthquake sequence from January 23 through March 31, 1989. See Figure 2-5 for further explanation.

TABLE 2 - 1

STATIONS USED FOR MASTER-EVENT RELOCATIONS OF THE SAN RAFAEL SWELL EARTHQUAKE SEQUENCE

Station Name	Type†	Latitude N	Longitude W	Elevation (m)	P-wave Station Correction (sec)	First Event Recorded (UTC)* Date	First Event Recorded (UTC)* Time	Last Event Recorded (UTC)* Date	Last Event Recorded (UTC)* Time
FUL	M	39° 06.26′	110° 51.32′	1640	−.03	8-17	07:04	8-31	08:34
FAV	M	39° 08.21′	110° 52.53′	1646	+.03	8-16	18:27	8-31	08:34
FLUT	P	39° 06.00′	110° 50.33′	1682	−.01	8-21	02:21	12-11	13:29
RLUT	P	39° 09.13′	110° 49.12′	1779	−.02	8-20	22:00	12-11	13:29
TWUT	P	39° 05.42′	110° 46.30′	1878	−.01	8-20	22:00	12-11	13:29
WEG	M	39° 05.33′	110° 45.32′	1902	+.01	8-20	22:00	8-31	08:34
OPUT	P	39° 04.07′	110° 57.21′	1768	−.01	8-21	02:21	12-11	13:29
OIL	M	39° 12.26′	110° 56.20′	1768	−.02	8-20	22:00	8-31	08:34
CMU	R	39° 10.28′	110° 37.16′	2332	.00	8-14	18:58	3-21	15:02
SNO	R	39° 18.86′	111° 32.28′	2446	+.25	8-14	18:58	3-21	15:02
SGU	R	39° 10.97′	111° 38.60′	2365	+.24	8-14	18:58	3-21	15:02
EMUT	R	39° 48.84′	110° 48.92′	2268	+.04	8-14	18:58	3-21	15:02
LVU	R	39° 29.50′	111° 49.60′	2530	+.07	8-14	18:58	3-21	15:02
WCU	R	38° 57.88′	112° 05.40′	2714	+.12	8-14	19:07	3-21	15:02
MMU	R	38° 11.91′	111° 17.66′	2387	−.05	8-14	18:58	3-21	15:02
FLU	R	39° 22.69′	112° 10.23′	1950	+.24	8-14	18:58	3-21	15:02
MSU	R	38° 30.80′	112° 10.45′	2141	+.06	8-14	18:58	3-21	15:02

†R= UUSS regional network, M= microearthquake recorder, P= portable telemetry
*From August 14, 1988, through March 31, 1989

TABLE 2 - 2

STATIONS USED FOR MASTER-EVENT RELOCATIONS OF THE SOUTHERN WASATCH PLATEAU EARTHQUAKE SEQUENCE

Station Name	Type†	Latitude N	Longitude W	Elevation (m)	P-wave Station Correction (sec)	First Event Recorded (UTC)* Date	First Event Recorded (UTC)* Time	Last Event Recorded (UTC)* Date	Last Event Recorded (UTC)* Time
SKUT	M	38° 52.81′	111° 32.91′	2522	.00	1-31	16:17	2-8	00:47
WHOT	M	38° 48.19′	111° 31.16′	2755	+.01	1-31	21:42	2-4	01:13
GOOT	M	38° 51.74′	111° 44.80′	2398	+.09	1-31	16:17	2-8	10:29
TWIT	M	38° 33.07′	111° 43.37′	3251	−.12	1-31	21:42	2-8	10:29
GPUT	P	38° 48.91′	111° 37.63′	2755	+.10	2-09	21:24	5-14	23:47
OWUT	P	38° 46.80′	111° 25.42′	2568	+.14	2-09	21:24	5-14	23:47
SGU	R	39° 10.97′	111° 38.60′	2365	+.04	1-23	13:20	7-19	16:29
WCU	R	39° 57.88′	112° 05.40′	2714	−.17	1-23	13:20	7-19	16:29
SNO	R	39° 18.86′	111° 32.28′	2446	+.02	1-23	13:20	7-19	16:29
MSU	R	38° 30.80′	112° 10.45′	2141	−.02	1-23	13:20	7-19	16:29
LVU	R	39° 29.50′	111° 49.60′	2530	+.03	1-30	04:06	7-19	16:29
MMU	R	38° 11.91′	111° 17.66′	2387	+.03	1-23	13:20	7-19	16:29
CMU	R	39° 10.28′	110° 37.16′	2332	.00	1-23	13:20	7-19	16:29
NMUT	R	38° 30.99′	112° 51.00′	1853	+.28	1-23	13:20	7-19	16:29
SUU	R	39° 53.32′	111° 47.50′	1987	−.12	1-23	13:20	7-19	16:29
EMUT	R	39° 48.84′	110° 48.92′	2268	−.28	1-23	13:20	7-19	16:29
NLU	R	39° 57.29′	112° 04.50′	2036	+.24	1-23	13:20	7-19	16:29
WMUT	R	40° 04.60′	111° 50.00′	1981	+.38	1-30	04:15	7-19	16:29

†R= UUSS regional network, M= microearthquake recorder, P= portable telemetry
*From January 23 through July 31, 1989

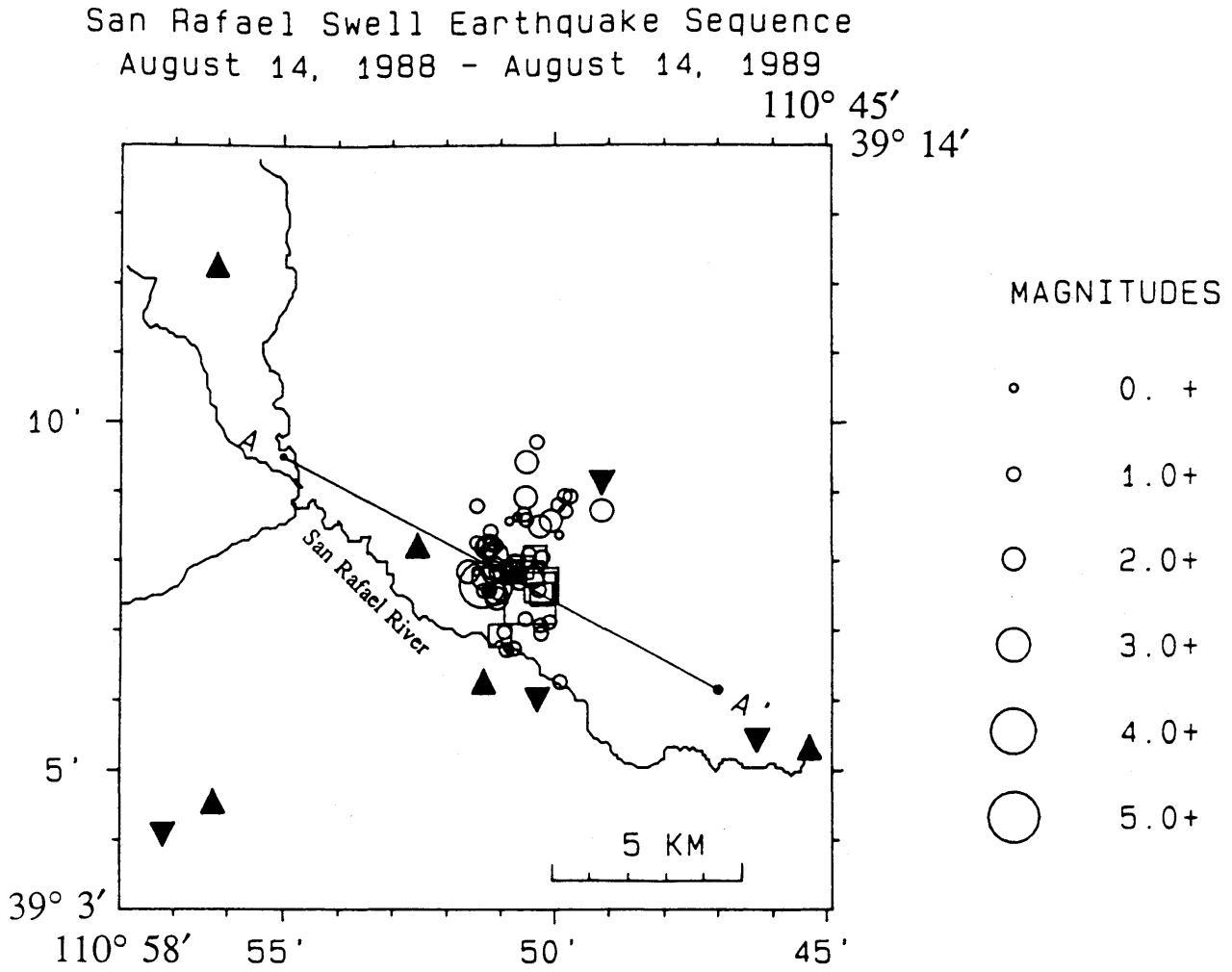

Fig. 2-7. Epicenter map of the 68 best-located earthquakes in the San Rafael swell sequence from August 14, 1988, through August 14, 1989. See text for selection criteria. Circles indicate earthquakes that occurred when the portable stations were operating, and squares indicate earlier and later events. Symbol sizes are scaled by magnitude as shown. Portable analog seismograph stations (Sprengnether MEQ-800 smoked-paper recorders), operated during the period August 16 to 31, are represented by triangles, and the portable telemetry stations, deployed from August 20-21 until December 12, 1988, are represented by inverted triangles. The line A-A′ shows the direction of the cross section in Figure 2-8.

to a permanent station in the spring of 1989, and continues to function as of December 1991. The other was removed on May 25, 1989. The seismometers at all of the temporary stations installed for these aftershock studies were high-gain, short-period, vertical-component velocity transducers.

Velocity Models

We computed the earthquake locations for this study using P-wave arrival times and two different one-dimensional velocity models, one for each of the two areas of interest (Table 2-3). We did not use any S-wave arrival times for our locations because the stations in the vicinity were equipped only with vertical-component seismometers, and S-wave arrival-time picks from vertical-component records are notoriously unreliable.

The lower part of both velocity models is taken, with some slight modifications, from a P-wave velocity model determined by Roller (1965) from a 300-km-long reversed refraction line across the Colorado Plateau in southeastern Utah and northwestern Arizona. The uppermost 2.7 km of the velocity model for the San Rafael swell area was adapted from the velocity model of Williams and Arabasz (1989) for the East Mountain area of the Wasatch Plateau. Williams and Arabasz derived their model from interval velocities determined from high-resolution seismic-reflection profiles on East Mountain and from sonic logs of an oil well located south of East Mountain and 28 km NW of the San Rafael swell main shock epicenter. We modified their model for the San Rafael swell area based on a comparison between the stratigraphic section in their paper and a stratigraphic section for the west flank of the San Rafael swell published in Hintze (1988, p. 180). The uppermost 3.7 km of the southern Wasatch Plateau velocity model was generalized by J. Bott from sonic logs for the Maple Springs #1 well of the Philips Petroleum Company, located 4 km WNW of the epicenter for the 1989 main shock (W, Figure 2-10).

We attempted to compensate for the substantial elevation differences among the recording stations, typically a few hundred meters even for the closest sites (Tables 2-1 and 2-2), by subtracting elevation corrections from the observed arrival times. These corrections were calculated from the standard expression $(h/v)\cos i$, where h is the elevation of the station above the datum, v is the velocity of the topmost layer in the velocity model, and i is the calculated incidence angle in this layer. This correction is exact for refracted waves and an excellent approximation for direct waves, provided that the near-surface velocity is constant over the range of elevation of the stations. In reality, P-wave velocities increase rapidly with depth near the earth's surface in both areas (see Williams and Arabasz, 1989). To make the elevation corrections as accurate as possible, we set the velocity of the top layer in each model equal to the average velocity measured in the uppermost few hundred meters of the crust. Note that the earthquake locations for this study are not very sensitive to the details of the velocity models for the uppermost few kilometers of the crust, since most of the hypocenters are deeper than 10 km. The total calculated travel time through the uppermost layers does, however, affect the absolute depths of the calculated hypocenters.

TABLE 2 - 3

VELOCITY MODELS FOR THE NORTHWESTERN COLORADO PLATEAU

Region	P-Wave Velocity (km/sec)	Depth to Top of Layer (km)
San Rafael Swell†	3.0	0.0
	3.5	0.3
	4.04	0.6
	4.40	0.7
	4.84	1.0
	5.81	2.1
	6.18	2.7
	6.8	27.5
	7.8	40.0
	7.9	80.0
Southern Wasatch Plateau*	3.0	0.0
	4.0	0.5
	5.1	2.8
	5.6	3.5
	6.2	3.7
	6.8	27.5
	7.8	40.0
	7.9	80.0

†Datum is 1800 meters above sea level.
*Datum is 2600 meters above sea level.

Station Delays

In order to improve the relative locations of the earthquakes in each sequence, we employed a master event technique to calibrate station delays for both the temporary stations and the nearby permanent stations of the regional network (see Johnson and Hadley, 1976, and Corbett, 1984). The earthquakes selected as master events are well-located aftershocks that (1) occurred during the times when the maximum number of temporary stations was operating and (2) were large enough to produce clear P-wave arrivals on key regional network stations. For the San Rafael swell sequence, we chose three events of $2.5 \leq M_c$ (coda magnitude) ≤ 2.8, which occurred on August 25 and 26, 1988, when eight of the portable stations were operational. For the southern Wasatch Plateau sequence, we chose four events of $1.7 \leq M_c \leq 2.3$ that were recorded by all four smoked-paper seismographs as well as by regional network stations. Because there was no overlap in the time periods of operation of the smoked-paper seismographs and the two portable telemetry stations in the southern Wasatch Plateau, it was necessary to determine station delays separately for the latter using three other master events of M_c 2.2 to M_L 4.2.

We located each set of master events with the computer program HYPOINVERSE (Klein, 1978) using the appropriate velocity model from Table 2-3. For these initial locations, we set the distance weighting parameters within the program to give full weight to all of the temporary stations and to the minimum number of regional network stations needed to obtain good locations for the master events. Arrival times from the more distant regional network stations were downweighted with a cosine taper from a weight of one at a distance "dmin" (set to 30 km for the San Rafael swell master events and 100 km for the southern Wasatch Plateau events) to a weight of zero at a distance "dmax" (set to 40 km for the San Rafael swell events and 150 km for the southern Wasatch Plateau events) (see Klein, 1978). This distance weighing served to minimize or eliminate the influence of arrival times from the more distant stations, which tend to be the most affected by differences between the actual seismic velocities and those in the model. Downweighting these stations was desirable in order to get the best locations possible for the master events, and thereby reduce location bias in the computation of station delays from travel-time residuals (observed arrival time minus calculated arrival time).

The station delays for the two areas of interest were set equal to the median of the travel-time residuals for the master events in that area (Tables 2-1, 2-2). We then simply subtracted these station delays, along with the elevation delays, from the observed arrival times before locating the earthquakes with HYPOINVERSE. In computing the final sets of locations, we used only those stations for which we had determined a station delay, and we applied no distance weighting. The trial hypocenter for the locations in each area was the median hypocenter of the master events.

Compilation of Data Set

All of the arrival-time data from the temporary stations were combined with the data from the permanent stations of the regional seismic network and processed according to standard procedures to compute locations for the University of Utah earthquake catalog (see Nava et al., 1990). This data set included a few earthquakes that were recorded only on the continuously recording portable analog seismographs, either because they were not large enough to trigger the centralized digital recording system for the regional network, or because the digital recording system was temporarily out of operation when they occurred. Subsequently, we used the master event technique to relocate all earthquakes in the catalog within a 15 km radius of each main shock epicenter that occurred during the one-year period prior to each main shock and the one-year period following them. We were able to obtain good relocations for 161 of the 216 earthquakes in the San Rafael swell data set and 58 of the 64 earthquakes in the southern Wasatch Plateau data set. These locations are listed in the Appendix. The rest of the earthquakes could not be reliably relocated using our master event method because there were less than five P-wave arrival times available for them from the stations for which we determined station delays.

AFTERSHOCK SEQUENCES

San Rafael Swell

A plot of magnitude versus time for the San Rafael swell earthquakes (Figure 2-5) shows a typical foreshock-main shock-aftershock sequence. The largest aftershock was an M_L 4.4 event at 12:44 UTC on August 18, 1988, that was felt (maximum MMI V) throughout much of central Utah and in western Colorado (U.S. Geological Survey, 1988). All but 12 of the 202 locatable aftershocks during the year following the main shock occurred during the 4½-month time period shown on Figure 2-5. However, the detection and location capability of the network in this area decreased significantly after December 12, 1988, when the four portable telemetry stations were removed.

Figure 2-7 is an epicenter map of the master event locations for the San Rafael swell earthquake and 67 of its best-located foreshocks and aftershocks. Figure 2-8 shows the hypocenters of these earthquakes projected onto a vertical plane parallel to line A-A′ on Figure 2-7. The locations for all of the earthquakes on these two plots meet the following selection criteria: (1) maximum azimuthal gap between stations of 130°, (2) minimum of six arrival times used for the location, (3) maximum root-mean-square of the weighted travel-time residuals of 0.10 sec, (4) maximum horizontal standard error of 1.5 km, and (5) maximum vertical standard error of 3.0 km. The circles represent the earthquakes that took place while there were portable stations operating in this area. For all of these earthquakes, the epicentral distance to the

nearest station was less than 4 km. The squares represent earthquakes that were located with the permanent regional network stations only, the closest station of which was about 20 km away.

In map view, the San Rafael swell earthquakes occupy a 3 × 5 km zone which is slightly elongated NNE-SSW and is adjacent to the main shock epicenter (Figure 2-7). In three dimensions, the hypocenters define an aftershock zone dipping 60° ± 5° ESE between 11 and 18 km depth (Figure 2-8), with a length along strike of 5 km and a downdip extent of 7 km. The main shock hypocenter is located at the base of the aftershock zone at a depth of 17 km. Although the depth control on the main shock hypocenter is not as good as it is for most of the others on the cross section, this observation suggests that the rupture began near the base of the fault break and propagated primarily updip.

Space-time plots of the best-located hypocenters (Figure 2-9) show that, within the resolution of the study, the entire aftershock zone became active shortly after the main shock. Although no aftershocks were located southwest of the main shock epicenter during the first several days of the sequence, the apparent expansion of the zone 2 km in this direction took place shortly after the deployment of the portable telemetry stations. Thus, this apparent southwest migration may be an artifact of the change in the station distribution.

Southern Wasatch Plateau

The plot of magnitude versus time for the southern Wasatch Plateau earthquakes (Figure 2-6) shows far fewer aftershocks than the plot for the San Rafael swell earthquakes (Figure 2-5), even though the local magnitudes of the two main shocks are nearly identical. During the one-year period following the southern Wasatch Plateau main shock, the University of Utah located 59 aftershocks, all but four of which occurred during the two-month time period covered by Figure 2-6. Sixteen of these aftershocks were of $M \geq 2.0$ and only one exceeded M_L 2.8—an M_L 4.2 aftershock that occurred nearly a month after the main shock on February 27, 1989, at 15:13 UTC and was felt in central Utah with a maximum MMI of V. The corresponding aftershock totals for the San Rafael swell sequence are 202 locatable aftershocks during the year after the main shock, including 40 of $M \geq 2.0$ and two of $M_L \geq 3.0$. For both aftershock sequences, these totals include all earthquakes during these time periods that have catalog epicenters within 15 km of that of the main shock, but the great majority of the relocated epicenters for these events are within 5 km of their respective main shock epicenters.

In order to evaluate this difference between the number of recorded aftershocks for the southern Wasatch Plateau and San Rafael swell earthquakes, it is necessary to consider the size of the smallest aftershocks that could be routinely located in the two aftershock zones. This threshold size changed with time during both aftershock sequences as the number and distribution of stations changed, but was evidently higher, on the average, for the southern Wasatch Plateau sequence than for the San Rafael swell sequence (compare Figures 2-5 and 2-6). This difference is not surprising, given the sparser station distribution and the greater depth of the

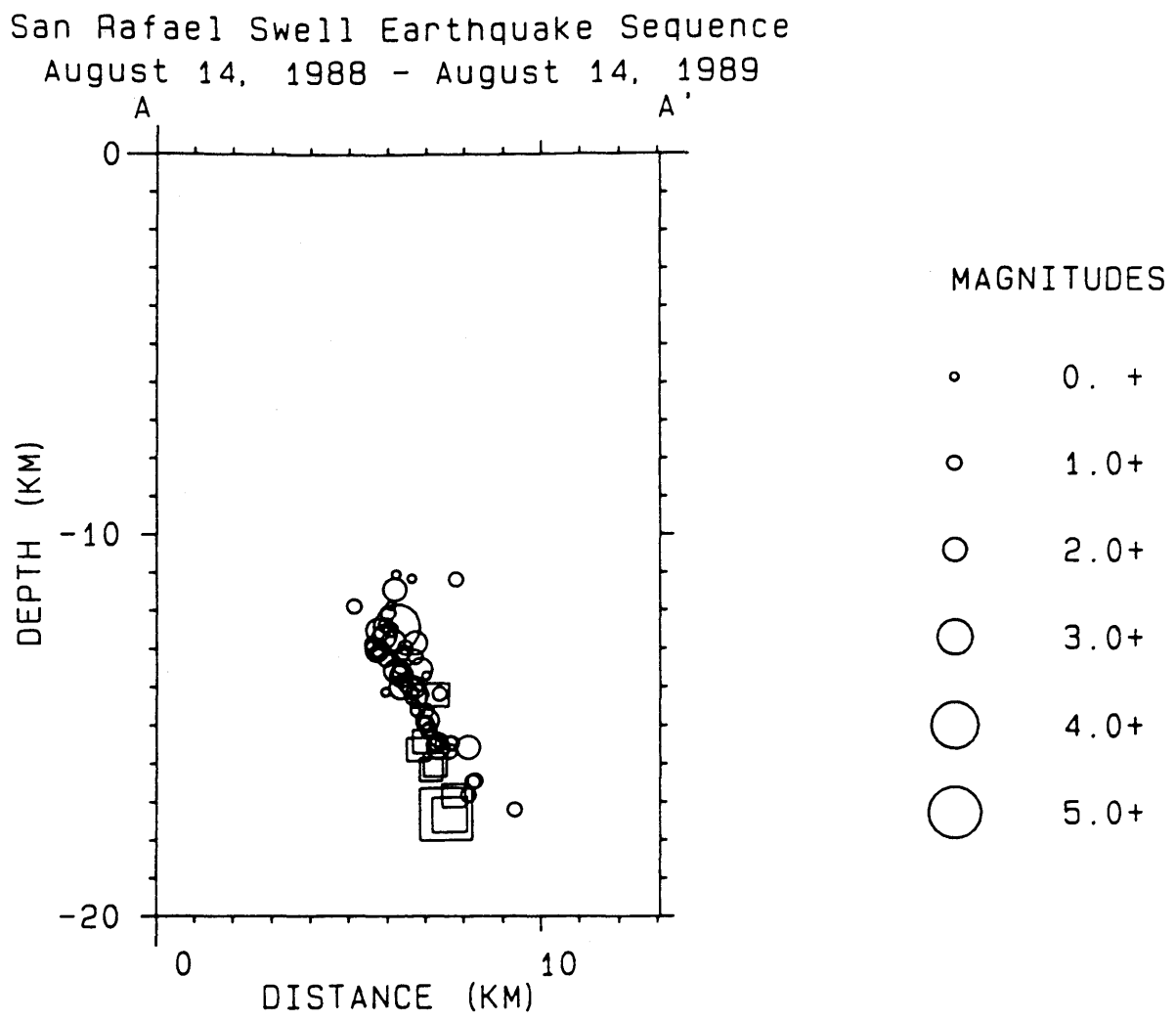

Fig. 2-8. Hypocentral cross section of the earthquakes in Figure 2-7, taken along line A-A′ on Figure 2-7. Squares and circles as in Figure 2-7.

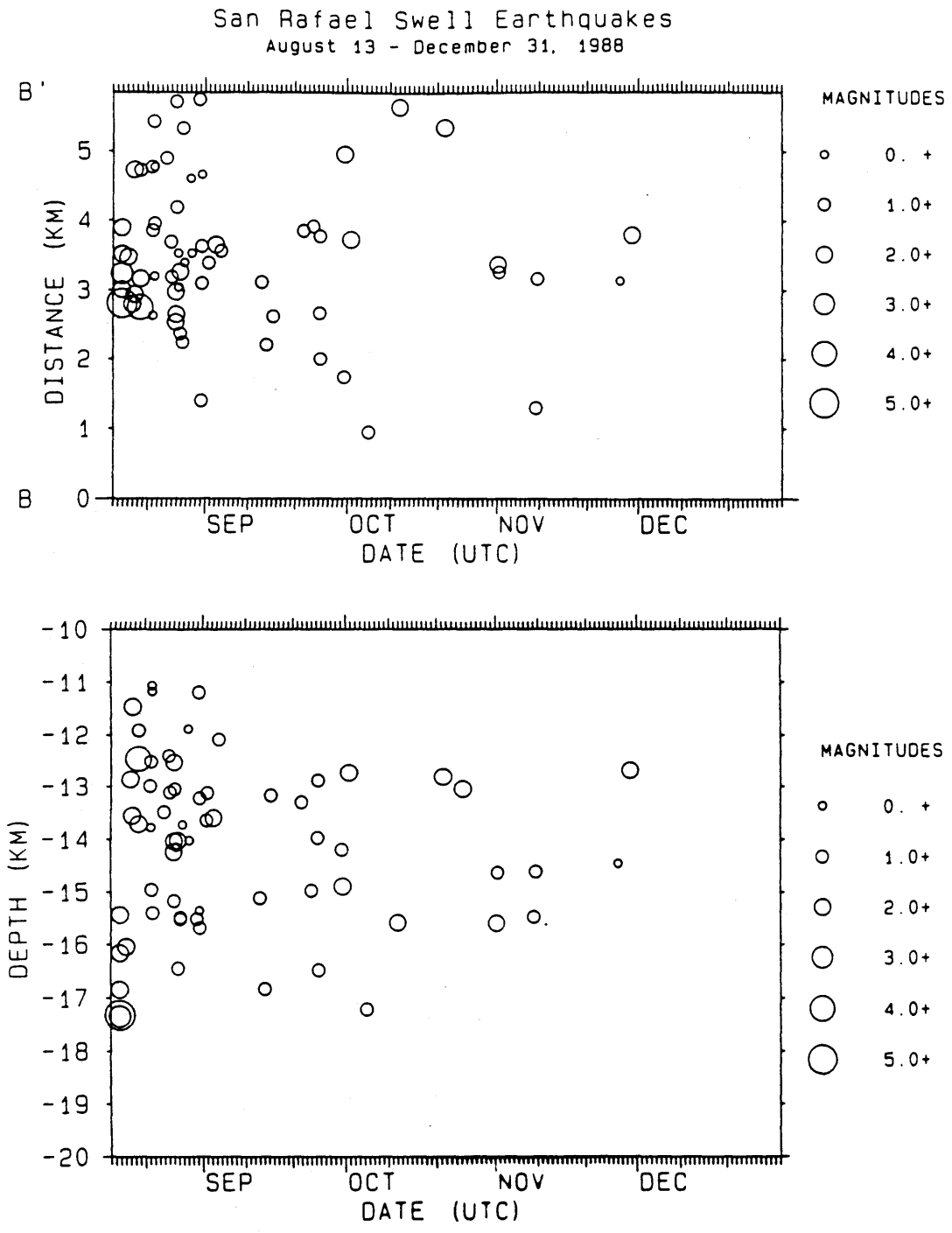

Fig. 2-9. Space-time plots of the best-located earthquakes in the San Rafael swell earthquake sequence from Figures 2-7 and 2-8. The space coordinate of the top plot is the distance along the strike of the inferred fault plane, i.e., along a line perpendicular to line A-A′ on Figure 2-7. The space coordinate of the bottom plot is hypocentral depth.

hypocenters in the southern Wasatch Plateau area. We believe that both lists of aftershocks should be complete for at least $M \geq 2$, however, and the difference in the number of $M \geq 2.0$ aftershocks is a factor of 2½. Thus, it appears that the aftershock sequence for the southern Wasatch Plateau earthquake was considerably less energetic than that of the San Rafael swell earthquake, but a careful analysis of detection thresholds would be needed to rigorously demonstrate this.

Figures 2-10 and 2-11 are a map and vertical cross section, respectively, of hypocenters for the 33 best-located earthquakes of the southern Wasatch Plateau earthquake sequence. The definition of "best-located" is the same as that used above for the San Rafael swell sequence. The squares and circles distinguish, respectively, earthquakes that took place before and after the first portable stations were installed in the area. For all but one of the earthquakes indicated by the circles, the epicentral distance of the closest station used in the location was between 1 and 20 km and was less than one focal depth.

The epicenters of the best-located southern Wasatch Plateau earthquakes form a discontinuous NNE-trending zone approximately 8 km long. In cross section, the hypocenters define an aftershock zone dipping 90° ± 10° between 21 and 25 km depth. The location of the main shock hypocenter near the center of the base of the aftershock zone suggests upward and bilateral propagation of the rupture. However, the depth of the southern Wasatch Plateau main shock is not particularly well constrained, given that the nearest station was 40 km away. Space-time plots of the best-located hypocenters imply that the entire aftershock zone became active immediately after the main shock (Figure 2-12).

A swarm of 59 locatable earthquakes—including 20 of $2.0 \leq M_c \leq 2.8$—took place during April and May of 1990 in a small (< 6 km diameter) area centered 15 km SE of the 1989 main shock epicenter (Figure 2-4). An M_c 3.2 earthquake and three smaller events followed later that year in this same area. We do not consider these earthquakes to be aftershocks, at least in the ordinary sense of the word, because of their clear space-time separation from the activity immediately following the 1989 main shock. To our knowledge, there are no operating coal mines in the vicinity of the 1990 swarm.

FOCAL MECHANISMS

Focal mechanisms of earthquakes in the San Rafael swell and the southern Wasatch Plateau are difficult to constrain from P-wave first motion data because they are near the eastern edge of the University of Utah seismic network. In order to augment the azimuthal coverage of the University of Utah network, we obtained data from seismograph stations in Utah, Colorado, New Mexico, Arizona, and Nevada that are operated by other institutions. We attempted to determine focal mechanisms for all four earthquakes in the San Rafael swell sequence of $M_L \geq 3.0$, plus an M_L 2.9 foreshock, but could obtain acceptably well-constrained solutions only for the main shock and for the largest aftershock. We also determined focal mechanisms for the southern Wasatch Plateau main shock and its largest aftershock. The rest

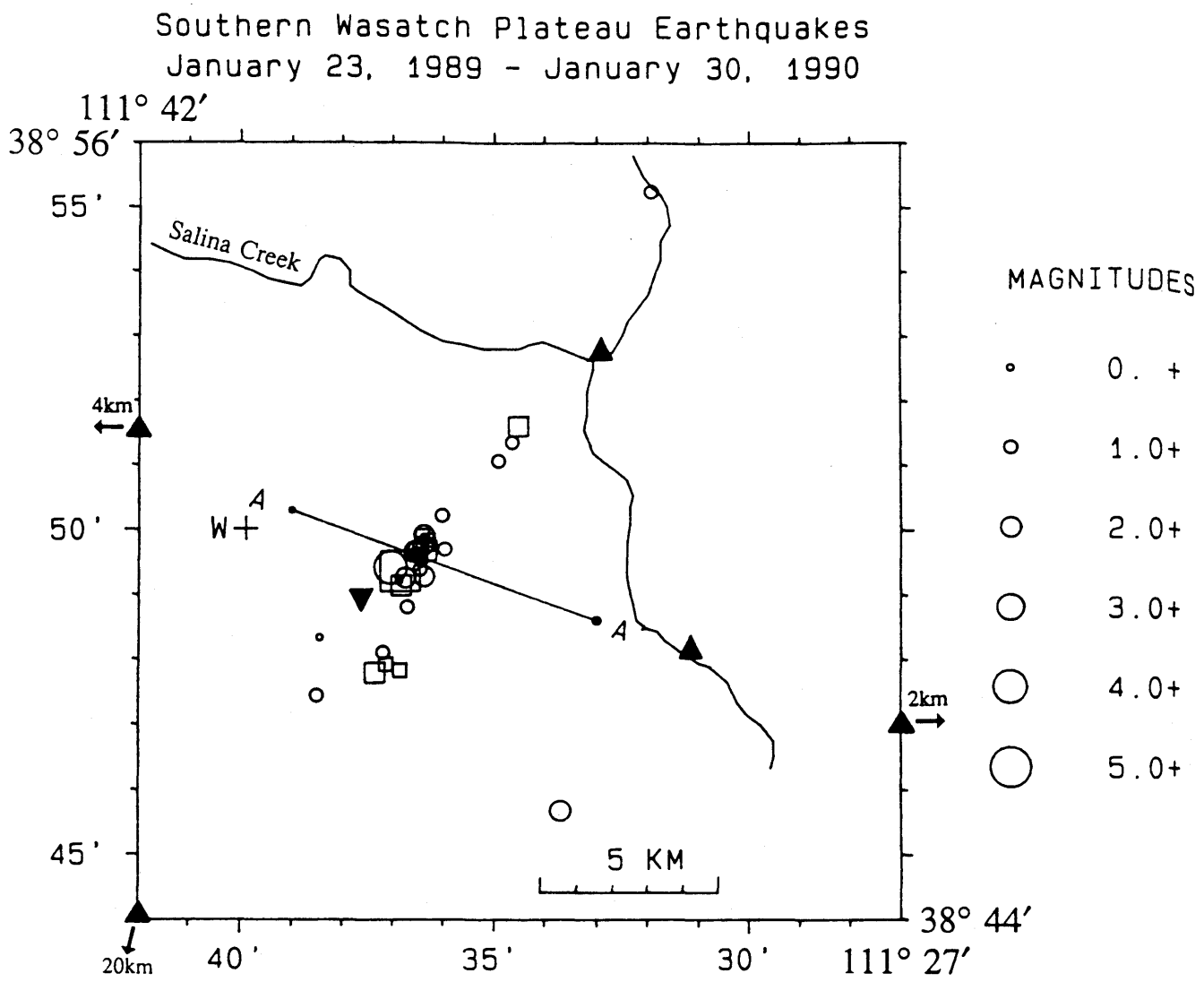

Fig. 2-10. Epicenter map of the 33 best-located earthquakes in the southern Wasatch Plateau earthquake sequence from January 23, 1989, through January 30, 1990. The selection criteria are the same as for Figure 2-7 (see text). Circles indicate earthquakes that occurred after the first portable stations were installed, and squares indicate earlier events. Symbol sizes are scaled by magnitude as shown. Portable seismograph stations, operated during the period January 31 to February 8, 1989, are represented by triangles, and two portable telemetry stations, deployed from February 8 until May 25, 1989, are represented by inverted triangles. The easternmost temporary telemetry station was converted to a permanent station and is still operating as of December 1991. The line A-A′ shows the direction of the cross section in Figure 2-11. W is the location of the petroleum exploration well where the sonic logs used to determine the uppermost part of the southern Wasatch Plateau velocity model were measured.

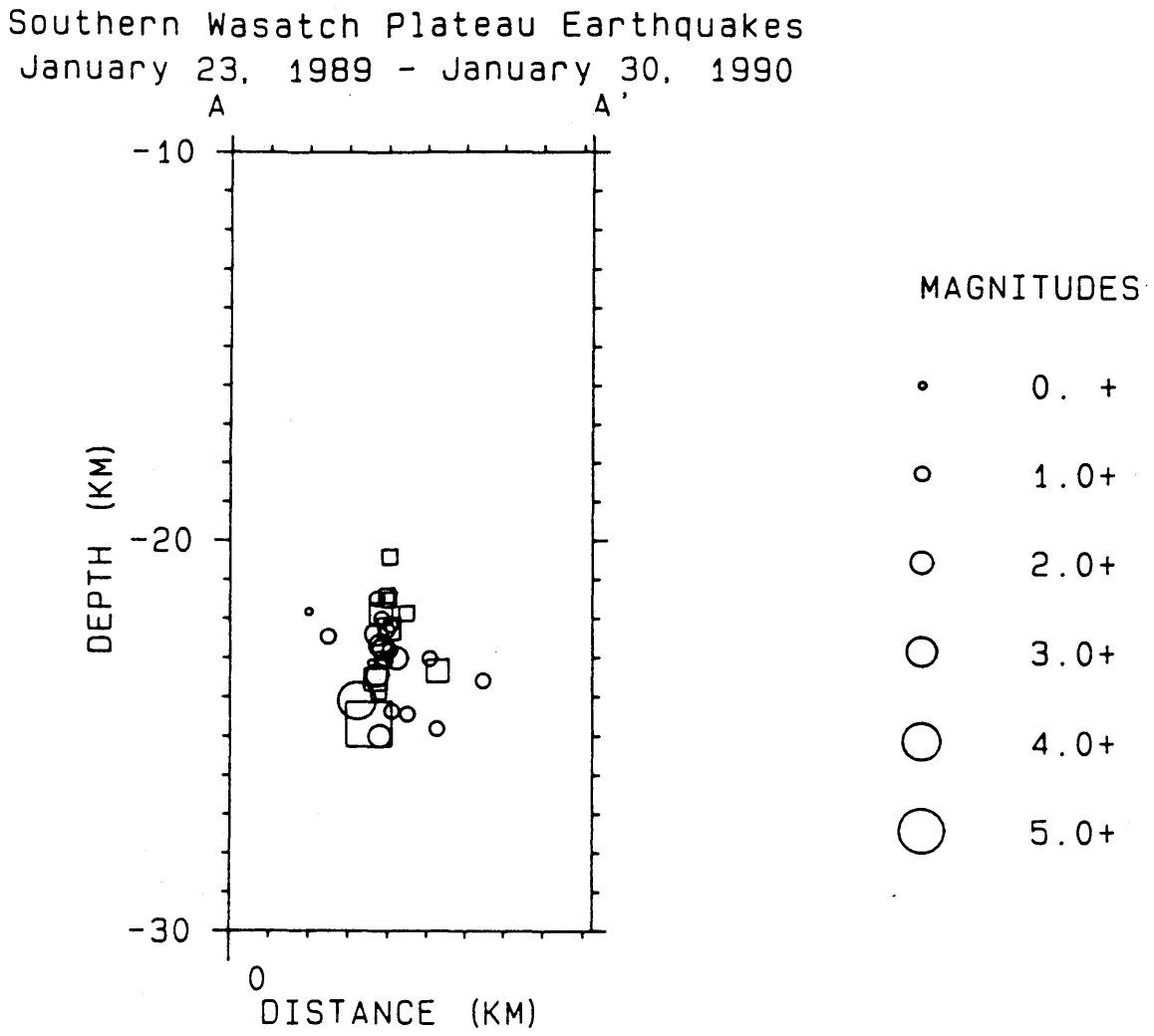

Fig. 2-11. Hypocentral cross section of the earthquakes in Figure 2-10, taken along line A-A′ on Figure 2-10. The cross section line A-A′ is perpendicular to the strike of the preferred (N 20° E-striking) nodal plane of the focal mechanism for the southern Wasatch Plateau main shock shown in Figure 2-13. Squares and circles as in Figure 2-10.

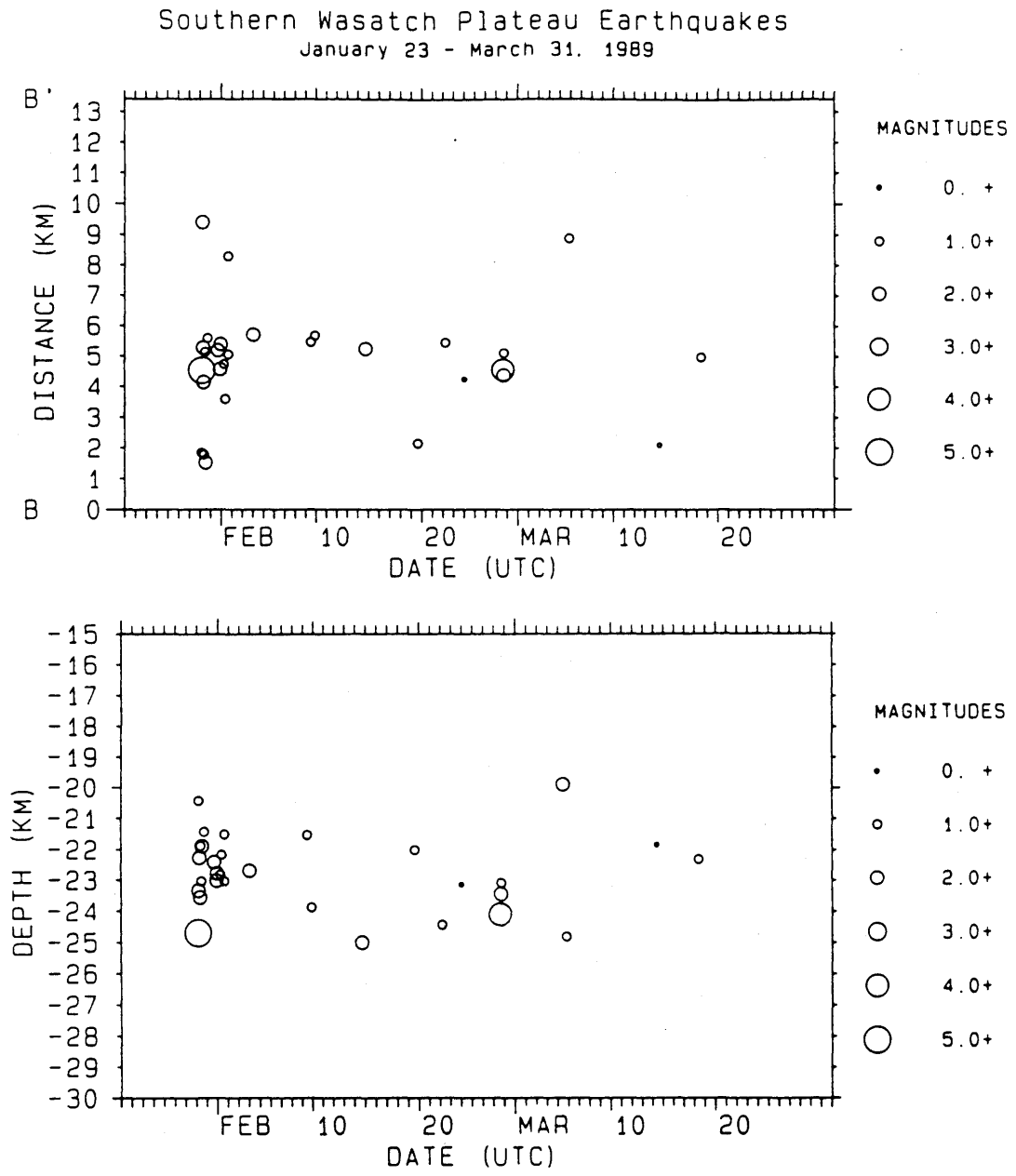

Fig. 2-12. Space-time plots of the best-located earthquakes in the southern Wasatch Plateau earthquake sequence from Figures 2-10 and 2-11. The space coordinate of the top plot is the distance along the strike of the inferred fault plane, i.e., along a line perpendicular to line A-A′ on Figure 2-10. The space coordinate of the bottom plot is hypocentral depth.

of the southern Wasatch Plateau aftershocks are too small for focal mechanism determination with the available station coverage. As a check on the validity of the takeoff angles calculated from the master-event locations and the velocity models in Table 2-3, we plotted reduced P-wave travel time versus distance for the two main shocks and their largest aftershocks (see Bjarnason and Pechmann, 1989). For all four of these earthquakes, the agreement between the observed and theoretical arrival times is acceptable out to distances of at least 300 or 400 km, implying that the locations and velocity models are adequate for the focal mechanism calculations.

The focal mechanism for the San Rafael swell main shock (upper left, Figure 2-13) shows oblique-normal faulting, with the left-lateral nodal plane striking between 20° and 42° and dipping between 45° ESE and 80° SE. This nodal plane has an orientation similar to that of the aftershock zone (Figure 2-8) and is therefore assumed to be the fault plane. The data restrict the rake angle on this plane to lie between -20° and -60° (following the sign convention for rake angle of Aki and Richards, 1980, p. 106). The tension (T) axis of the main shock focal mechanism has a shallow plunge and an azimuth within 25° of E-W. The focal mechanism for the largest San Rafael swell aftershock (upper right, Figure 2-13) is somewhat better constrained than that of the main shock because of the availability of first motion readings from two of the portable seismographs. This mechanism indicates oblique-normal faulting on a plane that dips either to the E or SW, and has a shallowly-plunging T axis oriented N60°E - S60°W (±10°).

The focal mechanisms for the southern Wasatch Plateau main shock and its largest aftershock (bottom row, Figure 2-13) both show dominantly strike-slip faulting, with the left-lateral nodal plane striking NNE. On the basis of the aftershock distribution, we again choose the left-lateral nodal plane of the main shock as the fault plane. The first motion data constrain this plane to have a strike of 20° ± 10°, a dip of 79° ± 15°, and a rake angle between -25° and +10° (the rake angle of the solution shown is -10°). Our focal mechanism for the southern Wasatch Plateau main shock agrees very well with a focal mechanism for this earthquake determined by moment tenor inversion of very long-period teleseismic body waves (Harvard solution published by the U.S. Geological Survey, 1989): strike = 25°, dip = 90°, and rake = 0°. The seismic moment resulting from this inversion is 1.1×10^{24} dyne-cm. The T axis for the main shock focal mechanism has a shallow plunge and trends ENE-WSW. The T axis for the aftershock focal mechanism also has a shallow plunge and a trend constrained by the first-motion data to lie between E-W and ENE-WSW.

DISCUSSION

Focal Depths

The depths of the San Rafael swell and southern Wasatch Plateau earthquakes place both shocks near the middle of the 40-km-deep crust of the Colorado Plateau (Table 2-3) and well

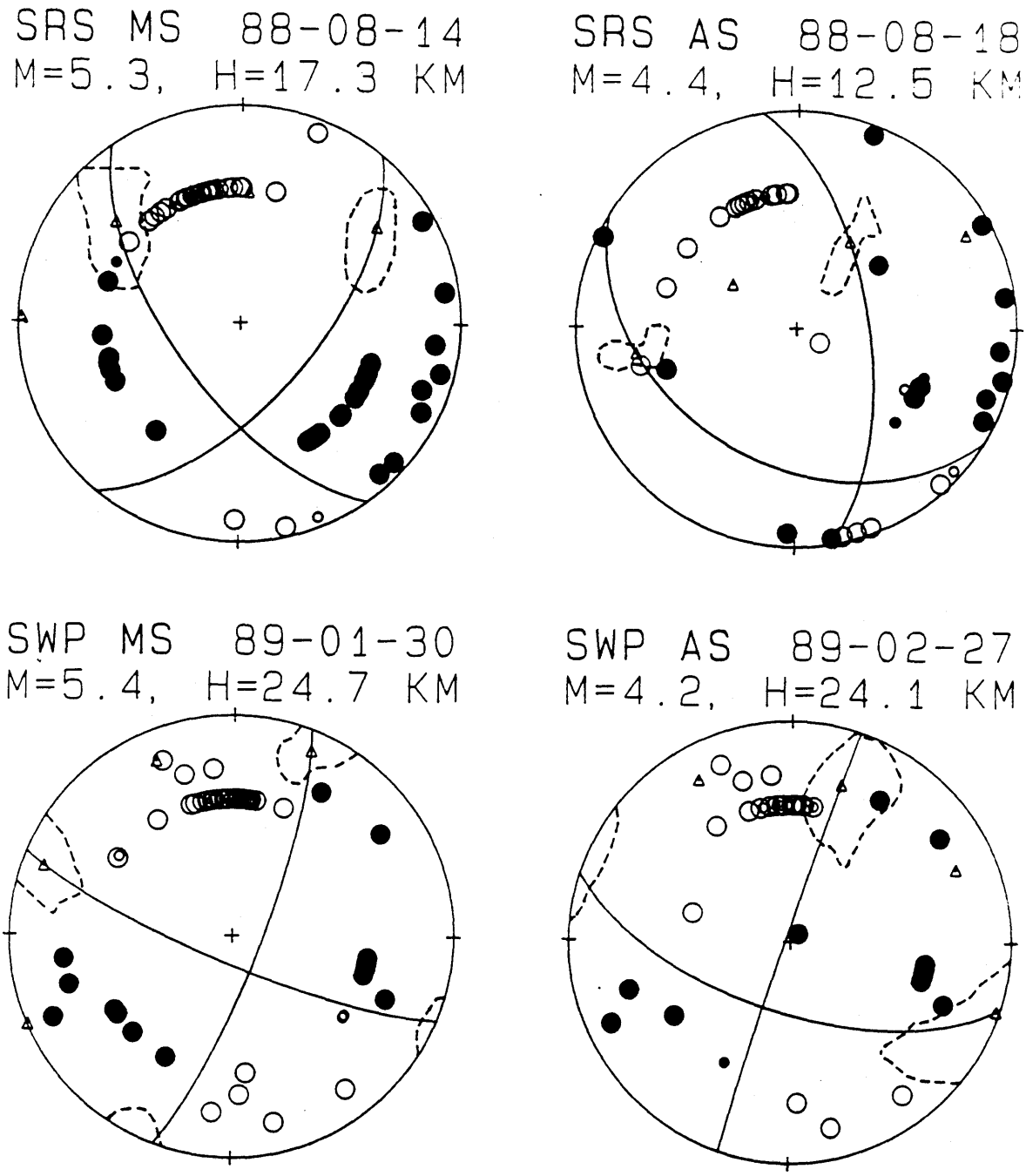

Fig. 2-13. Focal mechanisms for the 1988 San Rafael swell earthquake (SRS MS) and its largest aftershock (SRS AS), and for the 1989 southern Wasatch Plateau earthquake (SWP MS), and its largest aftershock (SWP AS). P-wave first motions are plotted on lower hemisphere equal area projections, with compressions shown as solid circles and dilatations as open circles. Smaller circles indicate readings of lower confidence. The triangles show slip vectors and P and T axes. The dashed contours show the error bars on the slip vectors, allowing up to one good or two lesser-quality readings in error. On the basis of the aftershock distributions, we choose the left-lateral (north-northeast- to northeast-striking) nodal plane of each main shock as the fault plane.

within the Precambrian basement (Figure 2-3). The depth ranges of the aftershocks suggest that the main shock ruptures did not propagate to the surface. The fact that no surface faulting was observed after either earthquake supports this inference. However no one, to our knowledge, thoroughly searched either of the epicentral areas. The apparent absence of surface faulting is consistent with a typical threshold magnitude of about 6.0 to 6.5 for surface faulting in the Utah region (Arabasz et al., 1987).

Both the San Rafael swell and southern Wasatch Plateau events are unusually deep for earthquakes in the Intermountain Seismic Belt. In the Intermountain Seismic Belt in north-central Utah, the depth above which 90 percent of the well-constrained focal depths lie ranges from 11 to 17 km, with very few events occurring as deep as 25 km (Arabasz et al., 1987). In contrast, earthquakes with focal depths of up to 30 km are common in the interior of the Colorado Plateau in southeastern Utah, and events with focal depths as deep as 58 km have been reported there (Wong and Humphrey, 1989).

Wong and Humphrey (1989) and Wong and Chapman (1990) explain the unusually deep seismicity in the central Colorado Plateau as a consequence of the relatively low heat flow in this region, which presumably increases the depth to the brittle-ductile transition. Examination of local heat flow data shows that this explanation also applies to the San Rafael swell earthquake, because it occurred within the relatively low heat flow thermal interior of the Colorado Plateau. The mean of six heat flow measurements by Bodell and Chapman (1982) from sites within 20 km of the epicenter of the San Rafael swell main shock is 61 mW/m^2, with a standard deviation of 6 mW/m^2. This mean heat flow is essentially the same as that which Bodell and Chapman (1982) calculate for the interior of the Colorado Plateau. Using a heat flow of 61 ± 6 mW/m^2 and the average continental geotherms given by Wong and Chapman (1990), the estimated temperatures within the aftershock zone of the San Rafael swell earthquake range from 180 to 360° C. These temperatures are below the maximum temperature for earthquake occurrence in the crust of 350 ± 100°C that has been suggested by various investigators (e.g., Brace and Byerlee, 1970; Chen and Molnar, 1983).

The depth of the southern Wasatch Plateau earthquake is more difficult to reconcile with the heat flow data, because this earthquake occurred within the relatively warm thermal periphery of the Colorado Plateau where the heat flow is 80 to 90 mW/m^2 (Bodell and Chapman, 1982; Eggleston and Reiter, 1984). The closest heat flow measurement to the earthquake is a value of 82 ± 16 mW/m^2, calculated by Eggleston and Reiter (1984) from temperatures measured at depths of 3734 and 5107 m in a petroleum exploration well located 9.5 km NNE of the relocated epicenter. Three heat flow measurements by Bodell and Chapman (1982) from locations 30 to 32 km east of the epicenter range from 75 to 116 mW/m^2 and average 92 ± 21 mW/m^2 (one S.D error bar). For a heat flow of 80 to 90 mW/m^2, the average continental geotherms of Wong and Chapman (1990) predict temperatures within the aftershock zone of the southern Wasatch Plateau earthquake to be 520 to 690° C. These estimated temperatures are well above the typical threshold temperature for earthquake occurrence. If these tempera-

tures are correct, then other factors must be responsible for the exceptionally deep brittle-ductile transition beneath the southern Wasatch Plateau, perhaps high strain rate or unusual minerology.

Rupture Dimensions

Aftershocks that occur within the first few days following an earthquake are usually observed to cluster on or near the main shock rupture surface, at least in cases where the dimensions of the rupture can be determined independently from surface faulting, geodetic data, or other seismological observations. Such clustering can occur even when most of the aftershocks represent movement on subsidiary faults instead of additional slip on the main fault (Richins et al., 1987; Oppenheimer, 1990). Consequently, when the initial aftershock zone of an earthquake defines a planar surface, the orientation and size of this surface is generally believed to be indicative of the orientation and size of the main shock rupture.

Based on the aftershock distribution and focal mechanism for the San Rafael swell earthquake, we infer that this earthquake resulted from a combination of left-lateral and normal slip on a fault segment with a strike between NNE and NE, a dip of about 60° ESE, a depth extent from 11 to 18 km, and approximate dimensions of 5 km along strike and 7 km downdip (Figures 2-7 to 2-9, 2-13). Similarly, we infer that the southern Wasatch Plateau earthquake resulted from primarily left-lateral slip on a fault segment with a NNE strike, a near-vertical dip, a depth extent from 21 to 25 km, and approximate dimensions of 8 km along strike and 4 km downdip (Figures 2-10 to 2-13). Alternatively, the length along strike of the southern Wasatch Plateau fault break could be interpreted to be as short as 3 km, the length of the central continuous part of the aftershock zone adjacent to the main shock epicenter (Figures 2-10, 2-12).

Our estimates of the rupture areas for these earthquakes are based on the aftershock zones defined by the best-located hypocenters determined in this study. These hypocenters constitute 42% and 57% of the total number of hypocenters that we were able to relocate for the San Rafael swell and southern Wasatch Plateau earthquake sequences, respectively. The aftershock zones defined by the complete sets of relocated hypocenters are somewhat larger, but less well defined, due to the inclusion of hypocenters with larger location errors.

The rupture dimensions that we are inferring for the San Rafael swell and southern Wasatch Plateau earthquakes appear to be reasonable for events of this size (e.g., see Wells et al., 1992). Although surface faulting from earthquakes in the lower-magnitude-five range is rare, two unusually shallow strike-slip earthquakes in this magnitude range in the Mojave Desert of California produced clear tectonic surface ruptures with lengths comparable to those that we are inferring for the 1988 and 1989 main shocks in the Colorado Plateau. The June 1, 1975 (UTC), Galway Lake earthquake of M_L 5.0 (Hutton et al., 1985) was accompanied by surface rupture along a 6.8-km-long zone, with right-lateral displacements of up to 1.5 cm on individual fractures (Hill and Beeby, 1977). The March 15, 1979, Homestead Valley

earthquake of M_L 5.3 (Hutton et al., 1985) caused right-lateral surface slip of up to at least 10 cm on a 3.25-km-long fault break (Hill et al., 1980). Measurements of source durations for earthquakes with moments similar to that of the M_L5.4 southern Wasatch Plateau earthquake (~10^{24} dyne-cm) are typically in the range 0.5 to 1.5 sec, which give model-dependent source diameter estimates of ~1-4 km (e.g., Somerville et al., 1987).

Stress Drops

If the stress drop caused by a strike-slip earthquake on a buried, rectangular, vertical fault is assumed to be constant everywhere on the rupture surface, then this stress drop, $\Delta\sigma$, can be calculated from the equation

$$\Delta\sigma = C M_0 / L W^2$$

where M_0 = seismic moment, L = rupture length, W = rupture width, and C is a dimensionless factor that depends on the ratios L/W and h/W, h being the depth of the upper edge of the fault (Boore and Dunbar, 1977). For the southern Wasatch Plateau earthquake, $M_0 = 1.1 \times 10^{24}$ dyne-cm (U.S. Geological Survey, 1989) and from the aftershock distribution, L ≈ 3 to 8 km, W ≈ 4 km, and h ≈ 21 km. If L = 8 km, then from Figure 1 of Boore and Dunbar (1977), C = 1.37 and the calculated stress drop is 12 bars. To calculate an approximate upper-bound stress drop, we set L = 4 km instead of 3 km because Boore and Dunbar do not give C values for L/W < 1. For L = 4 km, C = 2.08 and the calculated stress drop is 36 bars. Our stress drop estimate of 12 to 36 bars for the southern Wasatch Plateau earthquake falls within the lower end of the range of stress drops typically observed for intraplate earthquakes (ten to several hundred bars; see, for example, Kanamori and Anderson, 1975, and Somerville et al., 1987). It is not possible to calculate the stress drop for the San Rafael swell earthquake without a measurement of its seismic moment. However, its stress drop is probably similar to that of the southern Wasatch Plateau earthquake, since the local magnitudes of the two earthquakes are nearly identical and the estimated rupture dimensions are comparable.

Implications for Regional Tectonics and Earthquake Hazards

The focal mechanisms for the San Rafael swell and southern Wasatch Plateau earthquakes provide new information to help piece together the present-day stress state and kinematics of deformation in the northwestern Colorado Plateau. Figure 2-14 compares the compression (P) and tension (T) axes of the main shock focal mechanisms with compilations of these parameters for earthquakes in the Basin and Range–Colorado Plateau transition zone (left plot, from Arabasz and Julander, 1986) and in the interior of the Colorado Plateau (right plot, from Wong and Humphrey, 1989). The plot of P and T axes for the Basin and Range–Colorado Plateau transition zone indicates a mixture of strike-slip and normal faulting with an approximately ESE-WNW extension direction. The plot for the Colorado Plateau interior indicates predominantly normal faulting with a NE-SW extension direction. The T axes for the San

P and T Axes from Focal Mechanisms

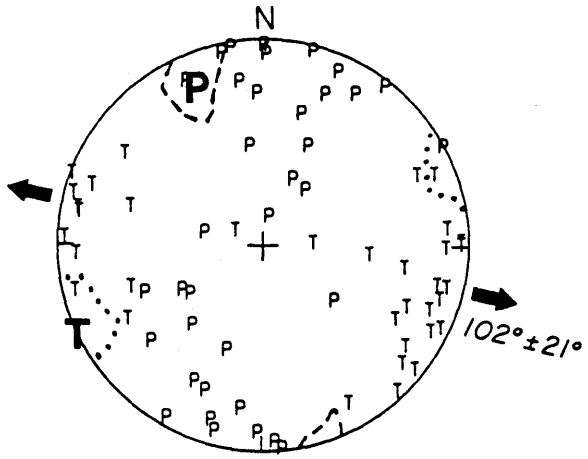

Basin & Range - Colorado Plateau Transition Zone
(After Arabasz and Julander, 1986)

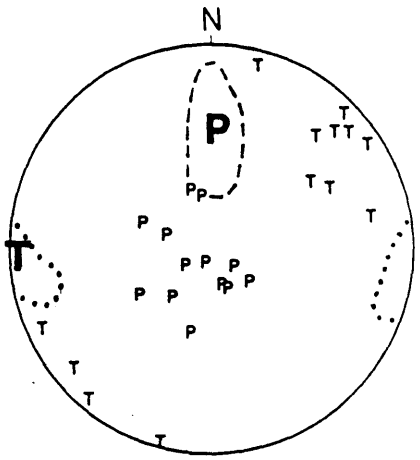

Colorado Plateau Interior
(After Wong and Humphrey, 1989)

Fig. 2-14. Summary plots of P and T axes from earthquake focal mechanisms. Bold letters identify P and T axes for the southern Wasatch Plateau main shock (left diagram) and the San Rafael swell main shock (right diagram). The dashed contours around the bold P and T axes show error bars on their orientations, allowing up to one good or two lesser-quality reading in error.

Rafael swell and the southern Wasatch Plateau earthquakes are both intermediate in trend between the extension directions for the transition zone and the Colorado Plateau. This observation suggests that in the vicinity of the eastern boundary of the transition zone, where these two earthquakes occurred, the extension direction rotates progressively counter-clockwise going towards the southeast, i.e., towards the center of the Colorado Plateau.

To put the 1988 and 1989 earthquakes into a regional perspective, Figure 2-15 summarizes our current understanding of contemporary seismotectonic deformation in Utah as inferred from both earthquake focal mechanisms and geological studies. Along the Wasatch Front in northern Utah (the boundary between the Basin and Range Province and the Middle Rocky Mountains), the crust is well known from geological and seismological observations to be undergoing E-W extension. The extension in this region is accommodated primarily by normal and oblique-normal faulting (Jones, 1987; Eddington et al., 1987; Bjarnason and Pechmann, 1989; Zoback, 1989; Patton and Zandt, 1991). In the Basin and Range–Colorado Plateau transition zone, both focal mechanism data (Figure 2-14; see also Bjarnason and Pechmann, 1989; Patton and Zandt, 1991) and geologic studies of Pleistocene and Holocene faults (Anderson and Barnhard, 1987) indicate a mixture of normal, oblique-normal, and strike-slip faulting with an E-W to ESE-WNW extension direction. In the interior of the Colorado Plateau, focal mechanisms show predominantly normal faulting with a NE-SW extension direction (Figure 2-14). There is no corroborative geological evidence for this NE-SW extension that we are aware of. However, volcanic dike trends, cinder cone alignments, and hydrofracture measurements from near the northern and southern edges of the Colorado Plateau are consistent with a NNE-SSW orientation for the least principal stress axis (Zoback and Zoback, 1980). In the northwest corner of the Colorado Plateau, the shallow mining-related earthquakes that were discussed earlier have mostly reverse focal mechanisms with variable P-axis orientations (Smith et al., 1974; McKee, 1982; Williams and Arabasz, 1989; Wong and Humphrey, 1989)

The focal mechanism diagrams and solid arrows in Figure 2-15 illustrate what the results of our analyses of the San Rafael swell and the southern Wasatch Plateau earthquakes have contributed to the picture. We consider these earthquakes to be of particular tectonic significance because of their relatively large size (M_L 5.3 and 5.4) and their unusual mid-crustal focal depths (17 and 25 km). The fact that both involved large amounts of left-lateral slip on NNE- to NE-striking faults suggests the possibility of large-scale left-lateral shear at depth beneath the northwestern Colorado Plateau (solid arrows, Figure 2-15). Although strike-slip focal mechanisms have been observed previously for other earthquakes in the Basin and Range–Colorado Plateau transition zone (Figure 2-14; Arabasz and Julander, 1986; Bjarnason and Pechmann, 1989), those other earthquakes were much smaller ($M_L \leq 4.4$) and shallower (focal depths < 10 km). Anderson and Barnhard (1987) interpreted those strike-slip earthquakes and the strike-slip faults that they discovered in their geologic field studies in the transition zone to represent only shallow deformation above upper crustal detachments. But it now appears that there is deep-seated left-lateral strike-slip movement taking place beneath the northwestern Colorado Plateau on faults that are roughly parallel to the northwest boundary of the province (Figure 2-15). This left-lateral motion may be a kinematic adjustment to the

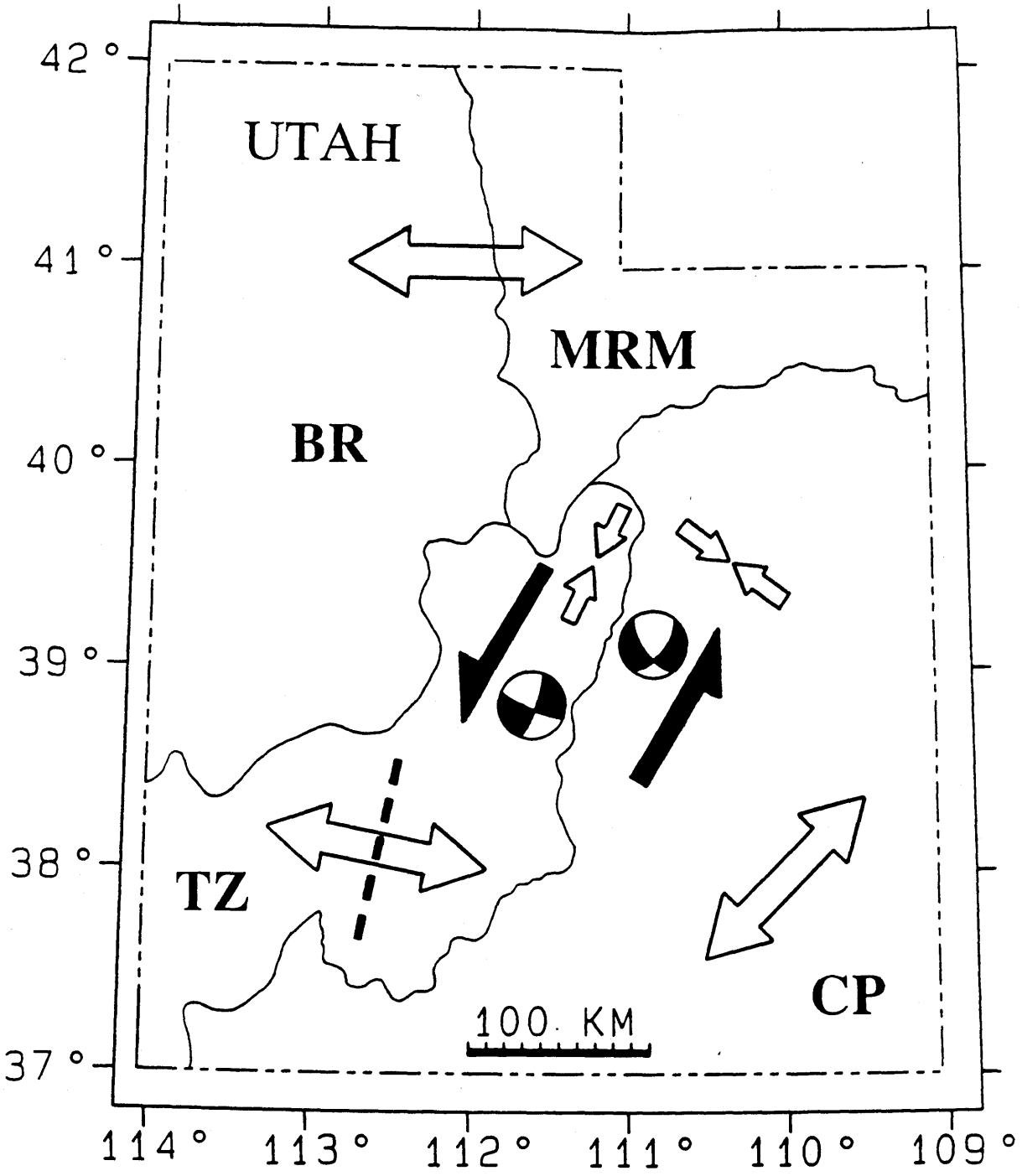

Fig. 2-15. Schematic summary of contemporary seismotectonic deformation in Utah as inferred from earthquake focal mechanisms and geological observations (see text for sources of information). Thin solid lines show boundaries of physiographic provinces from Stokes (1986), labeled as in Figure 2-4. The open arrows show extension and compression directions in regions dominated by normal and reverse faulting, respectively. The open arrow with the heavy dashed line through it indicates the extension direction in a region of mixed normal, oblique-normal, and strike-slip faulting. Focal mechanisms for the 1988 San Rafael swell and the 1989 southern Wasatch Plateau earthquakes are also shown, with the compressional quadrants shaded. The solid arrows illustrate the north-northeast left-lateral shear that we are inferring to exist at mid-crustal depths beneath the northwestern Colorado Plateau, based on the results of this study.

approximately 45° to 55° rotation in extension directions between the eastern edge of the Basin and Range Province and the interior of the Colorado Plateau (Figure 2-15).

Hamilton (1988) has proposed that the Colorado Plateau rotated ~3° clockwise relative to the interior of the North American Continent during the middle and late Cenozoic opening of the Rio Grande Rift on the southeastern margin of the Colorado Plateau (Figure 2-1). The latest phase of extension across the rift, and the one primarily responsible for its present structure and geomorphology, occurred primarily during the late Miocene (10 to 5 m.y. ago), with minor E-W extension continuing to the present (Morgan et al., 1986; Baldridge and Olsen, 1989). The basis for Hamilton's rotation hypothesis is the observation that the extensional terrain of the rift narrows northward from southern New Mexico to the northern end of the rift in central Colorado. This observation suggests that separation between the Colorado Plateau and the continental interior has occurred about an Euler pole of rotation that is located near the northern terminus of the rift in central Colorado (Hamilton, 1988). If the current pole of rotation is in south-central Colorado or north-central New Mexico, and if the Basin and Range Province in Utah is rotating more slowly than the Colorado Plateau, or not at all, then left-lateral shear would occur along the NNE- to NE-trending boundary between the Colorado Plateau and the Basin and Range Province in Utah. Note that this scenario is not incompatible with the NE-SW extension of the interior of the Colorado Plateau inferred by Wong and Humphrey (1989) from focal mechanism data. This NE-SW extension represents internal deformation of the Colorado Plateau block, which could occur, for instance, if the northeastern part of the Colorado Plateau is rotating slightly faster than the southwestern part.

The 1988 and 1989 earthquakes in the northwestern Colorado Plateau could not easily have been anticipated on the basis of either late Quaternary faulting or historical seismicity in the epicentral areas. The San Rafael swell earthquake occurred in an area where there was very little recorded seismicity before 1988 and where there is no known Quaternary surface faulting. It is possible that this earthquake occurred on a subsurface extension of one of the NE-striking faults which displace Cretaceous and older sedimentary rocks in the area (Hintze, 1980; Figure 2-2). If any of these faults have had Quaternary movement at the surface, it might be difficult to identify since there are few Quaternary deposits in the San Rafael swell. Most of the prior instrumental seismicity in the vicinity of the southern Wasatch Plateau earthquake was at shallower (but poorly constrained) focal depths. Although there are post-Eocene faults extending the length of the Wasatch Plateau, and some of them appear to be still active, the sense of motion on these fault is normal and not strike-slip. These normal faults in the Wasatch Plateau form a series of N-S-striking, right-stepping, en-echelon graben, which are typically 10 to 30 km wide (Figure 2-2). The focal mechanisms of the southern Wasatch Plateau and San Rafael swell earthquakes raise the possibility that these en-echelon graben may have formed as a result of stresses induced in the near-surface sedimentary rocks by left-lateral displacements on NNE- to NE-striking faults in the underlying Precambrian basement. In such a case, the grabens would be surficial features confined to the sedimentary rocks in the uppermost 10 km or so of the crust (Figure 2-3). These grabens might be separated from the strike-slip faults in the Precambrian basement by a low-angle detachment fault like the one interpreted (with some uncertainty) by Allmendinger et al. (1986) from seismic reflection data.

Earthquakes of moderate size ($5 \leq M_L \leq 6.5$) are capable of causing considerable damage in urban areas, as evidenced by the M_L 5.9 Whittier Narrows earthquake that struck southern California on October 1, 1987 (Hauksson et al. 1988). Earthquakes in this size range can occur without surface rupture on buried faults with no clear surface expression, as did the San Rafael swell and southern Wasatch Plateau earthquakes. The occurrence of these two earthquakes emphasizes the potential for moderate but potentially damaging earthquakes on buried faults anywhere in the Utah region—including the Colorado Plateau.

CONCLUSIONS

1. The 1988 M_L 5.3 San Rafael swell earthquake and the 1989 M_L 5.4 southern Wasatch Plateau earthquake were both caused by buried left-lateral or oblique left-lateral and normal slip on NNE- to NE-striking faults in Precambrian basement rocks at mid-crustal depths. This observation suggests that the crust beneath the northwestern Colorado Plateau may be undergoing left-lateral shear in a NNE-SSW direction. Left-lateral shear at depth could explain some of the complexities of the surficial tectonics in this region, such as the right-stepping, en-echelon pattern of young, N-S-trending grabens in the sedimentary rocks of the Wasatch Plateau.

2. Focal mechanisms for these two earthquakes and their largest aftershocks suggest a local extension direction that is intermediate between the E-W to ESE-WNW extension direction of the Basin and Range–Colorado Plateau transition zone and the NE-SW extension direction of the interior of the Colorado Plateau.

3. The San Rafael swell main shock was preceded by a cluster of seven recorded earthquakes ($M_L \leq 2.5$) which occurred seven months before the main shock, and by six immediate foreshocks of $M_L \leq 3.8$. The southern Wasatch Plateau earthquake was preceded by only one possible recorded foreshock of M_c 2.0, which occurred a week before the main shock.

4. Based on the aftershock distribution, we infer that the San Rafael swell main shock took place on a 5 by 7 km fault break which dips approximately 60° ESE and extends from 11 to 18 km depth. Similarly, we infer that the southern Wasatch Plateau main shock took place on a fault break 3 to 8 km long and 4 km wide which is nearly vertical and extends from 21 to 25 km depth.

5. The temperatures along the inferred rupture surface of the southern Wasatch Plateau earthquake appear to be unusually warm for brittle rock failure. The stress drop estimated for this earthquake is 12 to 36 bars, a value which lies within the normal range of stress drops for intraplate earthquakes.

6. Moderate earthquakes ($5 \leq M_L \leq 6.5$) on buried faults are a definite hazard in the northwestern Colorado Plateau—as in the rest of Utah—even in places where there is no recognized Quaternary surface faulting and only sparse historical seismicity.

ACKNOWLEDGEMENTS

We thank Ted Olson and Allan Stevens of Snow College and Erwin McPherson, Ken Whipp, Julie Shemeta, and Mary Murphy of the University of Utah for installing and operating seismographic instrumentation in the field. Linda Hall measured the arrival times, Paula Oehmich computed the local magnitudes, and Jackie Bott determined the upper part of the southern Wasatch Plateau velocity model from sonic log data. Rick Martin of the U.S. Bureau of Reclamation, Pingsheng Chang of the U.S. Geological Survey, Joyce Wolff of Los Alamos National Laboratory, Allan Sanford of the New Mexico Institute of Mining and Technology, George Zandt and Cheryl Short of Lawrence Livermore National Laboratory, and Doug Bausch of Northern Arizona University kindly supplied data from other seismic networks. We appreciate helpful discussions with David Chapman and Ivan Wong. This research was supported by the U.S. Geological Survey, Department of the Interior, under award numbers 14-08-0001-G1349 and 14-08-0001-G1762, and by the Utah Geological Survey through contract number 89-3659. The views and conclusions contained in this report are those of the authors and should not be interpreted as necessarily representing the official policies, either expressed or implied, of either the U.S. Government or the Utah State Government.

REFERENCES

Aki, K. and P. G. Richards (1980). *Quantitative Seismology: Theory and Methods*, W. H. Freeman, San Francisco, California, 932 pp.

Allmendinger, R. W., H. Farmer, E. Hauser, J. Sharp, D. Von Tish, J. Oliver, and S. Kaufman (1986). Phanerozoic tectonics of the Basin and Range-Colorado Plateau transition from COCORP data and geologic data: A review, in *Reflection Seismology: The Continental Crust*, Geodynamics Series, Vol. 14, M. Barazangi and L. D. Brown, Editors, American Geophysical Union, Washington, D.C., 257-268.

Anderson, R. E. and T. P. Barnhard (1987). Neotectonic framework of the central Sevier Valley area, Utah, and its relationship to seismicity, in *Assessment of Regional Earthquake Hazards and Risk Along the Wasatch Front, Utah*, P. L. Gori and W. W. Hays, Editors, *U.S. Geol. Surv., Open-File Rept. 87-585*, F1-F134.

Arabasz, W. J., R. B. Smith, and W. D. Richins, Editors (1979). *Earthquake Studies in Utah, 1850 to 1978*, Special Publication, University of Utah Seismograph Stations, Salt Lake City, Utah, 552 pp.

Arabasz, W. J., J. C. Pechmann, and E. D. Brown (1987). Observational seismology and the evaluation of earthquake hazards and risk in the Wasatch front area, Utah, in *Assessment of Regional Earthquake Hazards and Risk Along the Wasatch Front, Utah*, P. L. Gori and W. W. Hays, Editors, *U.S. Geol. Surv., Open-File Rept. 87-585*, D1-D58.

Arabasz, W. J. and D. R. Julander (1986). Geometry of seismically active faults and crustal deformation within the Basin and Range-Colorado Plateau transition, in *Cenozoic Tectonics of the Basin and Range Province: A Perspective on Processes and Kinematics of an Extensional Origin*, L. Mayer, Editor, *Geol. Soc. Am. Special Paper 208*, 43-74.

Baldridge, W. S. and K. H. Olsen (1989). The Rio Grande rift, *Am. Scientist* **77**, 240-247.

Best, M. G. and W. K. Hamblin (1978). Origin of the northern Basin and Range province: Implications from the geology of its eastern boundary, in *Cenozoic Tectonics and Regional Geophysics of the Western Cordillera*, R. B. Smith and G. P. Eaton, Editors, *Geol. Soc. Am. Mem. 152*, 313-340.

Bjarnason, I. T. and J. C. Pechmann (1989). Contemporary tectonics of the Wasatch Front region, Utah, from earthquake focal mechanisms, *Bull. Seism. Soc. Am.* **79**, 731-755.

Bodell, J. M. and D. S. Chapman (1982). Heat flow in the north-central Colorado Plateau, *J. Geophys. Res.* **87,** 2869-2884.

Boore, D. M. and W. S. Dunbar (1977). Effect of the free surface on calculated stress drops, *Bull. Seism. Soc. Am.* **67,** 1661-1664.

Brace, W. F. and J. D. Byerlee (1970). California earthquakes: Why only shallow focus?, *Science* **168,** 1573-1575.

Case, W. F. (1988). Geologic effects of the 14 and 18 August, 1988 earthquakes in Emery County, Utah, *Survey Notes (Utah Geological and Mineral Survey)* **22,** 8-15.

Chen, W. and P. Molnar (1983). Focal depths of intracontinental and intraplate earthquakes and their implications for the thermal and mechanical properties of the lithosphere, *J. Geophys. Res.* **88,** 4183-4214.

Corbett, E. J. (1984). Seismicity and crustal structure studies of southern California: Tectonic implications from improved earthquake locations, *Ph.D. Thesis,* California Institute of Technology, Pasadena, California, 231 pp.

Davis, G. H. (1978). Monocline fold pattern of the Colorado Plateau, in *Laramide Folding Associated with Basement Block Faulting in the Western United States,* V. Matthews, Editor, *Geol. Soc. Am. Mem. 151,* 215-233.

Dunrud, C. R., F. W. Osterwald, and J. Hernandez (1973). Summary of activity and its relation to geology and mining in the Sunnyside mining district, Carbon and Emery Counties, Utah during 1967-1970, *U.S. Geol. Surv., Open-File Rept. 73-63.*

Ebel, J. E. (1981). Evidence for fault asperities from systematic time-domain modeling of teleseismic waveforms, *Ph.D. Thesis,* California Institute of Technology, Pasadena, California, 141 pp.

Eddington, P. K., R. B. Smith, and C. Renggli (1987). Kinematics of Basin and Range intraplate extension, in *Continental Extensional Tectonics,* M. P. Coward, J. F. Dewey, and P. L. Hancock, Editors, *Geol. Soc. London Special Publication 28,* 371-392.

Eggleston, R. E. and M. Reiter (1984). Terrestrial heat-flow estimates from petroleum bottom-hole temperature data in the Colorado Plateau and the eastern Basin and Range Province, *Geol. Soc. Am. Bull.* **95,** 1027-1034.

Evison, F. F. (1977). The precursory earthquake swarm, *Phys. Earth Planet. Interiors* **15,** P19-P23.

Foley, L. L., R. A. Martin Jr., and J. T. Sullivan (1986). Seismotectonic study for Joes Valley, Scofield and Huntington North dams, Emery County and Scofield projects, Utah, *U.S. Bureau of Reclamation, Seismotectonic Report No. 86-7.*

Hamilton, W. B. (1988). Laramide crustal shortening, in *Interaction of the Rocky Mountain Foreland and the Cordilleran Thrust Belt*, C. J. Schmidt and W. J. Perry, Jr., Editors, *Geol. Soc. Am. Mem. 171*, 27-39.

Hauksson, E., L. M. Jones, T. L. Davis, L. K. Hutton, A. G. Brady, P. A. Reasenberg, A. J. Michael, R. F. Yerkes, P. Williams, G. Reagor, C. W. Stover, A. L. Bent, A. K. Shakal, E. Etheredge, R. L. Porcella, C. G. Bufe, M. J. S. Johnston, and E. Cranswick (1988). The 1987 Whittier Narrows earthquake in the Los Angeles metropolitan area, California, *Science* **239**, 1409-1412.

Hill, R. L. and D. J. Beeby (1977). Surface faulting associated with the 5.2 magnitude Galway Lake earthquake of May 31, 1975: Mojave Desert, San Bernardino County, California, *Geol. Soc. Am. Bull.* **88**, 1378-1384.

Hill, R. L., J. C. Pechmann, J. A. Treiman, J. R. McMillan, J. W. Given, and J. E. Ebel (1980). Geologic study of the Homestead Valley earthquake swarm of March 15, 1979, *California Geology* **33**, 60-67.

Hintze, L. F. (1980). Geologic map of Utah, Utah Geological and Mineral Survey Map, scale 1:500,000.

Hintze, L. F. (1988). *Geologic History of Utah*, Brigham Young University Geology Studies Special Publication 7, Department of Geology, Brigham Young University, Provo, Utah, 202 pp.

Humphrey, J. R. and I. G. Wong (1983). Recent seismicity near Capitol Reef National Park, Utah, and its tectonic implications, *Geology* **11**, 447-451.

Hutton, L. K., C. R. Allen, and C. E. Johnson (1985). *Seismicity of Southern California: Earthquakes of ML 3.0 and Greater, 1975 through 1983*, Special Publication, California Institute of Technology, Pasadena, California, 142 pp.

Johnson, C. E. and D. M. Hadley (1976). Tectonic implications of the Brawley earthquake swarm, Imperial Valley, California, January 1975, *Bull. Seism. Soc. Am.* **66**, 1133-1144.

Jones, C. H. (1987). A geophysical and geological investigation of extensional structures, Great Basin, western United States, *Ph.D. Thesis*, Massachusetts Institute of Technology, Cambridge, Massachusetts, 226 pp.

Kanamori, H. (1981). The nature of seismicity patterns before large earthquakes, in *Earthquake Prediction: An International Review*, Maurice Ewing Series, Vol. 4, D. W. Simpson and P. G. Richards, Editors, American Geophysical Union, Washington, D.C., 1-19.

Kanamori, H. and D. L. Anderson (1975). Theoretical basis of some empirical relations in seismology, *Bull. Seism. Soc. Am.* **65**, 1073-1095.

Keller, G. R., L. W. Braile, and P. Morgan (1979). Crustal structure, geophysical models and contemporary tectonism of the Colorado plateau, *Tectonophysics* **61**, 131-147.

Klein, F. W. (1978). Hypocenter location program HYPOINVERSE, *U.S. Geol. Surv., Open-File Rept. 78-694*, 113 pp.

Lawton, T. F. (1985). Style and timing of frontal structures, thrust belt, central Utah, *Am. Assoc. Petrol. Geol. Bull.* **69**, 1145-1159.

McKee, M. E. (1982). Microearthquake studies across the Basin and Range-Colorado Plateau transition zone in central Utah, *M.S. Thesis*, University of Utah, Salt Lake City, Utah.

McKee, M. E. and W. J. Arabasz (1982). Microearthquake studies across the Basin and Range-Colorado Plateau transition in central Utah, in *Overthrust Belt of Utah*, D. L. Nielson, Editor, *Utah Geological Association, Publication 10*, 137-149.

Morgan, P., W. R. Seager, and M. P. Golombek (1986). Cenozoic thermal, mechanical and tectonic evolution of the Rio Grande rift, *J. Geophys. Res.* **91**, 6263-6276.

Nava, S. J., J. C. Pechmann, W. J. Arabasz, E. D. Brown, L. L. Hall, P. J. Oehmich, E. McPherson, and J. K. Whipp (1990). *Earthquake Catalog for the Utah Region, January 1, 1986 to December 31, 1988*, Special Publication, University of Utah Seismograph Stations, Salt Lake City, Utah, 96 pp.

Neuhauser, K. R. (1988). Sevier-age ramp-style thrust faults at Cedar Mountain, northwestern San Rafael swell (Colorado Plateau), Emery County, Utah, *Geology* **16**, 299-302.

Oppenheimer, D. H. (1990). Aftershock slip behavior of the 1989 Loma Prieta, California earthquake, *Geophys. Res. Lett.* **17**, 1199-1202.

Pack, F. J. (1921). The Elsinore earthquakes in central Utah, September 29 and October 1, 1921, *Bull. Seism. Soc. Am.* **11**, 155-165.

Patton, H. J. and G. Zandt (1991). Seismic moment tensors of western U.S. earthquakes and implications for the tectonic stress field, *J. Geophys. Res.* **96**, 18,245-18,259.

Powell, W. G. and D. S. Chapman (1990). A detailed study of heat flow at the Fifth Water Site, Utah, in the Basin and Range-Colorado Plateaus transition, *Tectonophysics* **176,** 291-314.

Richins, W. D., J. C. Pechmann, R. B. Smith, C. J. Langer, S. K. Goter, J. E. Zollweg, and J. J. King (1987). The 1983 Borah Peak, Idaho, earthquake and its aftershocks, *Bull. Seism. Soc. Am.* **77,** 694-723.

Roller, R. C. (1965). Crustal structure in the eastern Colorado Plateaus province from seismic refraction measurements, *Bull. Seism. Soc. Am.* **55,** 107-119.

Rowley, P. D., J. J. Anderson, P. L. Williams and R. J. Fleck (1978). Age of structural differentiation between the Colorado Plateaus and Basin and Range provinces in southwestern Utah, *Geology* **6,** 51-55.

Rowley, P. D., T. A. Steven, J. J. Anderson, and C. C. Cunningham (1979). Cenozoic stratigraphic and structural framework of southwestern Utah, *U.S. Geol. Surv. Profess. Paper 1149,* 22 pp.

Smith, R. B., P. L. Winkler, J. G. Anderson, and C. H. Scholz (1974). Source mechanisms of microearthquakes associated with underground mines in eastern Utah, *Bull. Seism. Soc. Am.* **64,** 1295-1317.

Somerville, P. G., J. P. McLaren, L. V. LeFevre, R. W. Burger, and D. V. Helmberger (1987). Comparison of source scaling relations of eastern and western North American earthquakes, *Bull. Seism. Soc. Am.* **77,** 322-346.

Spieker, E. M. (1949). *The Transition Between the Colorado Plateaus and the Great Basin in Central Utah,* Utah Geological Society Guidebook 4, 106 pp.

Standlee, L. A. (1982). Structure and stratigraphy of Jurassic rocks in central Utah: Their influence on tectonic development of the Cordilleran foreland thrust belt, in *Geologic Studies of the Cordilleran Thrust Belt,* R. B. Powers, Editor, Rocky Mountain Association of Geologists, Denver, Colorado, 357-382.

Stokes, W. L. (1986). *Geology of Utah,* Utah Museum of Natural History and Utah Geological and Mineral Survey, Salt Lake City, Utah, 280 pp.

Thompson, G. A. and M. L. Zoback (1979). Regional geophysics of the Colorado Plateau, *Tectonophysics* **61,** 149-181.

Tingey, J. and F. May (1988). CEM ALERT report summary of August 14, 1988 earthquake in Emery County, *Survey Notes (Utah Geological and Mineral Survey)* **22,** 20-21.

United States Geological Survey (1988). Preliminary determination of epicenters: Monthly listings, U.S. Government Printing Office, Washington, D.C.

United States Geological Survey (1989). Preliminary determination of epicenters: Monthly listings, U.S. Government Printing Office, Washington, D.C.

Wells, D. L., K. J. Coppersmith, D. B. Slemmons, and X. Zhang (1992). Earthquake source parameters: Updated empirical relationships among magnitude, rupture length, rupture area, and surface displacement, in preparation for *Bull. Seism. Soc. Am.*

Williams, D. J. and W. J. Arabasz (1989). Mining-related and tectonic seismicity in the East Mountain area, Wasatch Plateau, Utah, U.S.A., *Pure Appl. Geophys.* **129,** 345-368.

Williams, J. S. and M. L. Tapper (1953). Earthquake history of Utah, 1850-1949, *Bull. Seism. Soc. Am.* **43,** 191-218.

Wong, I. G. and D. S. Chapman (1990). Deep intraplate earthquakes in the western United States and their relationship to lithospheric temperatures, *Bull. Seism. Soc. Am.* **80,** 589-599.

Wong, I. G. and J. R. Humphrey (1989). Contemporary seismicity, faulting, and the state of stress in the Colorado Plateau, *Geol. Soc. Am. Bull.* **101,** 1127-1146.

Wong, I. G., J. R. Humphrey, J. A. Adams, and W. J. Silva (1989). Observations of possible non-double-couple failure in mine seismicity, eastern Wasatch Plateau, Utah, *Pure Appl. Geophys.* **129,** 369-405.

Zoback, M. L. (1989). State of stress and modern deformation of the northern Basin and Range province, *J. Geophys. Res.* **94,** 7105-7128.

Zoback, M. L. and M. Zoback (1980). State of stress in the conterminous United States, *J. Geophys. Res.* **85,** 6113-6156.

APPENDIX

This appendix contains listings of the relocated hypocenters determined in this study for earthquakes associated with the August 14, 1988, M_L 5.3 San Rafael swell earthquake and the January 30, 1989, M_L 5.4 southern Wasatch Plateau earthquake. These listings include all earthquakes in the University of Utah catalog which (1) had epicenters within 15 km of the relocated epicenter for each main shock, (2) occurred during the year preceding or following each main shock, and (3) had at least five P-wave arrival time picks. At the time that these earthquakes were sorted from the catalog, the catalog was final through 1988 (see Nava et al., 1990). The relocations were done with the computer program HYPOINVERSE (Klein, 1978) using P-wave arrival times only, the stations and station corrections in Tables 2-1 and 2-2, the velocity models in Table 2-3, elevation corrections calculated using the top layer velocity of 3.0 km/sec, and trial hypocenters of 39° 7.6′ N, 110° 51.1′ W, 14.1 km depth for the San Rafael swell events and 38° 49.7′ N, 111° 36.5′ W, 23.2 km depth for the southern Wasatch Plateau events. See text for further explanation.

The following data are listed for each earthquake:

- Year (YR), date and origin time in Universal Coordinated Time (UTC). Subtract seven hours to convert to Mountain Standard Time (MST) and six hours to convert to Mountain Daylight Time (MDT).
- Earthquake location coordinates in degrees and minutes of north latitude and west longitude, and depth in kilometers. "*" indicates poor depth resolution: no recording stations within 10 km or twice the depth.
- MAG, the computed local magnitude (M_L) for each earthquake. "W" indicates magnitude based on peak amplitude measurements from Wood-Anderson records. Otherwise, the estimate is calculated from signal durations and is more correctly identified as coda magnitude, M_C . "--" indicates that a reliable magnitude estimate could not be made.
- NO, the number of P readings used in the solution.
- GAP, the largest azimuthal separation in degrees between recording stations used in the solution.
- DMN, the epicentral distance in kilometers to the closest station used in the solution.
- RMS, the root-mean-square of the travel-time residuals in seconds:

$$RMS = \left\{ \frac{\sum_i \left[W_i R_i \right]^2}{\sum_i \left[W_i \right]^2} \right\}^{\frac{1}{2}}$$

where: R_i is the observed minus the computed arrival time for the i-th reading, and W_i is the relative weight given to the i-th arrival time (0.0 for no weight through 1.0 for full weight).

San Rafael Swell, Utah, Earthquake Sequence

yr	*date*	*origin time*	*latitude*	*longitude*	*depth*	*mag*	*no*	*gap*	*dmin*	*rms*
88	114	558 32.80	39° 8.48′	110° 50.79′	14.1	1.5	5	159	20	0.01
88	115	1405 54.40	39° 7.80′	110° 51.07′	11.9	2.1	6	163	21	0.03
88	115	1408 18.94	39° 7.96′	110° 50.37′	15.7	2.3	8	124	19	0.06
88	115	1409 23.73	39° 6.79′	110° 49.78′	7.5*	1.8	6	171	19	0.04
88	119	1138 32.14	39° 8.06′	110° 50.54′	14.9	2.0	6	163	20	0.02
88	120	716 18.74	39° 8.61′	110° 50.79′	14.0	2.3	11	120	20	0.34
88	120	742 13.02	39° 8.39′	110° 51.19′	12.0	2.5W	7	144	20	0.10
88	814	1858 36.53	39° 7.52′	110° 50.25′	16.8	2.9W	8	128	20	0.01
88	814	1907 58.63	39° 7.65′	110° 50.25′	17.3	3.8W	9	127	19	0.04
88	814	1912 54.31	39° 8.33′	110° 51.35′	10.5	2.3	9	122	21	0.09
88	814	1914 43.20	39° 8.05′	110° 50.36′	16.2	2.6W	9	124	19	0.04
88	814	1918 55.75	39° 6.53′	110° 50.91′	6.6*	1.8	5	192	21	0.08
88	814	1954 1.13	39° 7.90′	110° 50.61′	15.4	2.7	8	124	20	0.03
88	814	2003 3.70	39° 7.46′	110° 50.46′	17.3	5.3W	8	127	20	0.06
88	814	2152 5.57	39° 5.83′	110° 47.76′	24.6	1.8	6	181	17	0.24
88	814	2219 46.28	39° 7.77′	110° 51.67′	10.9	2.0	6	123	21	0.01
88	815	149 53.76	39° 6.73′	110° 51.62′	7.8*	2.2	8	129	22	0.06
88	815	153 47.73	39° 7.97′	110° 51.11′	8.9*	1.9	8	124	21	0.05
88	815	632 4.17	39° 7.94′	110° 52.16′	5.5*	2.2	8	122	22	0.07
88	815	1247 18.34	39° 6.87′	110° 50.97′	9.9*	1.9	7	129	21	0.04
88	815	1450 23.36	39° 7.38′	110° 50.94′	14.8	3.0W	6	166	21	0.01
88	815	1652 18.75	39° 7.81′	110° 50.32′	16.8	2.7	9	125	19	0.14
88	816	213 49.11	39° 7.83′	110° 50.43′	16.0	2.9	9	125	20	0.02
88	816	1827 4.83	39° 8.95′	110° 51.05′	14.1	2.1	8	154	3	0.09
88	816	2127 2.95	39° 7.59′	110° 51.01′	12.9	2.4	10	126	3	0.04
88	816	2143 50.92	39° 8.19′	110° 51.07′	12.9	2.2	7	122	20	0.06
88	816	2157 22.85	39° 8.49′	110° 51.05′	13.0	1.7	7	121	20	0.04
88	817	704 27.59	39° 8.50′	110° 50.27′	13.6	2.1	10	120	3	0.07
88	817	929 59.06	39° 7.75′	110° 51.33′	11.5	2.0	8	102	2	0.06
88	818	1244 53.49	39° 7.65′	110° 51.35′	12.5	4.4W	9	125	2	0.03
88	818	1257 5.94	39° 7.60′	110° 51.42′	12.2	1.8	7	130	2	0.12
88	818	1437 54.45	39° 7.83′	110° 51.14′	13.7	2.2	9	109	2	0.07
88	818	1446 57.42	39° 8.79′	110° 51.44′	11.9	1.4	7	95	2	0.09
88	818	1719 46.82	39° 10.32′	110° 51.84′	10.0	1.9	8	168	4	0.12
88	820	2200 1.23	39° 8.59′	110° 50.53′	13.0	1.1	12	67	2	0.06
88	821	221 8.69	39° 8.21′	110° 51.09′	12.5	1.3	8	102	2	0.02
88	821	226 46.81	39° 7.55′	110° 51.22′	13.8	0.9	10	84	2	0.05
88	821	547 25.74	39° 8.81′	110° 49.93′	14.9	1.1	10	115	1	0.04
88	821	912 9.95	39° 7.90′	110° 50.23′	13.7	0.6	8	89	3	0.09
88	821	1043 30.37	39° 8.63′	110° 50.69′	11.1	0.8	7	116	2	0.03
88	821	1107 52.27	39° 7.80′	110° 50.94′	11.2	0.3	8	88	2	0.02
88	821	1158 15.52	39° 8.05′	110° 50.23′	15.4	1.1	11	87	3	0.05
88	821	1335 7.77	39° 4.51′	110° 52.56′	20.4	--	5	259	4	0.12
88	821	1435 40.24	39° 5.21′	110° 50.92′	17.9	--	5	242	2	0.07
88	821	2342 37.71	39° 7.22′	110° 50.03′	16.6	2.0	7	97	2	0.02

San Rafael Swell, Utah, Earthquake Sequence

yr	*date*	*origin time*	*latitude*	*longitude*	*depth*	*mag*	*no*	*gap*	*dmin*	*rms*
88	823	55 15.98	39° 6.11′	110° 52.70′	15.4	--	5	240	2	0.04
88	823	59 28.96	39° 6.33′	110° 52.39′	16.2	--	5	234	2	0.08
88	823	715 15.13	39° 14.49′	110° 44.94′	6.3	--	5	286	12	0.30
88	823	1055 41.57	39° 7.27′	110° 52.25′	20.8	--	5	185	2	0.04
88	823	1109 33.74	39° 5.94′	110° 50.75′	17.4	--	5	208	1	0.06
88	823	2010 44.72	39° 8.67′	110° 50.57′	13.5	1.7	12	66	2	0.06
88	823	2109 13.38	39° 7.50′	110° 51.18′	17.5	--	5	119	2	0.03
88	824	52 30.16	39° 8.32′	110° 49.46′	18.3	1.0	8	115	2	0.05
88	824	118 10.28	39° 9.64′	110° 49.10′	9.6	--	5	209	1	0.03
88	824	241 48.03	39° 9.55′	110° 49.40′	11.2	--	5	205	1	0.01
88	824	1642 29.34	39° 8.48′	110° 52.01′	8.4	--	5	113	1	0.03
88	824	2045 47.30	39° 8.15′	110° 51.23′	12.4	1.4	10	101	4	0.04
88	824	2245 10.20	39° 8.83′	110° 49.86′	14.3	0.6	6	190	1	0.01
88	825	26 56.93	39° 7.83′	110° 51.09′	13.1	1.9	14	72	2	0.04
88	825	47 10.98	39° 7.87′	110° 51.17′	13.3	1.3	5	179	4	0.01
88	825	1756 41.86	39° 7.24′	110° 50.62′	14.6	0.8	5	87	2	0.01
88	825	2032 30.97	39° 12.43′	110° 47.05′	30.2	0.7	5	241	7	0.06
88	825	2128 47.12	39° 8.94′	110° 49.81′	15.2	1.7	9	125	1	0.07
88	825	2136 24.35	39° 7.46′	110° 51.08′	14.2	2.5	17	41	2	0.02
88	825	2155 11.94	39° 7.84′	110° 51.61′	12.5	2.2	11	93	3	0.05
88	825	2333 10.88	39° 7.53′	110° 51.10′	14.0	2.8	16	43	2	0.03
88	826	113 16.79	39° 8.42′	110° 51.19′	13.1	1.6	9	110	2	0.03
88	826	856 27.62	39° 7.95′	110° 50.79′	14.1	0.6	8	91	3	0.02
88	826	1116 24.71	39° 7.84′	110° 51.46′	14.1	0.5	7	93	2	0.02
88	826	1927 17.53	39° 7.88′	110° 51.12′	14.0	2.6	16	48	2	0.03
88	826	1938 39.17	39° 7.12′	110° 50.10′	16.5	1.0	8	99	2	0.02
88	826	2243 11.55	39° 9.07′	110° 50.08′	15.1	1.5	5	216	1	0.
88	826	2252 37.01	39° 6.84′	110° 50.70′	14.4	1.2	5	146	1	0.01
88	827	625 49.67	39° 8.72′	110° 49.79′	15.5	1.3	6	123	1	0.02
88	827	652 41.44	39° 7.16′	110° 50.55′	15.5	2.0	6	99	2	0.03
88	827	1750 55.86	39° 7.83′	110° 50.62′	13.7	0.4	8	85	3	0.04
88	828	2231 26.07	39° 8.57′	110° 50.84′	11.9	1.0	7	114	3	0.03
88	829	521 0.88	39° 7.93′	110° 50.72′	14.0	0.9	8	89	3	0.03
88	829	2057 0.16	39° 7.83′	110° 50.72′	16.2	0.8	5	169	3	0.03
88	830	1832 6.00	39° 8.93′	110° 49.70′	15.5	1.0	8	120	1	0.02
88	831	514 53.83	39° 6.73′	110° 50.76′	11.2	1.1	8	81	1	0.05
88	831	738 48.40	39° 7.99′	110° 50.73′	13.2	1.1	7	91	3	0.02
88	831	809 16.08	39° 8.37′	110° 49.91′	15.4	0.6	8	92	2	0.03
88	831	834 13.44	39° 7.58′	110° 50.30′	15.7	1.2	9	74	3	0.02
88	901	1532 39.67	39° 7.46′	110° 50.96′	14.3	1.3	5	110	3	0.10
88	901	1959 16.07	39° 7.95′	110° 51.10′	13.6	1.2	6	123	4	0.
88	901	2326 10.02	39° 9.72′	110° 50.33′	13.1	1.8	11	85	2	0.09
88	902	2116 50.77	39° 8.62′	110° 49.99′	23.7	0.9	5	129	2	0.04
88	903	755 51.99	39° 8.09′	110° 51.08′	13.6	2.1	11	73	3	0.03
88	904	932 12.70	39° 8.08′	110° 51.24′	12.1	1.8	10	73	4	0.05

San Rafael Swell, Utah, Earthquake Sequence

yr	*date*	*origin time*	*latitude*	*longitude*	*depth*	*mag*	*no*	*gap*	*dmin*	*rms*
88	907	404 44.44	39° 8.70′	110° 49.71′	14.7	2.0	5	132	1	0.01
88	907	420 51.02	39° 6.75′	110° 49.77′	17.8	1.1	5	105	2	0.
88	909	547 40.70	39° 9.49′	110° 49.20′	14.4	1.1	7	159	1	0.01
88	911	123 40.93	39° 8.87′	110° 50.01′	14.4	1.4	6	141	1	0.01
88	912	2316 9.21	39° 7.68′	110° 50.66′	15.1	1.4	7	109	3	0.02
88	913	2314 58.04	39° 7.07′	110° 50.27′	16.8	1.9	7	93	2	0.03
88	915	719 54.43	39° 7.27′	110° 50.88′	14.3	1.7	5	120	2	0.01
88	915	859 7.72	39° 7.57′	110° 51.32′	13.2	1.3	7	117	3	0.01
88	916	209 12.68	39° 10.26′	110° 48.32′	19.1	0.8	5	220	2	0.03
88	920	1310 40.52	39° 8.98′	110° 49.43′	14.6	1.6	5	130	1	0.
88	921	2028 13.74	39° 8.23′	110° 51.18′	13.3	1.7	7	87	3	0.01
88	923	1433 40.44	39° 7.67′	110° 49.99′	14.8	1.0	5	146	3	0.01
88	923	2252 1.62	39° 8.09′	110° 50.48′	15.0	1.6	7	130	3	0.02
88	925	711 47.96	39° 7.57′	110° 51.22′	14.0	1.4	7	115	3	0.02
88	925	859 38.42	39° 8.25′	110° 51.44′	12.9	1.8	8	73	4	0.01
88	925	1143 11.96	39° 6.95′	110° 50.26′	16.5	1.5	7	90	2	0.02
88	930	645 42.29	39° 9.33′	110° 49.54′	16.8	1.6	5	215	1	0.01
88	930	810 50.98	39° 6.97′	110° 50.94′	14.2	1.9	6	101	2	0.01
88	930	1127 0.28	39° 8.58′	110° 50.07′	14.9	2.1	12	73	2	0.05
88	930	1130 35.46	39° 8.93′	110° 49.72′	15.0	1.6	5	138	1	0.
88	930	1138 58.00	39° 8.95′	110° 49.72′	15.1	1.9	5	140	1	0.
88	1001	248 10.02	39° 8.83′	110° 49.99′	14.0	1.1	5	195	1	0.01
88	1001	1844 49.77	39° 8.18′	110° 51.26′	12.7	2.0	12	73	4	0.02
88	1004	1323 6.82	39° 8.00′	110° 51.34′	12.9	2.0	5	186	4	0.02
88	1004	1508 1.06	39° 7.39′	110° 51.00′	10.3	1.3	5	163	3	0.05
88	1005	858 37.01	39° 6.26′	110° 49.90′	17.2	1.8	8	128	1	0.07
88	1008	104 52.76	39° 9.86′	110° 50.43′	23.6	1.8	5	224	2	0.06
88	1010	246 51.40	39° 8.58′	110° 49.64′	15.3	1.1	5	163	1	0.
88	1011	2306 17.95	39° 8.73′	110° 49.12′	15.6	2.8	7	80	1	0.02
88	1016	650 8.80	39° 7.93′	110° 50.49′	14.4	1.1	5	167	3	0.
88	1021	754 35.47	39° 8.92′	110° 50.54′	12.8	2.0	9	77	2	0.09
88	1024	1954 12.39	39° 8.95′	110° 51.69′	10.9	2.1	8	155	4	0.05
88	1025	808 47.34	39° 9.43′	110° 50.52′	13.0	2.3	12	84	2	0.06
88	1025	1633 15.51	39° 8.73′	110° 49.27′	15.5	0.7	5	142	1	0.01
88	1025	1929 27.08	39° 8.60′	110° 49.23′	15.5	1.1	5	134	1	0.01
88	1026	329 51.24	39° 8.81′	110° 49.30′	15.3	1.1	5	149	1	0.01
88	1101	331 52.11	39° 7.79′	110° 50.78′	14.9	0.1	5	169	3	0.
88	1101	612 54.18	39° 7.77′	110° 50.41′	15.6	2.3	12	72	3	0.09
88	1101	1114 13.92	39° 7.77′	110° 50.66′	14.6	1.6	7	111	3	0.01
88	1101	2220 45.52	39° 7.61′	110° 50.15′	15.4	1.4	5	149	3	0.01
88	1102	1549 1.13	39° 7.83′	110° 51.35′	13.1	1.5	5	191	4	0.02
88	1103	518 0.28	39° 7.35′	110° 51.43′	13.1	2.0	5	171	3	0.
88	1106	423 40.91	39° 8.13′	110° 51.37′	13.1	1.0	7	131	4	0.03
88	1109	442 7.58	39° 6.71′	110° 50.90′	15.5	1.6	7	98	2	0.06
88	1109	1353 52.10	39° 7.76′	110° 50.85′	14.6	1.2	6	114	3	0.01

San Rafael Swell, Utah, Earthquake Sequence

yr	*date*	*origin time*	*latitude*	*longitude*	*depth*	*mag*	*no*	*gap*	*dmin*	*rms*
88	1111	810 16.29	39° 7.12′	110° 50.85′	14.3	1.1	5	102	2	0.01
88	1112	1331 24.21	39° 6.78′	110° 50.15′	16.5	1.5	6	101	1	0.01
88	1118	2307 11.23	39° 11.32′	110° 50.43′	15.6	0.9	6	227	4	0.04
88	1119	733 38.32	39° 10.47′	110° 50.43′	17.1	1.6	7	141	3	0.03
88	1123	1631 33.91	39° 7.21′	110° 50.48′	13.7	0.5	5	148	2	0.02
88	1126	1938 12.92	39° 8.17′	110° 51.26′	14.5	0.9	5	190	4	0.02
88	1127	26 49.70	39° 7.76′	110° 50.90′	14.4	0.7	6	114	3	0.01
88	1127	722 37.27	39° 6.86′	110° 49.86′	17.4	1.5	6	103	2	0.01
88	1128	707 10.70	39° 8.71′	110° 49.21′	15.4	0.8	5	135	1	0.
88	1129	1436 11.32	39° 8.21′	110° 51.21′	12.7	2.4	11	73	3	0.04
88	1202	359 11.21	39° 8.76′	110° 50.83′	12.9	1.0	7	146	3	0.03
88	1207	1228 29.42	39° 7.68′	110° 47.89′	31.1	0.8	5	105	3	0.07
88	1211	1329 32.06	39° 7.39′	110° 49.73′	15.4	0.6	5	134	3	0.02
88	1219	29 15.44	39° 7.89′	110° 50.88′	11.7	2.1	6	124	20	0.04
89	108	1710 22.62	39° 8.15′	110° 51.56′	11.9	2.8	8	121	21	0.03
89	121	1029 52.93	39° 6.81′	110° 51.90′	4.5*	2.4	6	128	22	0.04
89	316	1516 20.09	39° 6.92′	110° 51.02′	14.2	2.9	6	129	21	0.01
89	321	1502 24.36	39° 7.84′	110° 50.78′	15.6	2.6	9	125	20	0.04
89	404	306 54.77	39° 6.86′	110° 50.63′	16.0	2.5	9	131	20	0.03
89	426	327 58.87	39° 8.77′	110° 50.08′	20.4	1.7	6	120	19	0.08
89	429	1429 53.71	39° 8.70′	110° 51.27′	11.0	1.9	7	119	21	0.07
89	514	942 15.11	39° 9.75′	110° 52.16′	11.8	2.2	7	113	22	0.06
89	514	1237 36.11	39° 9.68′	110° 52.31′	10.0*	1.8	6	112	22	0.03
89	520	425 43.63	39° 9.83′	110° 52.49′	10.5*	1.2	6	112	22	0.09
89	628	1805 14.58	39° 7.65′	110° 51.39′	12.0	2.3	8	125	21	0.08
89	714	2153 22.23	39° 8.54′	110° 51.21′	8.3*	2.5	7	121	20	0.07

number of earthquakes = 161

* indicates poor depth control
W indicates Wood-Anderson data used for magnitude calculation

Southern Wasatch Plateau, Utah, Earthquake Sequence

yr	*date*	*origin time*	*latitude*	*longitude*	*depth*	*mag*	*no*	*gap*	*dmin*	*rms*
88	319	2312 36.70	38° 44.09′	111° 29.13′	9.7*	1.8	9	139	52	0.25
88	320	209 7.78	38° 44.15′	111° 29.32′	9.8*	2.0	8	139	52	0.50
88	1113	1605 19.09	38° 55.44′	111° 30.29′	5.7*	2.8	9	109	31	0.48
89	123	1320 39.19	38° 48.54′	111° 30.62′	7.5*	2.0	10	102	43	0.36
89	130	406 22.82	38° 49.36′	111° 36.85′	24.7	5.4W	11	93	40	0.09
89	130	415 2.82	38° 47.92′	111° 37.14′	20.4*	1.9	12	93	43	0.05
89	130	419 33.08	38° 48.67′	111° 33.15′	21.5	1.1	8	160	42	0.11
89	130	422 24.54	38° 51.60′	111° 34.51′	23.3	2.1	11	130	36	0.09
89	130	432 20.45	38° 47.91′	111° 37.72′	19.8*	1.6	8	149	43	0.03
89	130	448 40.84	38° 49.76′	111° 36.46′	20.8	2.0	12	92	39	0.16
89	130	538 8.40	38° 48.82′	111° 36.83′	23.1	1.4	5	151	41	0.07
89	130	605 18.11	38° 50.74′	111° 35.43′	26.4	1.4	5	156	38	0.02
89	130	610 21.26	38° 52.24′	111° 33.96′	17.6*	1.7	9	131	35	0.12
89	130	618 10.26	38° 47.86′	111° 36.94′	13.5*	1.8	8	126	43	0.12
89	130	627 16.23	38° 49.67′	111° 36.33′	22.3	2.7	12	93	40	0.05
89	130	803 37.33	38° 49.14′	111° 36.83′	23.6	2.1	10	93	41	0.09
89	130	829 46.91	38° 48.70′	111° 36.76′	22.5	0.8	10	92	41	0.13
89	130	829 53.83	38° 49.00′	111° 37.73′	15.0*	2.3	11	92	41	0.27
89	130	904 41.92	38° 47.83′	111° 36.86′	21.9	1.8	7	126	43	0.07
89	130	1112 4.15	38° 49.62′	111° 36.47′	23.0	1.7	10	93	40	0.09
89	130	1240 2.55	38° 47.79′	111° 37.36′	21.9	2.5	11	92	43	0.08
89	130	1325 35.97	38° 49.14′	111° 36.66′	22.6	1.7	8	152	41	0.04
89	130	1444 38.96	38° 48.32′	111° 35.55′	20.3*	1.6	7	154	42	0.06
89	130	1732 12.69	38° 49.84′	111° 36.30′	21.4	2.0	10	92	39	0.03
89	131	1043 42.98	38° 47.07′	111° 34.96′	19.3*	1.6	8	155	45	0.04
89	131	1617 21.98	38° 49.67′	111° 36.57′	22.4	2.3	11	93	8	0.07
89	131	2142 2.83	38° 49.28′	111° 36.37′	23.0	2.6	13	67	8	0.06
89	131	2255 6.74	38° 49.75′	111° 36.40′	22.8	2.3	13	53	8	0.08
89	201	642 50.97	38° 49.39′	111° 36.45′	22.8	1.7	15	68	8	0.05
89	201	905 19.63	38° 48.81′	111° 36.71′	22.2	1.2	11	62	8	0.06
89	201	1537 21.05	38° 51.06′	111° 34.91′	23.0	1.5	10	93	4	0.09
89	201	1546 56.80	38° 49.60′	111° 36.59′	21.5	1.8	14	67	8	0.07
89	203	902 20.69	38° 49.32′	111° 34.39′	21.2	1.6	12	83	5	0.12
89	204	113 31.31	38° 49.92′	111° 36.38′	22.7	2.1	15	53	7	0.07
89	208	1029 36.27	38° 47.95′	111° 37.45′	15.8	1.6	9	149	13	0.10
89	209	1142 53.80	38° 49.77′	111° 36.29′	21.5*	1.6	7	127	45	0.02
89	209	2124 35.62	38° 49.91′	111° 36.41′	23.9	1.5	8	67	3	0.01
89	214	1656 33.13	38° 49.69′	111° 36.50′	25.0	2.6	12	72	2	0.09
89	218	158 41.11	38° 50.59′	111° 27.36′	4.0	1.6	8	131	8	0.18
89	219	1436 8.51	38° 48.10′	111° 37.20′	22.0	1.8	11	80	2	0.04
89	220	1938 51.04	38° 44.40′	111° 40.14′	16.0	1.0	7	105	9	0.11
89	222	506 1.78	38° 49.70′	111° 35.97′	24.4	1.1	7	114	3	0.05
89	224	17 16.40	38° 49.21′	111° 36.87′	23.1	0.8	6	108	1	0.05
89	225	317 48.03	38° 48.49′	111° 37.47′	22.4	1.3	6	97	1	0.13
89	227	1513 7.73	38° 49.42′	111° 37.04′	24.1	4.2W	12	66	1	0.09

Southern Wasatch Plateau, Utah, Earthquake Sequence

yr	*date*	*origin time*	*latitude*	*longitude*	*depth*	*mag*	*no*	*gap*	*dmin*	*rms*
89	227	1626 50.11	38° 49.26′	111° 36.74′	23.5	2.2	12	77	1	0.07
89	227	1741 54.19	38° 49.61′	111° 36.44′	23.1	1.6	10	77	2	0.07
89	305	1150 12.86	38° 45.68′	111° 33.69′	19.9	2.4	13	84	8	0.08
89	305	1931 42.82	38° 51.22′	111° 34.69′	24.6	1.3	5	195	6	0.02
89	305	1955 30.91	38° 51.35′	111° 34.64′	24.8	1.2	7	119	6	0.07
89	306	720 51.76	38° 48.39′	111° 30.21′	5.5	1.3	8	86	8	0.11
89	312	2321 38.96	38° 46.37′	111° 34.65′	7.5	2.8W	12	83	6	0.10
89	314	904 29.45	38° 48.33′	111° 38.45′	21.8	0.9	6	90	19	0.05
89	318	948 22.88	38° 49.53′	111° 36.43′	22.3	1.9	11	77	2	0.05
89	324	515 33.58	38° 49.99′	111° 36.56′	21.9	1.5	11	78	3	0.14
89	414	251 26.00	38° 55.25′	111° 31.93′	23.6	1.9	11	79	14	0.07
89	514	2347 1.72	38° 50.22′	111° 36.02′	24.4	1.1	6	117	3	0.03
90	126	1451 59.53	38° 47.44′	111° 38.50′	22.5	1.8	6	82	19	0.01

number of earthquakes = 58

* indicates poor depth control
W indicates Wood-Anderson data used for magnitude calculation

3. THE 1988 BEAR LAKE, UTAH, EARTHQUAKE

ABSTRACT

On November 19, 1988, an M_L 4.8 earthquake occurred near the Utah-Idaho border approximately 5 km west of Bear Lake. Historically, this region was the site of an earthquake of estimated magnitude 6 in 1884, believed to have occurred in the Bear Lake Valley. An M_L 2.6 foreshock occurred 5 minutes before the 1988 main shock. Twenty aftershocks of magnitude 2.0 and larger occurred from November 1988 through June 1989, with the largest (M_L 4.3) occurring 18 minutes after the main shock.

The University of Utah Seismograph Stations deployed five portable seismographs, within 12 km of the main shock epicenter, from November 20 through November 23 (severe snow conditions precluded longer monitoring). We used data from these stations and from the University of Utah's regional seismic network to relocate the Bear Lake earthquakes with a local velocity model and station delays determined from well-located aftershocks. Focal depths are poorly constrained, but the best-located hypocenters lie between 7 and 12 km depth. A preliminary focal-mechanism for the main shock indicates normal faulting, possibly with a strike-slip component of motion, on one of two possible fault planes: one is nearly vertical, with a north-south strike; the other has a dip of less than 38°, and perhaps as small as zero, but has a poorly-constrained strike.

INTRODUCTION

At 19:42 UTC (12:42 p.m. MST) on November 19, 1988, an M_L (local magnitude) 4.8 earthquake occurred along the Utah-Idaho border, 5 km west of Bear Lake (Figure 3-1). The earthquake was felt throughout northern Utah and southeastern Idaho, with a maximum Modified Mercalli Intensity of V (U.S. Geological Survey, 1988).

This report presents the results of an aftershock study carried out following the earthquake, along with a focal mechanism for the main shock. The preferred focal mechanism shows normal faulting on a fault that is either nearly vertical with a N-S strike or nearly horizontal. Unfortunately, we were unable to resolve the causative fault plane from the aftershock locations.

GEOLOGICAL SETTING

The 1988 Bear Lake earthquake took place in the Middle Rocky Mountains physiographic province in a region cut by NNE- to NNW-striking Quaternary normal faults (Figure 3-1; Evans,

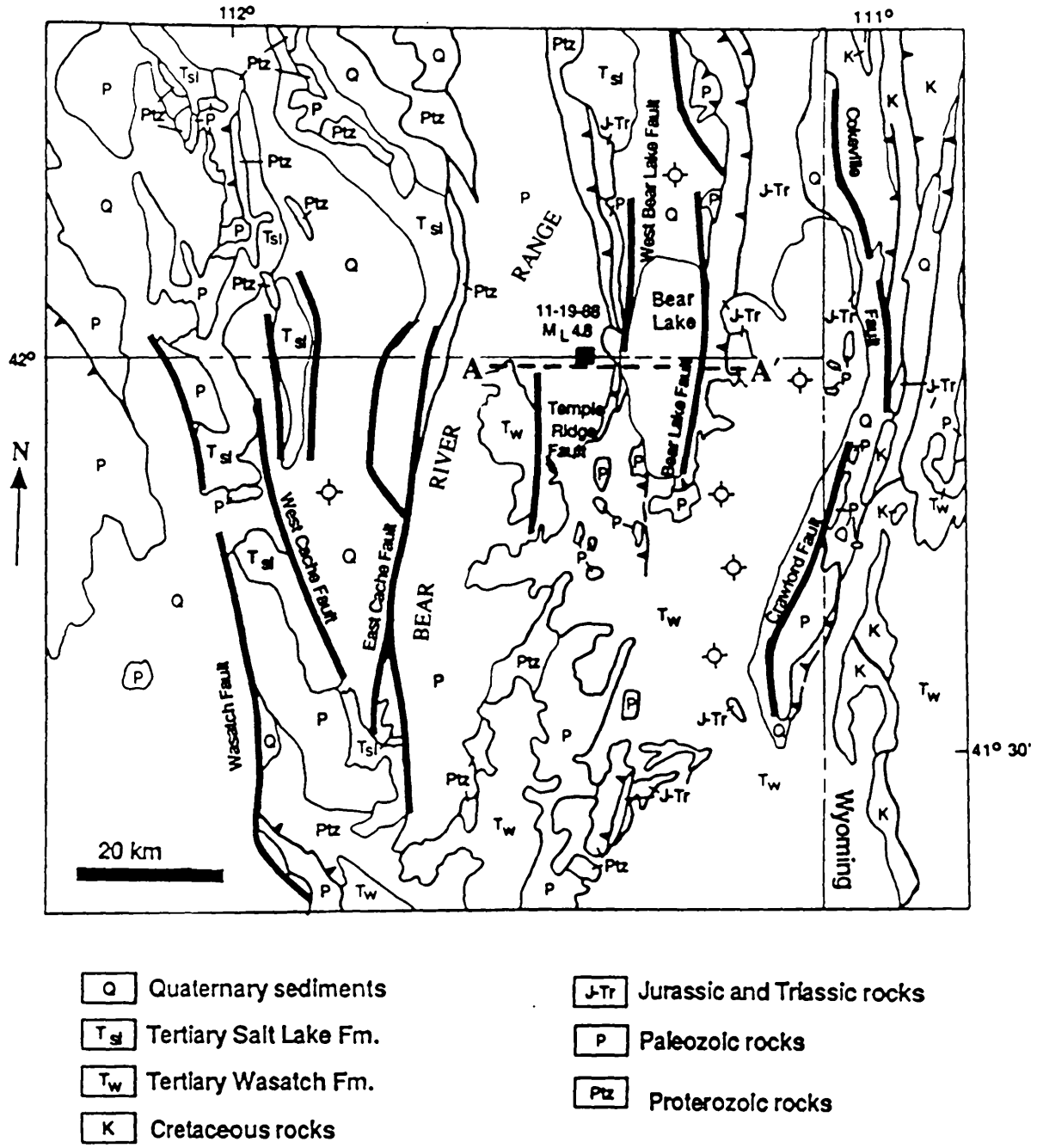

Fig. 3-1. Generalized geologic map of northern Utah, southern Idaho, and western Wyoming from Evans (1991). Major normal faults are indicated by heavy solid lines. The epicenter of the 1988 M_L 4.8 Bear Lake earthquake is shown as a square.

1991; Hecker, 1991). The epicenter of the earthquake is 18 km W of the surface trace of the active Bear Lake fault, a major W-dipping normal fault that follows the eastern shore of Bear Lake. Evans (1991) interprets the Bear Lake fault to be a listric normal fault which probably soles into the Sevier-age (Cretaceous) Meade thrust fault at depth (Figure 3-2). Evans bases his interpretation on an E-W-trending seismic reflection profile along the northern shore of Bear Lake. This same reflection profile also shows a zone of steeply-dipping normal faults at depths of 4 to 11 km in the hanging wall of the Meade thrust (Figure 3-2). Evans (1991) believes it likely that these faults extend southward along the strike direction of the regional structure into the vicinity of the epicenter of the 1988 earthquake. We refer the reader to Evans (1991) for further information on the geology of the Bear Lake region and its relationship to seismicity.

PRIOR SEISMICITY

Regional Seismicity

The 1988 Bear Lake earthquake occurred in a region of low to moderate seismicity within the Intermountain Seismic Belt (Smith and Arabasz, 1991; Figure 3-3). The largest earthquake to occur within 25 km of the 1988 shock took place on November 10, 1884, at 08:50 UTC. The 1884 earthquake was felt strongly in Idaho, Utah, and Wyoming over at least 15,000 km^2 (Williams and Tapper, 1953). Descriptions of damage, MMI = VIII, and reports of at least 6 shocks felt at Paris, Idaho, in the Bear Lake Valley led Arabasz and McKee (1979) to assign an epicenter at 42° 0′ N, and 111° 16′ W, arbitrarily on the Idaho-Utah border astride the active Bear Lake fault. They estimated a magnitude of 6.3 for this earthquake from a relationship between MMI and magnitude developed by Gutenberg and Richter (1956). According to Smith and Arabasz (1991), a magnitude of at least 5½ seems likely for the 1884 earthquake.

From July 1962, when the University of Utah regional seismic network began operating, through November 18, 1988, the University of Utah located 24 earthquakes of $M \geq 2.0$ and 4 earthquakes of $M \geq 3.0$ with epicenters within 25 km of that of the 1988 main shock. The most notable of these events was the M_L (local magnitude) 5.7 Cache Valley earthquake that occurred on August 30, 1962. Westaway and Smith (1989), relying on aftershock locations by Westphal and Lange (1966), revised the location of the 1962 Cache Valley epicenter to 13 km south of the University of Utah catalog location shown on Figure 3-3. Their revised epicenter for the earthquake is 23 km WSW of the 1988 main shock.

A prominent feature of the 1962-1988 seismicity in the Bear Lake region (Figure 3-3) is a linear band of earthquakes that trends roughly N-S underneath the Bear River Range near 111° 40′. At approximately 41° 48′ N latitude the seismicity of the band appears to diverge to the east and west, continuing northward along two linear zones. The eastern branch trends towards the location of the 1988 Bear Lake sequence.

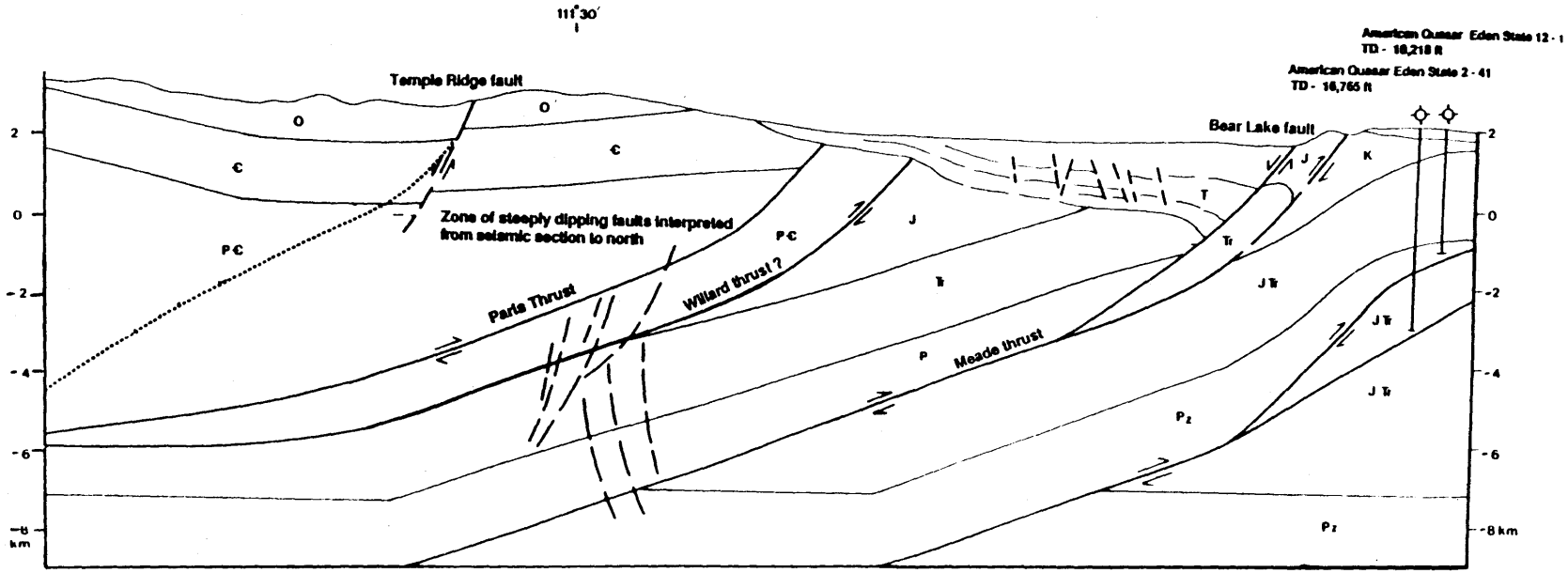

Fig. 3-2. Generalized geological cross-section from Evans (1991) along line A-A′ on Figure 3-1.

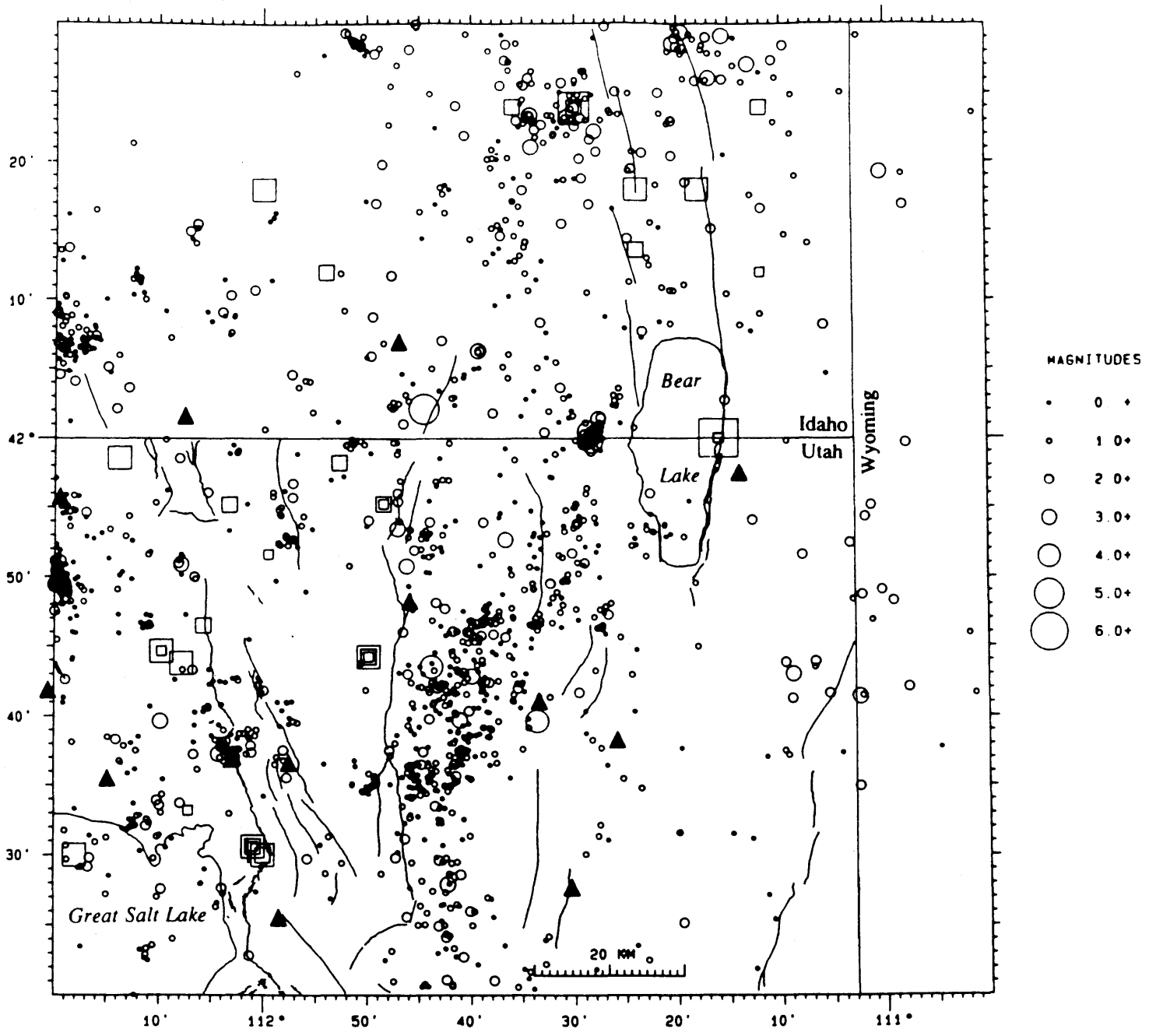

Fig. 3-3. Earthquake epicenter map of the region shown in Figure 3-1. The squares represent epicenters of earthquakes from 1850 through June 1962 (Arabasz et al., 1979). The circles represent earthquake epicenters located by the University of Utah Seismograph Stations from July 1962 through December 1988 (Arabasz et al., 1979; Richins et al., 1981, 1984; Brown et al., 1986; Nava et al., 1990). Both the circles and squares are scaled by magnitude. The solid lines represent Quaternary faults from Hecker (1991 and personal communication) and Witkind (1975). The solid triangles show stations of the University of Utah regional seismic network operating in November 1988.

Seismicity in the Epicentral Area

The area within 5 km of the University of Utah catalog epicenter for the 1988 Bear Lake earthquake (Nava et al., 1990) has been seismically active since at least the mid-1970's, when the University's regional seismic network was significantly upgraded and expanded. Within this 5-km-radius area, the catalog lists 9 earthquakes of M_c (coda magnitude) $\leq$ 1.6 from 1975 through 1985, an M_c 3.5 earthquake on October 18, 1986, a cluster of four earthquakes of 0.8 $\leq M_c \leq$ 2.4 on March 24, 1987, an M_c 2.0 earthquake on January 20, 1988, and an earthquake of M_L 2.6 on November 19, 1988, that occurred (as a foreshock) at 19:37 UTC, five minutes before the M_L 4.8 main shock.

The pattern of seismic activity observed during the two years prior to the 1988 Bear Lake main shock—an earthquake cluster or swarm, followed by relative quiescence, and then a foreshock—is similar to the pattern of activity observed before the 1988 San Rafael swell earthquake and a number of other main shocks elsewhere in the world (see Chapter 2 of this report). However, the time interval between the "precursory swarm" and the subsequent main shock was twenty months for the Bear Lake earthquake, versus seven months for the San Rafael swell earthquake. In the case of the Bear Lake earthquake, the significance of the swarm is more debatable given the previous seismicity in the epicentral area. Small earthquake swarms have occurred elsewhere in the Bear Lake region. Also, it is possible that some of the pre-1980 earthquakes near the epicenter of the 1988 main shock were part of temporal clusters that were only partially detected because of a lack of nearby seismograph stations. Note that the two stations of the regional network located closest to the 1988 main shock were installed in October 1974 (Bear River Range, Idaho, 30 km WNW) and October 1979 (Black Mountain, Utah, 20 km E) (see Figure 3-3 and Nava et al., 1990).

Nine days before the 1988 Bear Lake earthquake, an M_L 2.5 shock occurred 15 km south of the epicenter of the impending main shock. We do not regard this event as a foreshock because it occurred well outside the aftershock zone of the main shock (see discussion of foreshocks to the southern Wasatch Plateau earthquake in Chapter 2 of this report).

EARTHQUAKE LOCATIONS

Deployment of Portable Instruments

Approximately 24 hours after the M_L 4.8 Bear Lake earthquake occurred, personnel from the University of Utah began deployment of five portable analog seismographs with smoked-paper recorders in the snow-covered epicentral area to augment the station coverage of the permanent network (Table 3-1; triangles, Figure 3-5). These stations remained in operation through November 23, 1988. We removed the stations after only 3 days of recording because an impending storm threatened to bury the instruments under several feet of snow. If this had

TABLE 3 - 1

STATIONS USED FOR MASTER-EVENT RELOCATIONS
OF THE BEAR LAKE EARTHQUAKE SEQUENCE

Station Name	Type†	Latitude N	Longitude W	Elevation (m)	P-wave Station Correction (sec)	First Event Recorded (UTC)* Date	First Event Recorded (UTC)* Time	Last Event Recorded (UTC)* Date	Last Event Recorded (UTC)* Time
LAK	M	41° 59.09′	111° 25.64′	1890	+.07	11-20	21:39	11-23	16.41
GCU	M	41° 57.51′	111° 24.68′	1966	+.02	11-20	21:39	11-23	16:41
FHI	M	42° 02.97′	111° 27.46′	2097	+.05	11-20	21:39	11-23	16:41
SCI	M	42° 05.81′	111° 30.99′	2073	−.12	11-20	23:23	11-23	16:41
SKI	M	41° 58.22′	111° 32.49′	2219	+.05	11-20	21:39	11-23	16:41
BEI	R	42° 07.00′	111° 46.94′	1859	+.10	11-10	16:36	12-22	20:34
BMUT	R	41° 57.49′	111° 14.05′	2243	+.07	11-10	16:36	12-22	20:34
HDU	R	41° 48.27′	111° 45.89′	1853	−.08	11-10	16:36	12-22	20:34
LSUT	R	41° 41.09′	111° 33.45′	2225	−.03	11-10	16:36	12-22	20:34
LTU	R	41° 35.51′	112° 14.83′	1585	+.19	11-10	16:36	12-22	20:34
MCU	R	41° 27.70′	111° 30.45′	2664	+.08	11-10	16:36	12-22	20:34
PTU	R	41° 55.76′	112° 19.48′	2192	−.15	11-10	16:36	12-22	20:34
RSUT	R	41° 38.31′	111° 25.90′	2682	−.15	11-10	16:36	12-22	20:34
WVUT	R	41° 36.61′	111° 57.55′	1828	+.22	11-10	16:36	12-22	20:34

†R = UUSS regional network, M = microearthquake recorder
*From November 10 through December 31, 1988

happened, the instruments would likely have been lost for the winter. The seismometers of the temporary stations were all high-gain, short-period, vertical-component velocity transducers.

Velocity Model

We computed the earthquake locations for the study using P-wave arrival times and the one-dimensional velocity model in Table 3-2. As with the other aftershock studies in this report, we did not use any S-wave arrival times for our relocations because there were no horizontal-component records from nearby stations to provide reliable S-wave data.

The velocity model used to locate the earthquakes in the study derives from two sources. The velocities for the uppermost 4 km are adapted from a study by Evans (1991). He gives generalized velocity information for the Bear Lake region taken from "velocity profiles for several drill holes and from recommendations of several exploration geophysicists familiar with the area." The velocity information for the layers below 4 km is adapted from the "Wasatch Front" model of Bjarnason and Pechmann (1989). Their model is a modified version of velocity model B of Keller et al. (1975), which was determined from a 245-km-long unreversed seismic refraction profile that extended from Salt Lake City, Utah, southward along the Basin and Range-Colorado Plateau transition zone. A search for sonic logs from deep wells in the region covered by Figure 3-5 proved unsuccessful. We applied elevation corrections to the observed arrival times using the method explained in Chapter 2 of this report and assuming a near-surface velocity of 3.0 km/sec.

Station Delays

In order to improve the relative locations of the Bear Lake earthquakes, we used the master event technique described in Chapter 2 of this report to calibrate station delays for both the temporary stations and the nearby permanent stations of the regional network (see Johnson and Hadley, 1976, and Corbett, 1984). We chose as master events the three largest aftershocks ($1.9 \leq M_c \leq 2.6$), which occurred while the portable stations were operational.

We located these master events with the computer program HYPOINVERSE (Klein, 1978) and the velocity model in Table 3-2. For these initial locations, we set the distance weighting parameters within the program to give full weight to all of the temporary stations and to regional network stations within 30 km. Arrival times from the more distant regional network stations were downweighted with a cosine taper from a weight of one at a distance of 30 km to a weight of zero at a distance of 100 km (see Klein, 1978, and Chapter 2 of this report).

The station delays were set equal to the median of the travel-time residuals for the master events (Table 3-1). We then subtracted these station delays, along with the elevation delays, from the observed arrival times before locating the earthquakes with HYPOINVERSE. In

TABLE 3 - 2

BEAR LAKE VELOCITY MODEL

P-Wave Velocity (km/sec)	Depth to Top of Layer (km)*
4.9	0.0
5.8	1.2
5.9	4.0
6.4	17.6
7.5	28.5
7.9	42.5

*Datum is 2000 meters above sea level.

computing the final sets of locations, we used only those stations for which we had determined a station delay, and we applied no distance weighting. The trial hypocenter for the locations was the median hypocenter of the master events.

Compilation of Data Set

We used the master event technique to relocate 59 Bear Lake earthquakes that were recorded by the triggered digital recording system of the regional seismic network. The earthquakes selected for relocation (1) had an initial epicenter within 15 km of that of the 1988 main shock, and (2) occurred during the two-year period beginning one year before the main shock. In addition, we located 98 earthquakes that were recorded on the five portable seismographs during their three day deployment but were too small to trigger the centralized digital recording system of the regional network. For most of these 98 earthquakes, we supplemented the arrival time readings from the portable stations with readings from continuous analog records of the permanent station at Black Mountain, Utah. Magnitudes were calculated using the standard procedures described in Nava et al. (1990). Magnitudes and master-event locations for the 157 Bear Lake earthquakes that we analyzed are listed in the Appendix.

AFTERSHOCK SEQUENCE

Of the 152 aftershocks located in the study, 20 had magnitudes of 2.0 or greater and two had magnitudes of 3.0 or greater. The largest aftershock was an M_L 4.3 event at 20:00 UTC on November 19, 1988 (18 minutes after the main shock), which was felt in northern Utah and southeastern Idaho (U.S. Geological Survey, 1988). Of these 152 aftershocks, 72% occurred during the three-day time period when the portable seismograph stations were operational. Examination of a plot of magnitude versus time (Figure 3-4) confirms that this apparent concentration of activity is in large part due to the improved detection and location threshold during those three days. All aftershocks of $M_c \geq 1.8$ that were recorded by the temporary stations were also detected and located independently in the course of the routine analysis of the digital data from the regional network. Based on this fact, we infer that the magnitude threshold for uniformly complete detection by the regional seismic network is approximately M_c 1.8 in the Bear Lake region. When only events of $M \geq 1.8$ are considered the frequency of aftershock occurrence decreases gradually with time after the main shock (Figure 3-4). All but seven of the locatable aftershocks during the year following the main shock occurring during the 6-week time period shown in Figure 3-4.

An epicenter map of the master-event locations for the Bear Lake main shock and 111 of the best-located foreshocks and aftershocks is shown in Figure 3-5. Figure 3-6 shows the hypocenters of these earthquakes projected onto a vertical plane parallel to the line A-A′ in Figure 3-5. The locations for all of the earthquakes on these two plots meet the following selection criteria: (1) maximum azimuthal gap between stations of 180°, (2) minimum of six

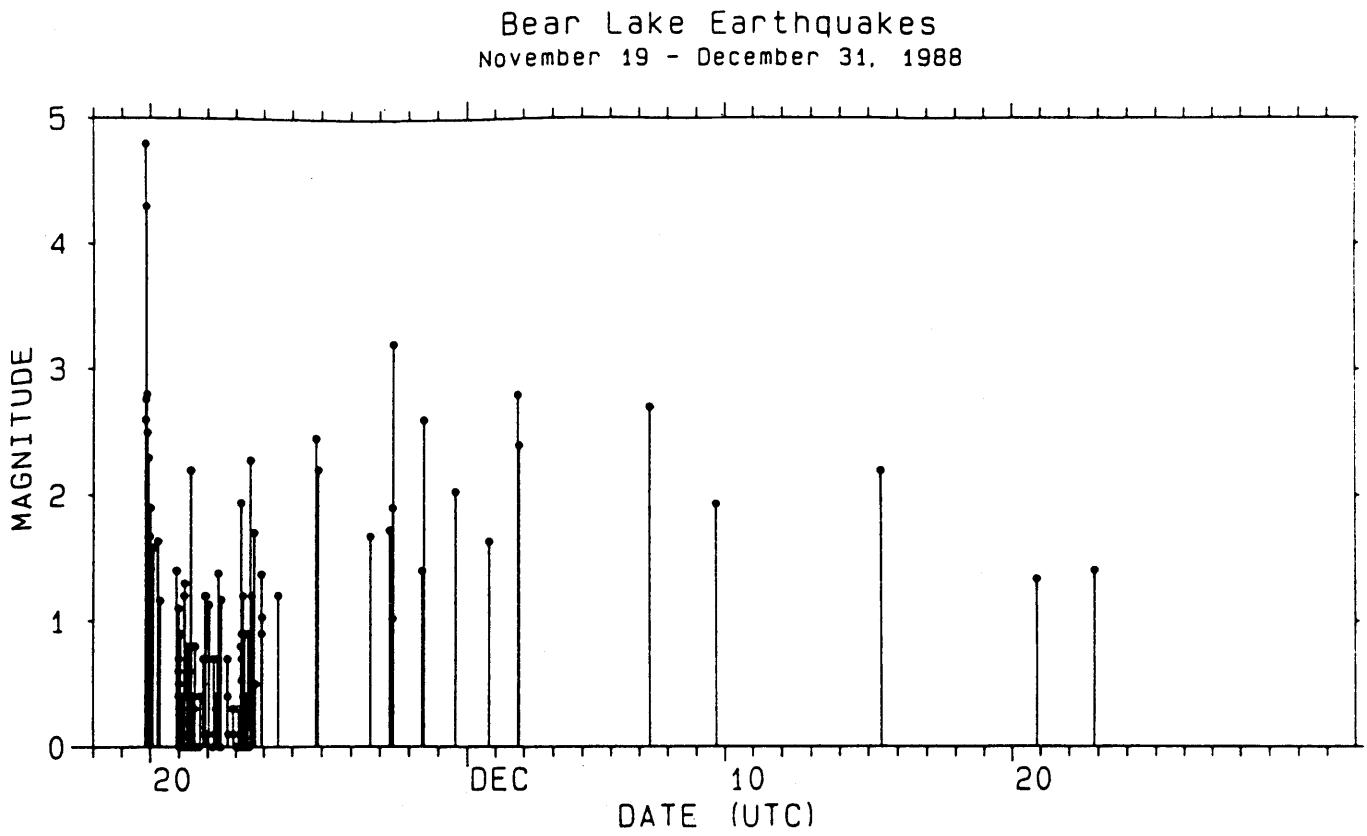

Fig. 3-4. Plot of magnitude versus time for the Bear Lake earthquake sequence from November 19 through December 31, 1988. This plot includes all earthquakes in the University of Utah catalog within 15 km of the main shock epicenter, plus additional earthquakes located in this study (see text). The sample is believed to be complete for $M \geq 1.8$. Small earthquakes not recorded on any stations of the permanent network were arbitrarily assigned a magnitude of 0.0, since we do not have a calibrated magnitude scale for use with the portable instruments.

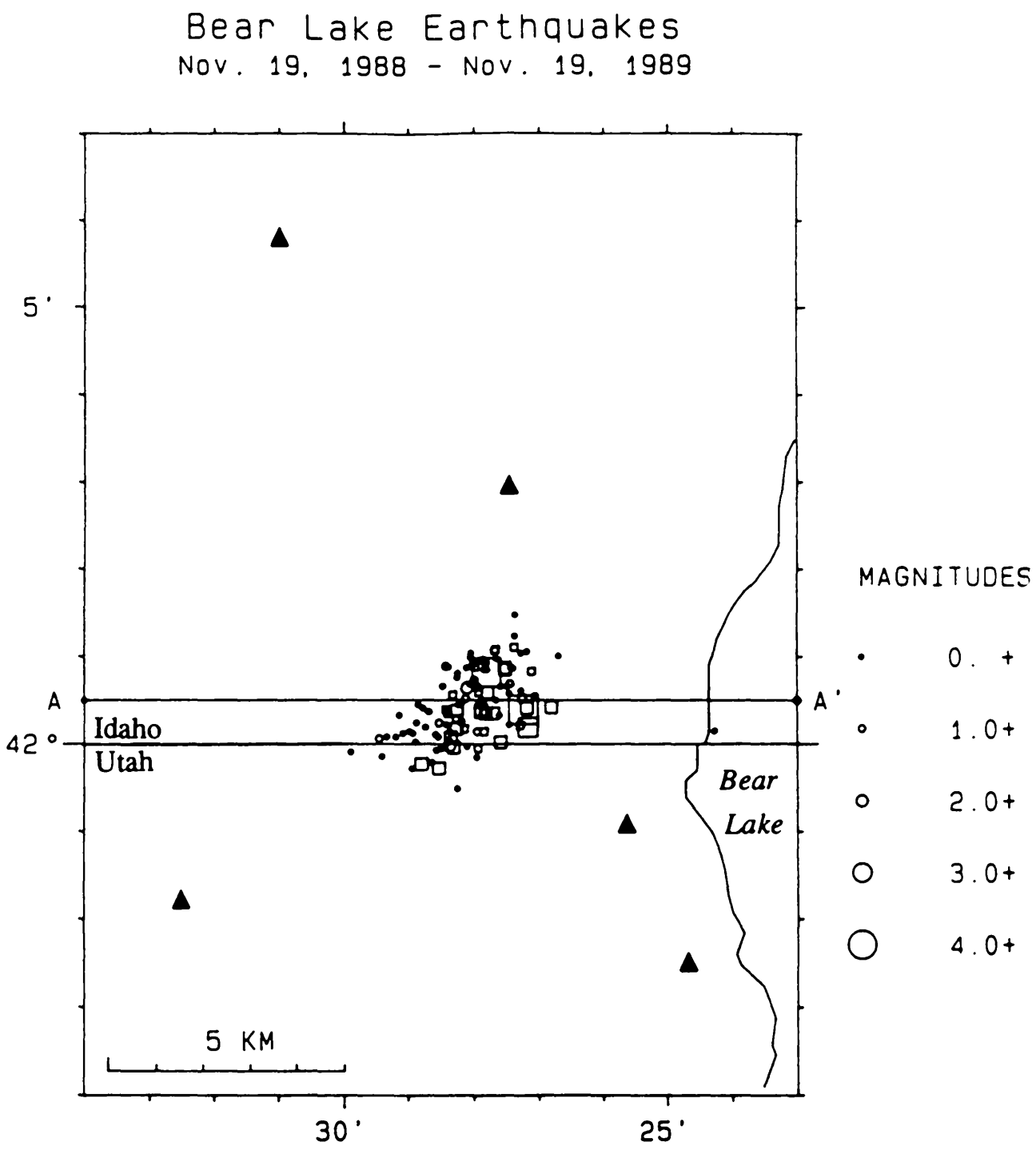

Fig. 3-5. Epicenter map of the 112 best-located earthquakes in the Bear Lake sequence from November 19, 1988, through November 19, 1989. See text for selection criteria. Circles indicate earthquakes that occurred when the portable stations were operating, and squares indicate earlier and later events. Symbol sizes are scaled by magnitude as shown. Portable analog seismograph stations (Sprengnether MEQ-800 smoked-paper recorders), deployed during the period November 20 to 23, 1988, are represented by triangles. The line A-A′ shows the surface projection of the cross-section in Figure 3-6. The NE-SW elongation of the aftershock zone is an artifact of location error (see text).

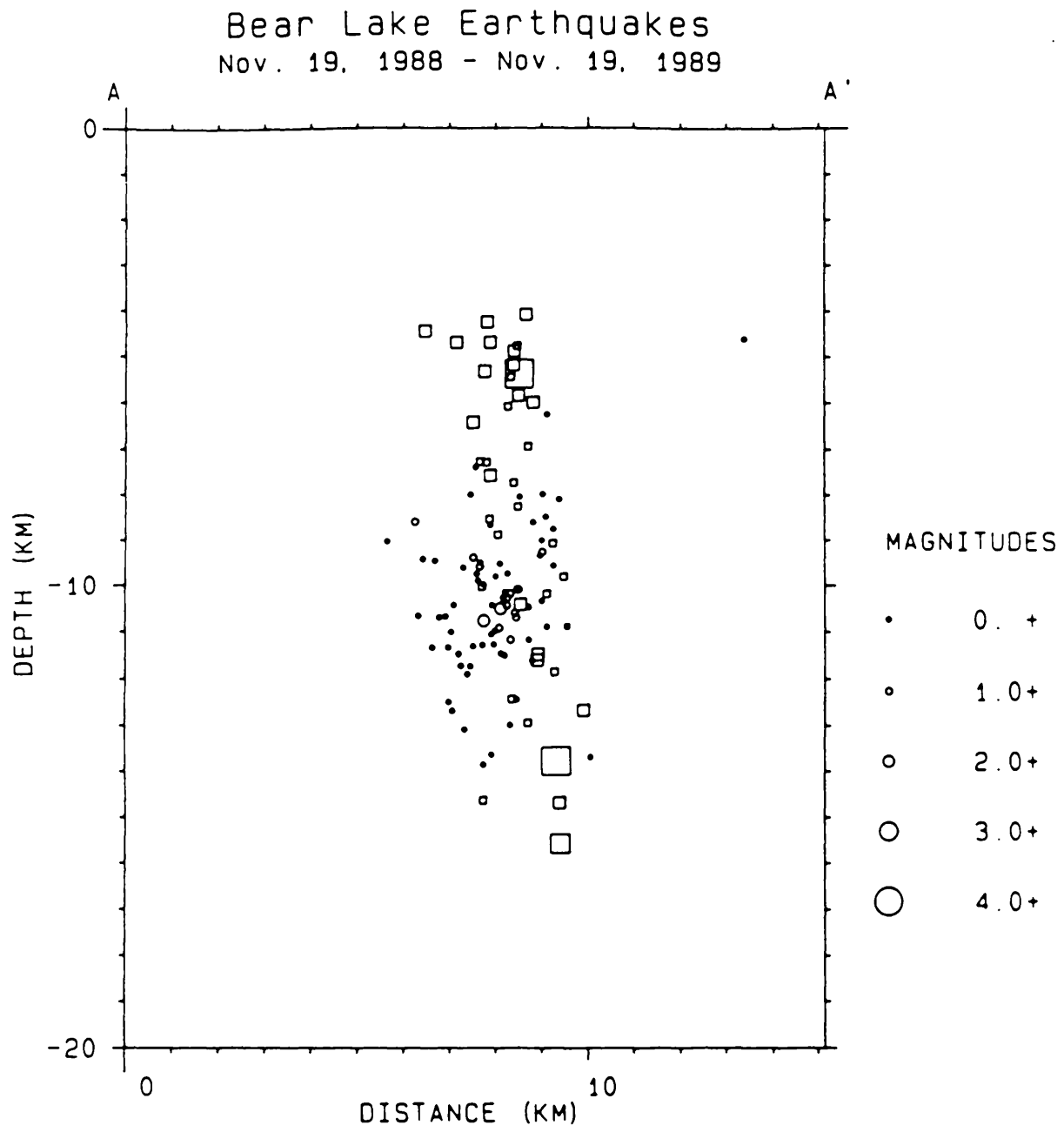

Fig. 3-6. Hypocentral cross-section of the earthquakes in Figure 3-5, taken along line A-A′ on Figure 3-5. Squares and circles as in Figure 3-5.

arrival times used for the location, (3) maximum root-mean-square of the weighted travel time residuals of 0.15 seconds, (4) maximum horizontal standard error of 1.5 km. The circles represent the earthquakes that took place while there were portable stations operating in the area. For all but one of these earthquakes, the epicentral distance to the nearest station was within 5 km. The squares represent earthquakes that were located with the permanent regional network stations only, the closest station of which was about 20 km away.

In map view, the epicenters of the best-located Bear Lake earthquakes form a NE-trending zone 4 km long and 2 km wide (Figure 3-5). Close examination of the data suggest that the NE trend of the aftershock zone is an artifact of location error. All but one of the epicenters west of 111° 28.5′ in Figure 3-5 are for aftershocks that occurred during the first two days of operation of the five portable stations (Figure 3-7). These epicenters were determined primarily with the data from the portable stations. Unfortunately, there is some uncertainty in the clock drift corrections applied to the P-wave arrival time picks obtained for this time period from station SKI, the only temporary station located SW of the aftershock activity. Because of this uncertainty, the arrival time picks from the first two days of records at SKI were given a maximum weight equal to one-half of the full weight. The downweighting of these SKI arrival times and/or improper clock drift corrections have apparently produced larger scatter in the aftershock epicenters along the azimuth to station SKI than in other directions (Figure 3-5). If the epicenters computed with the questionable SKI readings are removed from the data set, the remaining epicenters form a 2-km-wide roughly equidimensional distribution in map view. We examined other quality-selected subsets of the epicentral data, such as the 18 aftershocks that were recorded by both the temporary stations and at least two regional network stations. These other subsets of the data also failed to reveal any distinct azimuthal trends in the aftershock distribution.

The hypocenters plotted in the cross section shown in Figure 3-6 are distributed in a narrow zone ranging in depth from 4 to 16 km. However these data have erz (standard vertical error) values which average 3.6 km. Selecting those earthquakes with an erz $\leq$ 3 km results in a data set of 67 earthquakes in which 92% of the data cluster between depths of 7 and 12 km, with no discernible trends. Thus, it appears that the dimensions of the Bear Lake aftershock zone are relatively small, approximately 2 km (length) x 2 km (width) x 5 km (depth). These dimensions are comparable to the location errors of the hypocenters, which makes it difficult or impossible to resolve the true shape of the aftershock zone.

MAIN SHOCK FOCAL MECHANISM

We computed a focal mechanism for the 1988 Bear Lake main shock using P-wave first motion data primarily from the University of Utah seismic network, and velocity models and procedures described in Bjarnason and Pechmann (1989; Figure 3-8). The Jackson Lake seismic network in E Idaho and W Wyoming, operated by the U.S. Bureau of Reclamation, provided added data from stations to the north of the epicenter. The focal depth of 13.8 km that we computed for the main shock has a rather large standard error of 4.7 km. For this

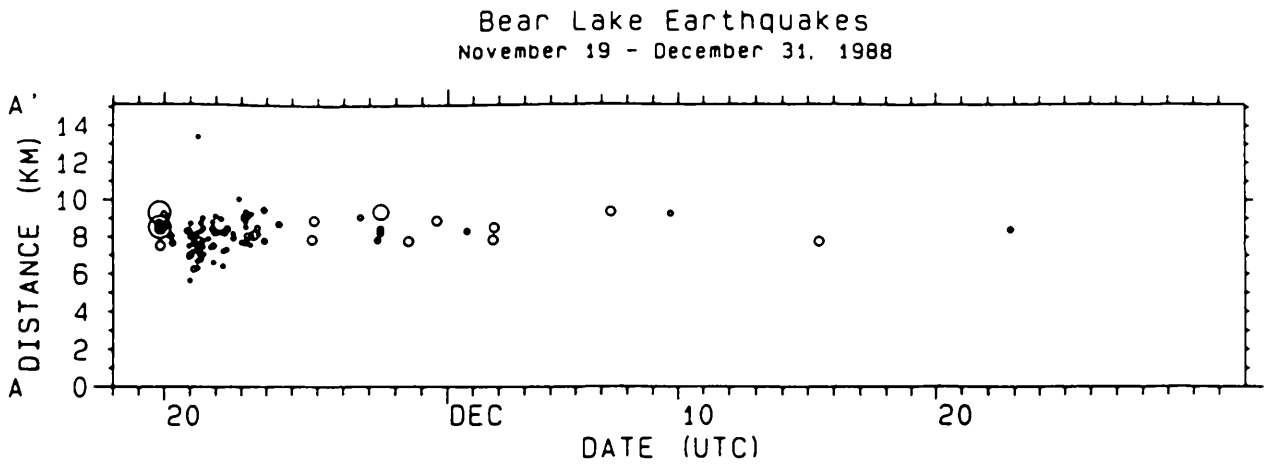

Fig. 3-7. Space-time plot of the best-located earthquakes of the 1988 Bear Lake sequence from Figure 3-5. The space coordinate of the plot is the distance parallel to line A-A′ on Figure 3-5.

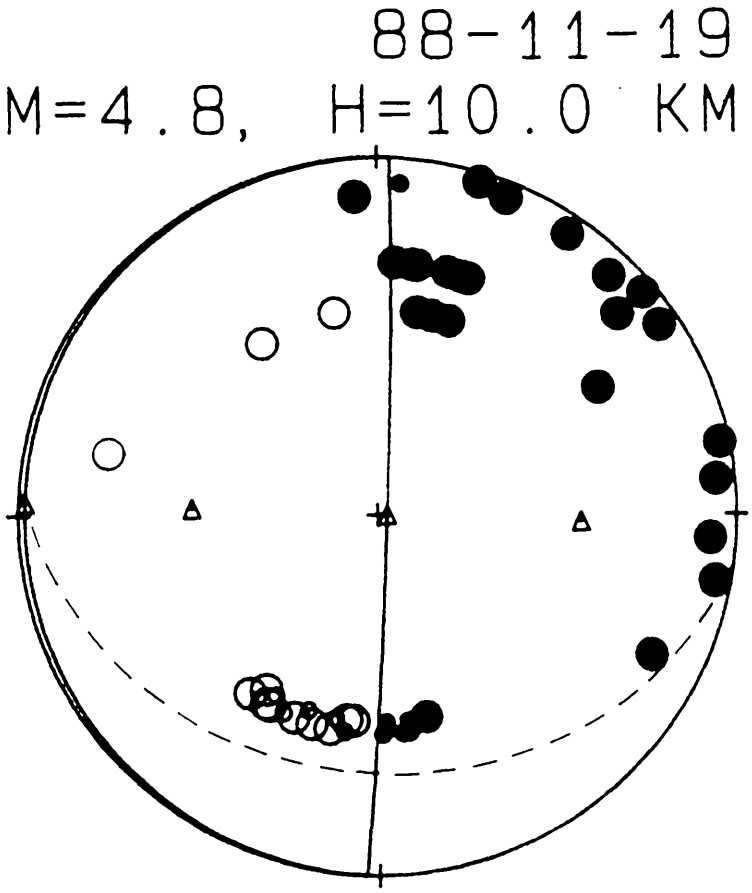

Fig. 3-8. Focal mechanism for the 1988 Bear Lake earthquake. P-wave first motions are plotted on a lower hemisphere equal area projection, with compressions shown as solid circles and dilatations as open circles. Smaller circles indicate readings of lower confidence. The triangles show slip vectors and P and T axes. The preferred nodal planes (one nearly vertical and one nearly horizontal) are shown by the solid lines. The dashed line shows an alternative orientation for the shallowly-dipping nodal plane.

reason, we decided to compute the focal mechanism for a fixed depth of 10 km, the median depth of the hypocenters with erz ≤ 3 km.

The focal mechanism indicated by the solid nodal planes in Figure 3-8 shows normal faulting on a fault that is either nearly vertical with a N-S strike or nearly horizontal. The steeply-dipping nodal plane is well constrained by the first-motion data to have a strike of 2° ± 10° and a dip of 88° ± 5°. The other nodal plane has a dip of less than 38°, and perhaps as small as zero, but a poorly-constrained strike. The dip of this plane can be significantly greater than zero only if its strike is close to E (dashed nodal plane, Figure 3-8). If the shallowly-dipping nodal plane is the fault plane, then the sense of motion on this plane could range from pure normal (solid nodal plane) to almost pure strike-slip (dashed nodal plane). The tension (T) axis of the focal mechanism plunges moderately to the E or ENE.

DISCUSSION

Hypocentral Resolution

The hypocentral data for the Bear Lake earthquake sequence cannot be easily interpreted, either because the location accuracy is inadequate to resolve the structure of this relatively small aftershock zone or because the distribution of the aftershocks was, in fact, diffuse. Our location accuracy for these earthquakes is not especially good, because the distribution of seismograph stations with respect to the activity was not ideal. Good hypocentral control requires high quality arrival time data from (1) at least one station at an epicentral distance which is less than the focal depth of the earthquake and (2) several more distant stations which are well-distributed in azimuth around the earthquake. The nearby stations constrain the focal depth of the earthquake, while the more distant stations constrain both the origin time and the epicentral location. Of the five temporary seismograph stations occupied after the main shock, the locations of four were approximately collinear because of siting constraints. Furthermore, all of the temporary stations were located within a distance of approximately one focal depth, resulting in poor epicentral control when these stations provided the bulk of the arrival time data. Unfortunately, very few aftershocks that occurred during the three-day deployment of the portable instruments were large enough to be recorded by more than one or two permanent network stations, in addition to the temporary stations.

Tectonic Implications

The focal mechanism for the 1988 Bear Lake earthquake is a rather unusual one. Focal mechanisms of earthquakes in the Utah-Idaho border region typically show normal or oblique-normal faulting on northerly-striking planes of moderate dip, although there are many exceptions (Jones, 1987; Bjarnason and Pechmann, 1989). Of the three largest instrumentally-

recorded earthquakes in this region, two involved normal faulting on N- to NE-striking planes with dips between 39° and 48°: the 1962 M_L 5.7 Cache Valley earthquake (Westaway and Smith, 1989) and the 1975 M_L 6.0 Pocatello Valley earthquake (Bache et al., 1980). The third earthquake, the 1934 M 6.6 Hansel Valley earthquake, involved left-lateral strike-slip faulting on a NE-striking plane with a dip greater than 84° (Doser, 1989). On a worldwide basis, only a small percentage of normal faulting earthquakes have a focal mechanism with a nodal plane that dips less than 30°, and for only a few of these earthquakes can the shallowly dipping plane be shown to be the fault plane (Abers, 1991; Jackson, 1987; Jackson and White, 1989). For this reason, there is considerable controversy about whether or not the many low-angle normal faults observed on seismic reflection profiles and in geological studies formed seismogenically at their current shallow dip (see, for example, Abers, 1991).

The aftershock locations determined in this study do not provide a reliable means to distinguish which of the two nodal planes of the focal mechanism for the 1988 Bear Lake earthquake is the fault plane. On geologic grounds, there does not appear to be any compelling reason to choose one nodal plane over the other. The geologic cross section of Evans (1991; Figure 3-2) shows both steeply-dipping and shallowly-dipping normal faults in the hypocentral region of the earthquake (located 5 to 10 km below sea level just E of 111° 30′ on Figure 3-2). Evans concluded that the 1988 Bear Lake earthquake could have occurred on either the steeply-dipping normal faults in the hanging wall of the Meade thrust, or on the Meade thrust itself, which he interprets to have been reactivated as part of the Bear Lake normal fault zone. Although Evans (1991) states that "slip along the steeply-dipping normal faults is the preferred solution" (p. 14), he does not explain the reasons for his preference. The available geological information does provide some basis for rejecting the dashed nodal plane (and similar nodal planes) as the fault plane, because all of the likely candidate faults in Figure 3-2 strike roughly N-S.

All of the possible focal mechanism solutions are difficult to reconcile with the regional stress field inferred from fault slip and focal mechanism data. The inferred stress field has principal stress axes oriented as follows: axis of minimum compressive principal stress, σ_3, horizontal and trending E-W; axis of intermediate principal stress, σ_2, horizontal and trending N-S; axis of maximum compressive principal stress, σ_1, vertical (Bjarnason and Pechmann, 1989; Zoback, 1989). The focal mechanism solution shown by the solid nodal planes in Figure 3-8 is the most consistent with the inferred σ_3 direction, and is therefore our preferred solution. However, both nodal planes of this focal mechanism are nearly perpendicular to one of the inferred principal stress axes, and would therefore be expected to have very little shear stress. The dashed nodal plane in Figure 3-8 has a strike that is nearly parallel to σ_3, and therefore the resolved shear stress across this plane should be nearly downdip. But if this plane is the fault plane, then this resolved shear stress direction would be nearly perpendicular to its slip vector.

CONCLUSIONS

1. The 1988 Bear Lake earthquake occurred in a region that had previously been seismically active and was preceded by an M_L 2.6 foreshock that occurred 5 minutes before the main shock.

2. The focal mechanism for the main shock indicates normal faulting, possibly with a strike-slip component of motion, on either a nearly vertical N-S-striking fault or a shallowly-dipping fault with a poorly-constrained strike. Regardless of which nodal plane is the fault plane, this focal mechanism is difficult to understand in the context of the currently accepted model for the regional stress field.

3. From depths of well-located aftershocks, we infer a focal depth for the main shock of between 7 and 12 km.

4. In map view, the size of the aftershock zone appears to be 2 km in diameter or less.

ACKNOWLEDGEMENTS

We thank Ken Whipp of the University of Utah and Jim Evans of Utah State University for helping to install and operate the portable seismographs. We also thank Jim Evans for keeping us informed about his work on the structural geology of the Bear Lake region. Linda Hall measured the arrival times and assisted with plotting the figures. Paula Oehmich computed the local magnitudes. Chris Wood of the U.S. Bureau of Reclamation kindly supplied arrival time and first motion data for the main shock from the Jackson Lake Seismograph Network. This research was supported by the U.S. Geological Survey, Department of the Interior, under award numbers 14-08-0001-G1349 and 14-08-0001-G1762, and by the Utah Geological Survey through contract number 89-3659. The views and conclusions contained in this report are those of the authors and should not be interpreted as necessarily representing the official policies, either expressed or implied, of either the U.S. Government or Utah State Government.

REFERENCES

Abers, G. A. (1991). Possible seismogenic shallow-dipping normal faults in the Woodlark-D'Entrecasteaux extensional province, Papua New Guinea, *Geology* **19,** 1205-1208.

Arabasz, W. J. and M. E. McKee (1979). Utah earthquake catalog 1850-June 1962, in *Earthquake Studies in Utah, 1850 to 1978*, W. J. Arabasz, R. B. Smith, and W. D. Richins, Editors, Special Publication, University of Utah Seismograph Stations, Salt Lake City, Utah, 119-121 and 133-143.

Arabasz, W. J., R. B. Smith, and W. D. Richins, Editors (1979). *Earthquake Studies in Utah, 1850 to 1978*, Special Publication, University of Utah Seismograph Stations, Salt Lake City, Utah, 552 pp.

Bache, T. C., D. G. Lambert, and T. G. Barker (1980). A source model for the March 28, 1975 Pocatello Valley earthquake from time domain modeling of teleseismic P waves, *Bull. Seism. Soc. Am.* **70,** 405-418.

Bjarnason, I. T. and J. C. Pechmann (1989). Contemporary tectonics of the Wasatch Front region, Utah, from earthquake focal mechanisms, *Bull. Seism. Soc. Am.* **79,** 731-755.

Brown, E. D., W. J. Arabasz, J. C. Pechmann, E. McPherson, L. L. Hall, P. J. Oehmich, and G. M. Hathaway (1986). *Earthquake Data for the Utah Region: January 1, 1984 to December 31, 1985*, Special Publication, University of Utah Seismograph Stations, Salt Lake City, Utah, 83 pp.

Corbett, E. J. (1984). Seismicity and crustal structure studies of southern California: Tectonic implications from improved earthquake locations, *Ph.D. Thesis*, California Institute of Technology, Pasadena, California, 231 pp.

Doser, D. I. (1989). Extensional tectonics in northern Utah–southern Idaho, U.S.A., and the 1934 Hansel Valley sequence, *Phys. Earth Planet. Interiors* **54,** 120-134.

Evans, J. P. (1991). Structural setting of seismicity in northern Utah, *Utah Geol. Surv., Contract Rept. 91-15*, 37 pp.

Gutenberg, B. and C. F. Richter (1956). Earthquake magnitude, intensity, and acceleration, *Bull. Seism. Soc. Am.* **46,** 105-145.

Hecker, S. (1991). Quaternary tectonics of Utah, *Survey Notes (Utah Geological and Mineral Survey)*, **24**, No. 3, 12-17.

Jackson, J. A. (1987). Active normal faulting and crustal extension, in *Continental Extensional Tectonics*, M. P. Coward, J. F. Dewey, and P. L. Hancock, Editors, *Geol. Soc. London Special Publication 28*, 3-17.

Jackson, J. A. and N. J. White (1989). Normal faulting in the upper continental crust: Observations from regions of active extension, *J. Struct. Geol.* **11**, 15-36.

Johnson, C. E. and D. M. Hadley (1976). Tectonic implications of the Brawley earthquake swarm, Imperial Valley, California, January 1975, *Bull. Seism. Soc. Am.* **66**, 1133-1144.

Jones, C. H. (1987). A geophysical and geological investigation of extensional structures, Great Basin, western United States, *Ph.D. Thesis*, Massachusetts Institute of Technology, Cambridge, Massachusetts, 226 pp.

Keller, G. R., R. B. Smith, and L. W. Braile (1975). Crustal structure along the Great Basin-Colorado Plateau transition from seismic refraction studies, *J. Geophys. Res.* **80**, 1093-1098.

Klein, F. W. (1978). Hypocenter location program HYPOINVERSE, *U.S. Geol. Surv., Open-File Rept. 78-694*, 113 pp.

Nava, S. J., J. C. Pechmann, W. J. Arabasz, E. D. Brown, L. L. Hall, P. J. Oehmich, E. McPherson, and J. K. Whipp (1990). *Earthquake Catalog for the Utah Region, January 1, 1986 to December 31, 1988*, Special Publication, University of Utah Seismograph Stations, Salt Lake City, Utah, 96 pp.

Richins, W. D., W. J. Arabasz, G. M. Hathaway, P. J. Oehmich, L. L. Sells, and G. Zandt (1981). *Earthquake Data for the Utah Region: July 1, 1978 to December 31, 1980*, Special Publication, University of Utah Seismograph Stations, Salt Lake City, Utah, 127 pp.

Richins, W. D., W. J. Arabasz, G. M. Hathaway, E. McPherson, P. J. Oehmich, and L. L. Sells (1984). *Earthquake Data for the Utah Region: January 1, 1981 to December 31, 1983*, Special Publication, University of Utah Seismograph Stations, Salt Lake City, Utah, 111 pp.

Smith, R. B. and W. J. Arabasz (1991). Seismicity of the Intermountain Seismic Belt, in *Neotectonics of North America*, D. B. Slemmons, E. R. Engdahl, M. D. Zoback, M. L. Zoback, and D. Blackwell, Editors, *Geol. Soc. Am. SMV V-1*, in press.

United States Geological Survey (1988). Preliminary determination of epicenters: Monthly listings, U.S. Government Printing Office, Washington, D.C.

Westaway, R. and R. B. Smith (1989). Source parameters of the Cache Valley (Logan), Utah, earthquake of 30 August 1962, *Bull. Seism. Soc. Am.* **79**, 1410-1425.

Westphal, W. H. and A. L. Lange (1966). The distribution of earthquake aftershock foci, Cache Valley, Utah, September 1962 (abstract), *Trans. Am. Geophys. Union* **47**, 428.

Williams, J. S. and M. L. Tapper (1953). Earthquake history of Utah, 1850-1949, *Bull. Seism. Soc. Am.* **43**, 191-218.

Witkind, I. J. (1975). Preliminary map showing known and suspected active faults in Idaho, *U.S. Geol. Surv., Open-File Rept. 75-278*, 71 pp.

Zoback, M. L. (1989). State of stress and modern deformation of the northern Basin and Range province, *J. Geophys. Res.* **94**, 7105-7128.

APPENDIX

This appendix contains a listing of the relocated hypocenters determined in this study for earthquakes associated with the November 19, 1988, M_L 4.8 Bear Lake earthquake. This listing includes all earthquakes in the University of Utah catalog which (1) had epicenters within 15 km of the relocated epicenter for the main shock, (2) occurred during the year preceding or following the main shock, and (3) had at least five P-wave arrival time picks. At the time that these earthquakes were sorted from the catalog, the catalog was final through 1988 (see Nava et al., 1990). This appendix also includes some small aftershocks which are not listed in the catalog. The relocations were done with the computer program HYPOINVERSE (Klein, 1978) using P-wave arrival times only, the stations and station corrections in Table 3-1, the velocity model in Table 3-2, elevation corrections calculated using a near-surface velocity of 3.0 km/sec, and a trial hypocenter of 42° 0.4′ N, 111° 28.0′ W, 10.3 km depth. See text for further explanation.

The following data are listed for each earthquake:

- Year (YR), date and origin time in Universal Coordinated Time (UTC). Subtract seven hours to convert to Mountain Standard Time (MST) and six hours to convert to Mountain Daylight Time (MDT).
- Earthquake location coordinates in degrees and minutes of north latitude and west longitude, and depth in kilometers. "*" indicates poor depth resolution: no recording stations within 10 km or twice the depth.
- MAG, the computed local magnitude (M_L) for each earthquake. "W" indicates magnitude based on peak amplitude measurements from Wood-Anderson records. Otherwise, the estimate is calculated from signal durations and is more correctly identified as coda magnitude, M_C . "--" indicates that a reliable magnitude estimate could not be made.
- NO, the number of P readings used in the solution.
- GAP, the largest azimuthal separation in degrees between recording stations used in the solution.
- DMN, the epicentral distance in kilometers to the closest station used in the solution.
- RMS, the root-mean-square of the travel-time residuals in seconds:

$$RMS = \left\{ \frac{\sum_i \left[W_i R_i \right]^2}{\sum_i \left[W_i \right]^2} \right\}^{\frac{1}{2}}$$

where: R_i is the observed minus the computed arrival time for the i-th reading, and W_i is the relative weight given to the i-th arrival time (0.0 for no weight through 1.0 for full weight).

Bear Lake (Utah/Idaho Border) Earthquake Sequence

yr	*date*	*origin time*	*latitude*	*longitude*	*depth*	*mag*	*no*	*gap*	*dmin*	*rms*
87	1127	2059 12.06	41° 54.29′	111° 29.30′	4.4*	2.1	8	119	22	0.09
87	1129	1612 1.28	41° 54.53′	111° 28.39′	14.6	1.8	8	121	21	0.11
88	120	1949 32.75	42° 1.43′	111° 27.02′	4.5*	2.0	7	181	19	0.08
88	1119	1937 26.29	42° 0.39′	111° 27.89′	4.9*	2.6W	7	170	20	0.05
88	1119	1942 37.21	42° 0.39′	111° 27.24′	13.8	4.8W	8	171	19	0.12
88	1119	1946 16.73	42° 0.35′	111° 27.70′	4.1*	2.8	8	170	20	0.08
88	1119	2000 53.31	42° 0.82′	111° 27.81′	5.4*	4.3W	7	174	20	0.10
88	1119	2033 25.36	41° 59.72′	111° 28.54′	6.4*	2.8W	8	163	20	0.13
88	1119	2106 28.50	42° 0.37′	111° 27.90′	5.2*	2.5W	7	169	20	0.05
88	1119	2215 11.48	42° 0.35′	111° 27.82′	5.8*	2.3	6	169	20	0.08
88	1119	2345 33.75	42° 0.55′	111° 27.75′	8.6*	1.7	5	171	20	0.04
88	1119	2359 58.61	42° 2.76′	111° 19.90′	12.8	0.9	5	284	10	0.03
88	1120	4 53.99	42° 0.21′	111° 27.29′	9.1*	1.9	7	170	19	0.07
88	1120	27 9.59	42° 0.14′	111° 27.84′	4.8*	1.4	7	168	20	0.09
88	1120	229 42.13	42° 1.07′	111° 27.68′	12.9	1.6	6	176	20	0.01
88	1120	623 46.72	42° 0.17′	111° 28.15′	8.9*	1.6	7	167	20	0.04
88	1120	805 43.89	42° 0.39′	111° 28.43′	7.3*	1.2	7	169	21	0.03
88	1120	2139 4.97	42° 0.65′	111° 27.95′	10.2	1.4	10	99	4	0.06
88	1120	2323 13.63	42° 0.08′	111° 28.55′	11.3	0.6	6	107	4	0.03
88	1120	2323 42.94	42° 0.14′	111° 27.95′	11.2	1.1	7	104	4	0.07
88	1120	2324 32.44	42° 0.14′	111° 28.98′	10.7	0.4	6	112	5	0.04
88	1120	2328 50.55	42° 0.02′	111° 28.89′	11.0	0.7	6	109	5	0.04
88	1120	2353 41.92	41° 59.91′	111° 29.90′	9.0	0.5	6	124	5	0.08
88	1121	9 24.54	41° 59.25′	111° 30.54′	9.2	0.2	5	246	7	0.01
88	1121	11 46.55	42° 0.45′	111° 28.20′	11.0	--	6	104	4	0.05
88	1121	54 20.30	42° 0.98′	111° 27.66′	10.5	0.9	6	105	4	0.03
88	1121	207 32.76	42° 0.12′	111° 28.93′	12.5	0.3	6	110	5	0.02
88	1121	235 52.96	42° 0.41′	111° 28.78′	11.5	0.4	6	111	5	0.02
88	1121	300 59.26	42° 0.26′	111° 28.19′	9.8	0.1	6	102	4	0.04
88	1121	316 21.66	42° 0.81′	111° 28.26′	11.1	0.1	6	107	4	0.03
88	1121	352 47.93	42° 0.42′	111° 29.05′	11.0	--	5	115	5	0.02
88	1121	355 0.26	42° 0.06′	111° 29.45′	8.6	1.2	7	106	5	0.07
88	1121	424 42.72	42° 0.89′	111° 28.44′	9.6	1.3	7	89	4	0.05
88	1121	450 48.69	41° 59.97′	111° 28.11′	11.5	--	6	108	4	0.01
88	1121	521 57.63	42° 0.42′	111° 28.50′	12.5	--	5	107	5	0.03
88	1121	550 29.25	42° 0.52′	111° 29.16′	9.7	--	5	119	5	0.01
88	1121	631 44.23	42° 0.37′	111° 28.70′	9.6	0.8	6	110	5	0.06
88	1121	646 0.99	42° 0.89′	111° 28.04′	10.1	0.2	6	105	4	0.04
88	1121	731 16.78	42° 0.33′	111° 29.14′	9.5	0.7	7	100	5	0.06
88	1121	733 24.37	41° 59.86′	111° 29.41′	10.7	--	6	114	5	0.06
88	1121	742 42.21	42° 0.15′	111° 24.27′	4.6	0.1	6	149	3	0.11
88	1121	750 41.22	42° 0.43′	111° 28.83′	12.0	--	5	113	5	0.02
88	1121	826 38.49	41° 59.97′	111° 28.47′	9.9	0.6	6	109	4	0.02
88	1121	852 25.30	42° 0.45′	111° 28.85′	10.4	0.8	6	113	5	0.03
88	1121	901 24.01	41° 59.81′	111° 28.04′	10.7	--	5	113	4	0.03

Bear Lake (Utah/Idaho Border) Earthquake Sequence

yr	*date*	*origin time*	*latitude*	*longitude*	*depth*	*mag*	*no*	*gap*	*dmin*	*rms*
88	1121	933 21.44	41° 59.95′	111° 28.50′	7.4	0.4	6	110	4	0.06
88	1121	933 50.44	41° 59.98′	111° 28.38′	10.8	2.2W	14	91	4	0.07
88	1121	1005 44.83	41° 59.83′	111° 27.93′	11.9	0.8	5	112	3	0.01
88	1121	1012 7.68	41° 59.72′	111° 28.94′	11.3	--	6	116	5	0.02
88	1121	1027 43.09	42° 0.50′	111° 27.66′	11.2	--	6	103	4	0.02
88	1121	1028 35.03	42° 0.26′	111° 28.53′	13.9	--	5	106	5	0.03
88	1121	1038 49.57	41° 59.79′	111° 28.64′	11.9	0.3	6	115	4	0.04
88	1121	1041 56.98	41° 59.85′	111° 27.96′	13.0	0.1	6	112	4	0.
88	1121	1049 38.30	42° 0.12′	111° 29.08′	10.7	0.3	6	113	5	0.04
88	1121	1118 56.99	41° 59.57′	111° 29.45′	8.9	0.9	5	230	5	0.05
88	1121	1124 55.43	41° 59.98′	111° 28.86′	17.3	0.6	6	109	5	0.06
88	1121	1138 38.40	42° 0.14′	111° 28.38′	10.0	--	6	105	4	0.01
88	1121	1151 4.39	41° 59.52′	111° 25.39′	11.1	--	5	189	1	0.35
88	1121	1202 46.55	41° 59.70′	111° 27.86′	8.5	--	5	115	3	0.11
88	1121	1208 4.67	42° 0.57′	111° 28.48′	13.6	--	5	109	5	0.05
88	1121	1214 45.30	42° 0.22′	111° 27.46′	9.0	0.4	6	105	3	0.03
88	1121	1239 53.43	41° 59.93′	111° 28.58′	8.0	0.3	6	111	4	0.08
88	1121	1248 46.34	42° 0.87′	111° 27.16′	15.7	--	5	153	4	0.01
88	1121	1300 1.64	42° 0.43′	111° 27.85′	12.4	--	6	100	4	0.05
88	1121	1310 24.47	42° 0.24′	111° 28.88′	12.7	0.8	6	112	5	0.04
88	1121	1405 23.14	42° 0.79′	111° 27.33′	13.3	--	5	145	4	0.01
88	1121	1413 42.50	42° 0.22′	111° 28.62′	7.4	--	5	108	5	0.06
88	1121	1422 57.04	41° 59.70′	111° 27.60′	13.9	--	5	113	3	0.01
88	1121	1458 58.61	42° 0.69′	111° 27.37′	13.7	--	6	108	4	0.09
88	1121	1525 15.87	42° 0.81′	111° 27.54′	11.5	--	5	139	4	0.02
88	1121	1655 13.94	42° 0.56′	111° 28.07′	11.1	--	5	119	4	0.02
88	1121	1724 3.45	41° 59.49′	111° 28.26′	13.6	0.4	6	122	4	0.05
88	1121	1726 2.35	41° 59.39′	111° 28.63′	13.7	0.8	5	126	4	0.02
88	1121	1949 40.84	42° 0.11′	111° 28.59′	11.7	0.7	6	106	5	0.04
88	1121	2107 52.48	42° 0.85′	111° 27.85′	10.1	0.7	12	101	4	0.09
88	1121	2125 4.76	42° 0.33′	111° 27.61′	11.6	0.7	6	103	4	0.06
88	1121	2125 49.76	42° 0.49′	111° 27.88′	10.6	1.2	8	99	4	0.05
88	1121	2139 38.29	42° 0.08′	111° 29.19′	11.3	0.1	6	114	5	0.03
88	1121	2200 6.15	42° 0.24′	111° 28.54′	9.4	1.2	9	88	5	0.07
88	1121	2202 1.38	41° 59.59′	111° 29.62′	13.7	0.4	5	232	6	0.02
88	1121	2254 12.74	42° 1.04′	111° 28.05′	11.5	0.1	6	106	4	0.02
88	1121	2359 2.45	42° 1.24′	111° 27.38′	10.9	0.1	6	111	3	0.06
88	1122	54 50.32	42° 0.73′	111° 28.00′	10.3	1.1	11	97	4	0.03
88	1122	416 37.14	42° 0.46′	111° 28.78′	11.1	--	5	112	5	0.02
88	1122	445 54.28	42° 0.74′	111° 28.00′	9.7	0.7	7	97	4	0.06
88	1122	515 18.85	42° 0.66′	111° 27.49′	9.3	0.1	6	107	4	0.06
88	1122	628 21.30	42° 0.08′	111° 29.33′	9.4	0.3	6	116	5	0.05
88	1122	637 45.73	42° 0.41′	111° 27.87′	15.6	0.4	6	99	4	0.06
88	1122	705 57.81	42° 0.19′	111° 28.74′	11.7	0.4	6	109	5	0.01
88	1122	755 15.82	42° 0.75′	111° 29.21′	7.5	0.7	5	122	5	0.03

Bear Lake (Utah/Idaho Border) Earthquake Sequence

yr	*date*	*origin time*	*latitude*	*longitude*	*depth*	*mag*	*no*	*gap*	*dmin*	*rms*
88	1122	835 24.91	42° 0.93′	111° 28.01′	10.4	1.4	10	132	5	0.05
88	1122	939 12.15	42° 0.97′	111° 27.35′	15.1	--	5	148	4	0.01
88	1122	1014 7.09	42° 0.37′	111° 28.69′	13.1	--	6	100	5	0.03
88	1122	1048 19.00	42° 0.12′	111° 29.03′	12.0	--	5	112	5	0.03
88	1122	1057 53.34	42° 0.96′	111° 27.86′	10.7	1.2	12	100	4	0.08
88	1122	1146 55.66	42° 0.02′	111° 28.84′	12.8	--	5	108	5	0.06
88	1122	1622 18.26	42° 0.45′	111° 28.25′	10.4	0.7	6	105	4	0.04
88	1122	1635 57.63	42° 0.99′	111° 28.06′	10.3	0.4	6	106	4	0.04
88	1122	1707 34.47	42° 0.24′	111° 28.22′	11.3	0.1	6	102	4	0.03
88	1122	2122 36.19	42° 1.10′	111° 27.70′	10.7	0.3	5	104	3	0.06
88	1122	2207 44.93	42° 1.01′	111° 26.70′	13.7	0.1	6	126	4	0.05
88	1123	20 22.52	42° 0.88′	111° 28.40′	11.3	--	6	110	4	0.02
88	1123	154 55.05	42° 0.58′	111° 27.46′	10.3	0.3	6	107	4	0.03
88	1123	205 41.72	42° 1.48′	111° 27.37′	6.2	--	6	114	3	0.06
88	1123	238 12.82	42° 0.87′	111° 27.44′	8.0	--	6	108	4	0.04
88	1123	316 25.36	42° 0.05′	111° 28.39′	13.9	--	6	107	4	0.04
88	1123	347 15.90	42° 0.22′	111° 28.43′	9.5	0.8	6	105	4	0.02
88	1123	413 59.87	42° 0.69′	111° 27.45′	9.3	1.9	12	107	4	0.04
88	1123	419 54.05	42° 0.66′	111° 27.59′	8.6	--	6	105	4	0.04
88	1123	423 18.43	42° 0.61′	111° 27.28′	9.6	0.5	9	135	4	0.05
88	1123	423 37.04	42° 1.06′	111° 27.19′	8.1	0.7	8	140	4	0.09
88	1123	434 17.68	42° 0.85′	111° 27.80′	8.0	0.9	6	102	4	0.03
88	1123	542 14.67	42° 0.76′	111° 28.27′	8.7	0.4	6	108	4	0.03
88	1123	556 52.49	42° 0.52′	111° 28.13′	10.9	1.2	10	95	4	0.03
88	1123	627 43.76	42° 0.87′	111° 27.40′	8.5	0.1	6	109	4	0.03
88	1123	714 24.98	42° 0.97′	111° 28.23′	10.0	--	5	118	4	0.02
88	1123	717 13.94	42° 0.71′	111° 28.31′	8.3	0.9	5	107	4	0.03
88	1123	840 54.44	42° 0.66′	111° 28.49′	9.8	0.4	6	110	5	0.05
88	1123	908 40.93	41° 59.99′	111° 30.46′	11.0	--	5	237	7	0.
88	1123	935 2.30	42° 1.04′	111° 27.28′	8.8	--	6	112	4	0.04
88	1123	1011 46.14	42° 0.87′	111° 28.12′	9.5	0.9	6	106	4	0.02
88	1123	1140 11.46	42° 0.93′	111° 27.32′	8.3	--	5	111	4	0.04
88	1123	1212 2.66	42° 0.64′	111° 28.11′	10.5	2.3	12	128	8	0.04
88	1123	1333 30.50	42° 0.71′	111° 28.32′	8.4	1.2	5	127	5	0.06
88	1123	1536 39.63	42° 0.93′	111° 27.82′	10.1	1.7	6	103	4	0.01
88	1123	1641 20.83	42° 0.68′	111° 28.07′	10.3	0.5	6	103	4	0.04
88	1123	2150 55.41	42° 0.55′	111° 27.07′	10.9	0.9	6	173	19	0.08
88	1123	2151 27.66	42° 0.83′	111° 27.12′	9.8	1.4	7	176	19	0.09
88	1123	2217 25.31	42° 0.56′	111° 28.33′	7.3*	1.0	6	171	20	0.02
88	1124	1205 46.15	42° 1.08′	111° 27.67′	6.9*	1.2	7	176	20	0.07
88	1125	1908 21.98	42° 0.17′	111° 28.27′	7.6*	2.5	7	167	20	0.04
88	1125	2056 10.36	42° 0.87′	111° 27.53′	11.6	2.2	8	175	20	0.06
88	1127	1600 21.03	42° 1.11′	111° 27.38′	10.2	1.7	6	178	20	0.02
88	1128	755 2.14	42° 0.29′	111° 28.28′	8.5*	1.7	7	168	20	0.08
88	1128	1018 23.53	42° 0.88′	111° 27.99′	6.1*	1.0	7	174	20	0.06

Bear Lake (Utah/Idaho Border) Earthquake Sequence

yr	*date*	*origin time*	*latitude*	*longitude*	*depth*	*mag*	*no*	*gap*	*dmin*	*rms*
88	1128	1021 53.18	42° 0.36′	111° 27.83′	8.3*	1.9	7	169	20	0.07
88	1128	1046 46.50	42° 0.19′	111° 27.17′	15.6	3.2W	9	170	19	0.12
88	1128	1830 39.77	42° 2.30′	111° 26.64′	16.3	1.5	6	189	20	0.07
88	1129	1031 27.58	42° 1.46′	111° 27.55′	10.2	1.4	5	180	20	0.11
88	1129	1207 8.00	41° 59.96′	111° 28.32′	4.3*	2.6W	8	166	20	0.09
88	1130	1356 17.62	42° 0.85′	111° 27.52′	11.5	2.0	9	174	20	0.08
88	1201	413 2.06	42° 1.04′	111° 27.98′	10.4	1.9	5	205	20	0.21
88	1201	1825 25.38	42° 0.59′	111° 27.93′	12.4	1.6	6	171	20	0.02
88	1202	1846 17.25	42° 0.38′	111° 28.27′	4.7*	2.8W	8	169	20	0.04
88	1202	1945 34.00	42° 0.59′	111° 27.79′	10.4	2.4W	8	171	20	0.02
88	1207	852 52.46	42° 0.41′	111° 27.19′	14.7	2.7W	9	171	19	0.14
88	1209	1639 24.53	42° 0.52′	111° 27.26′	11.9	1.9	6	173	19	0.04
88	1215	1042 15.40	42° 0.07′	111° 28.36′	5.3*	2.2	8	166	20	0.15
88	1220	2058 35.53	42° 0.44′	111° 28.26′	8.3*	1.3	5	169	20	0.09
88	1222	2034 37.26	42° 0.46′	111° 27.90′	7.7*	1.4	7	171	20	0.10
89	104	309 38.30	41° 59.77′	111° 28.80′	4.7*	2.7	7	162	21	0.03
89	115	1041 25.90	42° 1.02′	111° 26.86′	10.6*	1.8	6	246	30	0.02
89	202	2113 13.45	42° 0.35′	111° 28.41′	10.0*	1.5	6	169	20	0.01
89	218	2339 17.96	42° 0.55′	111° 27.65′	15.8	2.2W	7	241	29	0.12
89	319	952 49.54	42° 0.42′	111° 26.81′	12.7	2.2	8	173	18	0.10
89	319	2044 41.30	41° 59.95′	111° 27.94′	5.4*	1.7	7	166	20	0.12
89	605	457 39.51	42° 0.02′	111° 27.59′	6.0*	2.4	8	168	19	0.05

number of earthquakes = 157

* indicates poor depth control
W indicates Wood-Anderson data used for magnitude calculation